WIDEBAND ELECTROMAGNETIC BAND GAP (EBG) STRUCTURES, ANALYSIS AND APPLICATIONS TO ANTENNAS

Sandeep Palreddy

Dissertation submitted to the faculty of the Virginia Polytechnic Institute and State University in partial fulfillment of the requirements for the degree of

Doctor of Philosophy
In
Electrical Engineering

Amir I. Zaghloul (Chair)
William A. Davis
Gary S. Brown
Timothy Pratt
Konstantinos P. Triantis
William O'Keefe Coburn (External Examiner)

May 1, 2015

Blacksburg, VA

Keywords: electromagnetic band gap (EBG) structures, reflection phase, progressive EBG structures, stacked EBG structures, transmission line analysis, circuit analysis, EBG bandwidth, EBG applications.

WIDEBAND ELECTROMAGNETIC BAND GAP (EBG) STRUCTURES, ANALYSIS AND APPLICATIONS TO ANTENNAS

Sandeep Palreddy

ABSTRACT

In broadband antenna applications, the antenna cavity is usually loaded with absorbers to eliminate the backward radiation, but in doing so the radiation efficiency of the antenna is decreased. To enhance the radiation efficiency of the antennas electromagnetic band gap (EBG) structures are used, but they operate over a narrow band. Uniform EBG structures are usually periodic structures consisting of metal patches that are separated by small gaps and vias that connect the patches to the ground plane. The electrical equivalent circuit consists of a resonant tank circuit, whose capacitance is represented by the gap between the patches and inductance represented by the via. EBG structures are equivalent to a magnetic surface at the frequency of resonance and thus have very high surface impedance; this makes the EBG structures useful when mounting an antenna close to conducting ground plane, provided the antenna currents are parallel to the EBG structure. Because EBG structures are known to operate over a very narrow band, they are not useful when used with a broadband antenna. Mushroom-like uniform EBG structures (that use vias) are compact in size, have low loss, can be integrated into an antenna to minimize coupling effects of ground planes, and increase radiation efficiency of the antenna. The bandwidth of an EBG structure is defined as the band where the reflection-phase from the structure is between $+90^0$ to -90^0. In this dissertation analysis of EBG structures is established using circuit analysis and transmission line analysis. Methods of increasing the bandwidth of EBG structures are explored, by cascading uniform EBG structures of different sizes progressively and vertically (stacked), and applications with different types of antennas are presented. Analyses in this dissertation are compared with previously published results and with simulated results using 3D electromagnetic tools. Validation of applications with antennas is carried by manufacturing prototypes and comparing measured performance with analysis and 3D electromagnetic simulations. The improvements in performance by using wideband progressive EBG and wideband stacked EBG structures are noted.

ACKNOWLEDGEMENTS

I would like to express my special appreciation and thanks to my advisor Dr. Amir I. Zaghloul and the US Army Research Laboratory for helping me with my research. Amir has been a very good mentor and collaborator since my research started at Virginia Tech in 2010. As a mentor, he has provided me the freedom to explore on my own, and at the same time provided guidance to recover when my steps faltered. As a collaborator, he has dedicated countless hours to discuss, criticize and explore new solutions together with me in many aspects of several research topics. It was a great pleasure to work with him. I would like to thank the US Army Research Laboratory in prototyping my designs and providing me with measured results. I would like to thank Dr. Keefe Coburn and Mr. Theodore Anthony from ARL, for their guidance on the simulations and for doing the measurements, respectively. This five-year research was made possible through a continuous devotion, and using several right tools. I am greatly indebted to two distinguished companies and their colleagues. From 2008 through 2014 I worked at Microwave Engineering Corporation (MEC) as a Lead RF Design Engineer, where I honed my skills as Lead Antenna & Microwave Engineer which helped me prosper into a researcher. 2014 onwards I worked at ViaSat - Antenna Systems as a Member of Technical Staff where I appreciated the role of antenna engineers and scientists in delivering state of the art solutions to complex real world problems. Amir, MEC, US Army Research Laboratory and ViaSat have provided many practical advices and insights, which helped me understand my research problems and enrich my ideas.

My extended appreciation to the members of my advisory committee –Dr. William A. Davis, Dr. Gary S. Brown, Dr. Timothy Pratt and Dr. Konstantinos P. Triantis – for the advice and assistance provided throughout my research. Dr. Davis, Dr. Brown & Dr. Pratt deserve special thanks for the four EM courses taught to me over two years, and the numerous thought-provoking comments on EM modeling, programming and professional documentations, etc. My sincere thanks to my mother and sister who supported me emotionally through this journey and special thanks to my daughter Sanvi who provided me much needed final support in graduating. Special thanks to my wife, Spandana, for her emotional support, and being a patient listener and patiently typing all my equations and helping me put together my dissertation.

Table of Contents

LIST OF SYMBOLS

c	Speed of light in free space
f	Frequency
ω	Radian frequency
k	Wave number
l	Length
m	Electron mass
n	Refractive index
q	Charge of electron
B	Magnetic flux density
D	Electric flux density
E	Electric field
H	Magnetic Field
I	Current
J	Current density
Z	Surface impedance
σ	Material conductivity
α	Attenuation constant
β	Phase constant
η	Impedance
ε	Material Permittivity
μ	Material permeability
w	Patch width
g	Patch gap
h	Height
C	Capacitance
L	Inductance
δ	Skin depth
θ	Angle
∂	Scalar differential operator
∇	Vector differential operator

V	voltage
I	Current
τ	Transmission coefficient
Γ	Reflection coefficient

LIST OF FIGURES

1 INTRODUCTION

Antennas are essential to transmit and receive in a communication system [1]. The performance of an antenna is greatly affected by the surrounding medium and the presence of conducting ground planes [1, 2, 3]. A conducting surface close to a radiating antenna usually degrades the performance of the antenna. A parallel electric field is reflected out of phase from the conducting surface and when it interacts with the forward propagating electromagnetic wave, they often add destructively and thus affect the radiation characteristics of the antenna. A tangential current element close to a conducting plane is equivalent to two current elements, which are in opposite directions, as compared with the current in free space without the conducting plane. This causes the radiation from the current elements to cancel each other, thus affecting the radiation characteristics of the antenna. When an antenna is placed close to a parallel magnetic conductor, the electric field is reflected in phase and thus interacts constructively with the forward propagating electric field, enhancing the radiation in the forward direction instead of completely cancelling it. A tangential current element close to a magnetic conducting plane is equivalent to two electric current elements, in the same direction for the free space equivalent without the magnetic conducting plane. This causes the radiation from the current elements to add constructively, thus enhancing the radiation characteristics of the antenna. Similarly a current element that is normal to an electric conductor has an image that is also a normal current element aligned in the same direction, as shown in Figure 1.1, resulting in an enhancement of radiation pattern as the array factor adds constructively [2, 4]. A current element that is normal to a magnetic conductor has an image that is also a normal current element, but aligned in the opposite direction, as shown in Figure 1.1, resulting in destructive addition of radiation pattern as the array factor does not add constructively [2, 4].

Artificial magnetic conductors (AMC) enhance the radiation efficiency of antennas, but do not exist in reality [5, 6, 7]. One way to create AMCs is to design periodic structures that have electrical characteristics like a magnetic conductor in the desired frequency band, one such example is an electromagnetic band gap (EBG) structure [5, 6]. Electromagnetic band gap (EBG) structures are periodic structures. When they interact with electromagnetic waves, different electrical properties are observed at different frequencies [7, 8]. Periodic structures pass certain

frequency bands, reject some frequency bands, and behave like a magnetic conductor in a band of frequencies, known as the band gap [9, 10]. Different names have been used for periodic structures depending on the applications. These applications include filtering, frequency selective surfaces (FSS), and electromagnetic band gaps (EBG), etc [11, 12, 13, 14]. Usually electromagnetic band-gap structures are defined as artificial, periodic, high-surface impedance structures that reject or allow the propagation of electromagnetic waves in a specified frequency band.

Electromagnetic band gap structures are usually realized by etching periodic mushroom like square patches on a dielectric board, with or without vias connecting the patches to the ground plane [15]. EBG structures are widely used in antenna engineering applications, as they are compact, lightweight, easy to manufacture, and have low loss over a small band [15]. The band gap of EBG structures is usually defined as the frequency range where the reflection-phase from the EBG surface is between $+90^0$and -90^0. EBG structures behave as artificial magnetic conductors (AMC) about the frequency of resonance, as the reflection-phase from the EBG surface is 0^0 [16, 17]. In the EBG band gap the surface impedance of EBG structures is high; this makes them a good candidate to use under an antenna that needs to be placed close to a ground plane. EBG structures can be also used to suppress undesired surface waves in various antenna engineering applications [18].

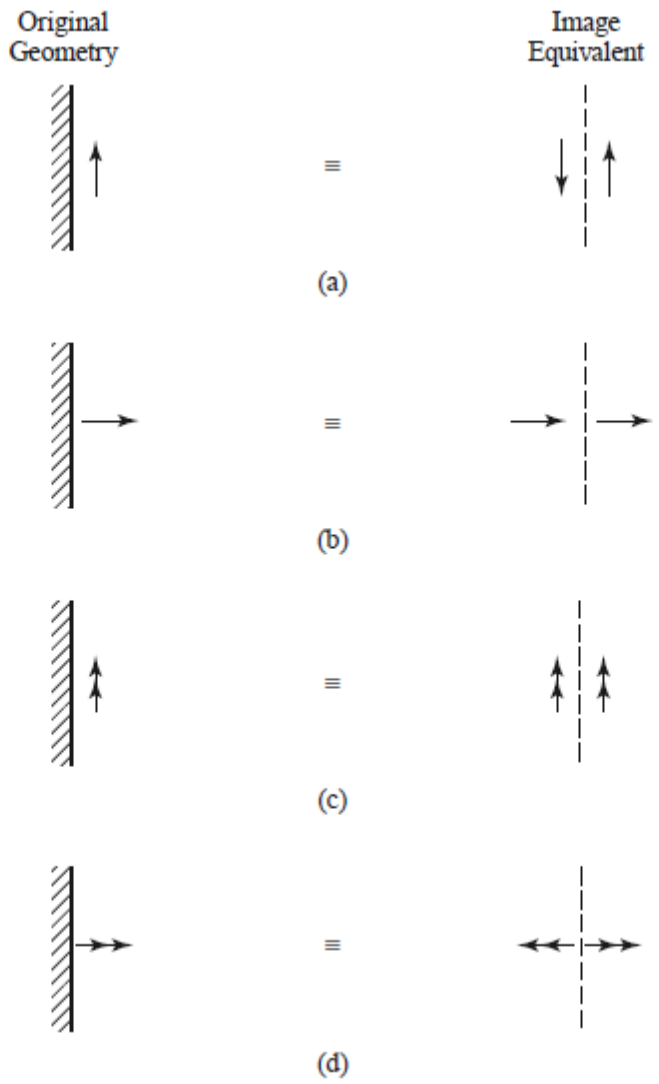

Figure 1.1: Image equivalents of (a) Electric current parallel to perfect electric conductor (b) Electric current perpendicular to perfect electric conductor (c) Electric current parallel to perfect magnetic conductor (d) Electric current perpendicular to perfect magnetic conductor. (with permission)

An EBG structure can be used around a microstrip patch antenna to increase the antenna gain by reducing the backward radiation [18]. EBG structures can also be used between antennas in an array to decrease coupling between adjacent antenna elements, helping eliminate blind scan angles [19]. EBG structures increase the efficiency of an antenna placed above them, provided the currents in the antenna are parallel to the EBG surface, by reflecting the backward radiated energy in-phase with respect to forward radiated energy, which results in constructive addition of the radiations [20]. An 1-D EBG structure can be used to design band pass, band reject and high Q

cavities. A 3-D EBG structure, formed by cascading EBG layers, can be used in a multiband communication system to separate multiple bands into the right feeds by employing them in sub-reflectors [21, 22].

A number of periodic structures can be designed and realized to have high surface impedance. Different types of EBG structures differ in the way they are implemented to achieve the wanted surface impedance in the band of interest. Although EBG surfaces have metal patches that conduct DC currents, they do not conduct AC currents in their band gaps and do not allow surface waves in their band gap. The EBG surface behaves like a band stop filter in its band gap, thus not supporting surface waves.

1.1 History of EBG Structures

Electromagnetic band gap (EBG) structures are periodic structures that exhibit special properties in a band of frequencies called the band gap. The special properties include very high surface-impedance and reflecting an incident wave, normally incident on the EBG surface with a near 0^0 reflection-phase. *Reflection-phase* is defined as the phase of the reflection coefficient measured at the surface of the EBG structure. Similarly, *reflection-magnitude* is defined as the magnitude of the reflection coefficient measured at the surface of the EBG structure. *Surface-impedance* is defined as the impedance measured on the surface of the EBG structure. This is the impedance an incident wave on the EBG surface encounters. Reflection-phase is important because when an antenna, which radiates in both directions, is mounted close to an EBG structure the backward radiated EM energy can be reflected in phase with respect to forward radiated EM energy. This enhances the total EM energy in the front half hemisphere of the antenna, which in turn increases the boresight gain of the antenna. Antennas are an important element in a communication system, which enable transmitting and receiving of RF signals. Performance of antennas in a communication system is an important metric, with importance placed on their efficiency. Antennas have evolved into an indispensable part in every communication system, from radios, TVs, wireless communication, navigation and wireless charging. Recently, new research and development has been taking place at a rapid pace on new antenna technologies, one such technology is electromagnetic band gap (EBG) structures and their applications to antennas. The central contribution of this dissertation is the design, analysis, and applications of broadband EBG

structures to different types of antennas. Recent popularity of EBG structures has encouraged development on new EBG applications. Applications to antennas used in radio communication system, satellite communication systems, and integrated packaged radios.

Antennas today are used in systems that communicate in multiple bands and such a number of requirements, such as low profile, compact size, broad bandwidth, and multiple functionalities are required from new antennas to be integrated into new communication systems. Due to better available computing machines and computational electromagnetic tools, design and development of new antenna technologies is made possible. These tools have made analysis and optimization of new antennas, not previously well characterized, easier and faster. The tools include various time domain solvers (e.g. finite-difference-time-domain or FDTD) and frequency domain solvers (e.g. method of moments or MoM and finite element method or FEM). Due to the available computing machines and full wave solvers, complex antenna packaging with feed networks and surrounding materials can be analyzed effectively and the entire packaging can be optimized to achieve the best possible performance. These new tools are the reason for renewed interest in electromagnetic band gap (EBG) structures and their applications to antennas.

1.2 Origin of EBG Structures

EBG structures were first introduced as frequency selective surfaces (FSS), and later adopted to reduce surface waves and increase the gain of antennas. EBG structures can be used to solve problems that arise when antennas are mounted close to conducting planes, problems that include degraded antenna performance when mounted close to a ground plane due to coupling to the ground plane. EBG structures are used in this scenario to minimize coupling to the ground plane, by creating a barrier that suppresses surface waves and enhances the efficiency of antenna by re-reflecting back lobe energy in phase with respect to forward lobe energy. EBG structures are also used in other applications, including miniaturization of antenna size, filtering etc[1, 2, 3]. Due to narrow band gaps of EBG structures, it is very hard to characterize them accurately using lumped-element modeling. Instead, computational electromagnetic tools are widely used. So far all the research involving characterizing the dispersion diagram, surface impedance, and reflection-phase of EBG structures has been carried out by writing lengthy code using computational electromagnetic techniques. EBG structures are periodic structures, so analyzing the until cell and

using appropriate boundary conditions can lead to faster and accurate analysis of EBG structures. Periodic structures, such as EBG structures, exhibit interesting properties in different bands. In a certain band they behave like high-impedance surfaces, in others they behave like a pass-band filter [4].

Electromagnetic band gap structures are defined as artificial periodic (or sometimes non-periodic) objects that prevent/assist the propagation of electromagnetic waves in a specified band of frequency for all incident angles and all polarization states[3, 4]. EBG structures typically consist of metal patches that are separated by a gap on a dielectric substrate with vias connecting the metal patches to the ground plane. The capacitance of the EBG structure is represented by the gap between the patches, while the inductance is represented by the via. Usually EBG structures are classified based on their arrangement, i.e. three dimensional EBG structures that are formed by stacking different EBG layers to form a three dimensional structure, two dimensional EBG structures formed by arranging an EBG unit cell in two dimensions on a plane and one dimension EBG structures that are formed by arranging an EBG unit cell in one dimension to form a transmission line with two ports.

Figure 1.2 shows an example of a three-dimensional EBG structure, formed by laying metal strips vertically and horizontally in different layers to form a three-dimensional structure [5, 6]. Figure 1.3 shows an example of two dimensional EBG structure formed by square patches, called mushroom like EBG structure [7, 8]. Figure 1.4shows an example of one dimensional EBG structure [9, 10], which is used in a filtering application with two ports on either end of the EBG structure. Two and three dimensional EBG structures exhibit some unusual properties in their band gap, when a plane wave is incident upon them it is reflected without a phase reversal as shown in Figure 1.5 [6, 7, 8], and they do not support surface waves, acting like a band-reject surface as shown in Figure 1.6.

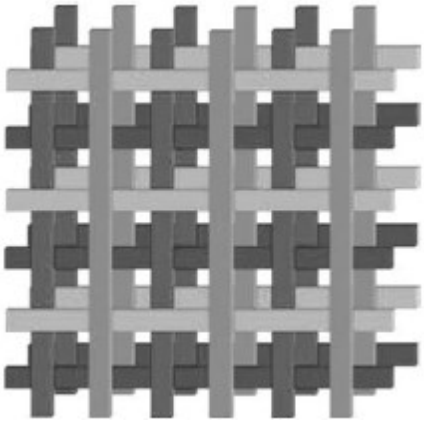

Figure 1.2: Example of a three-dimensional EBG structure. (with permission)

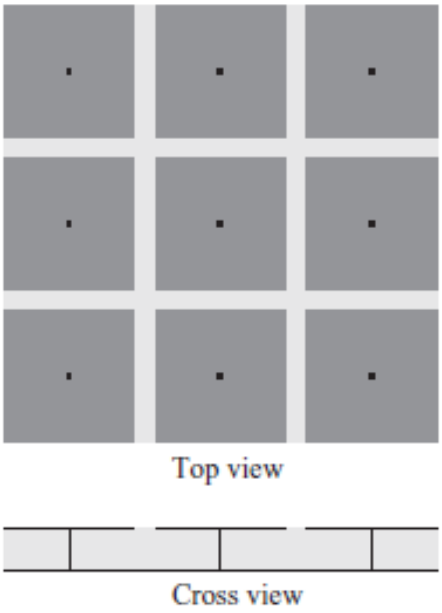

Figure 1.3: Example of a two-dimensional EBG structure. (with permission)

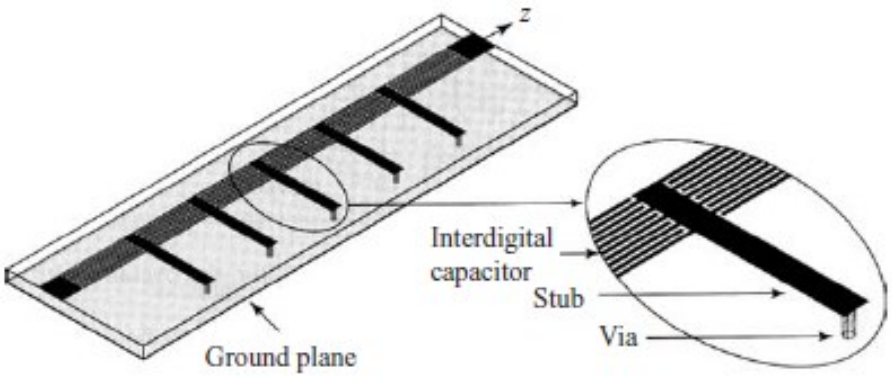

Figure 1.4: Example of an one-dimensional EBG structure. (with permission)

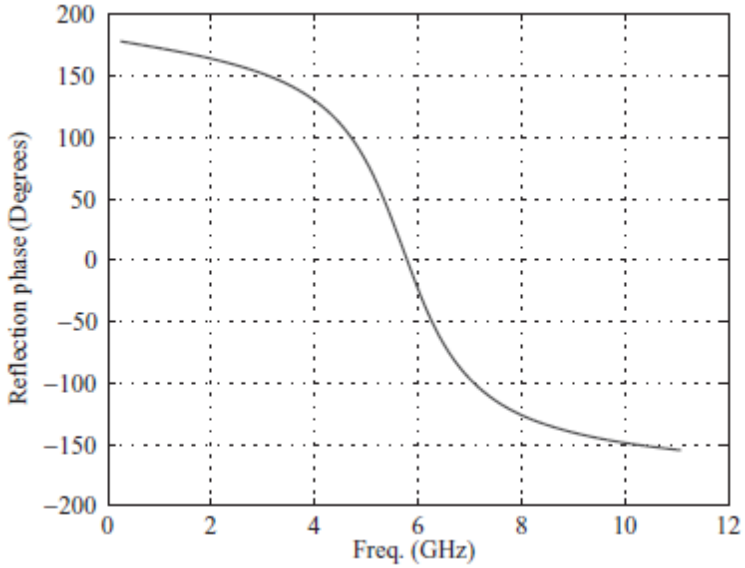

Figure 1.5: Reflection-phase from two-dimensional and three-dimensional EBG structures around their band gap. (with permission)

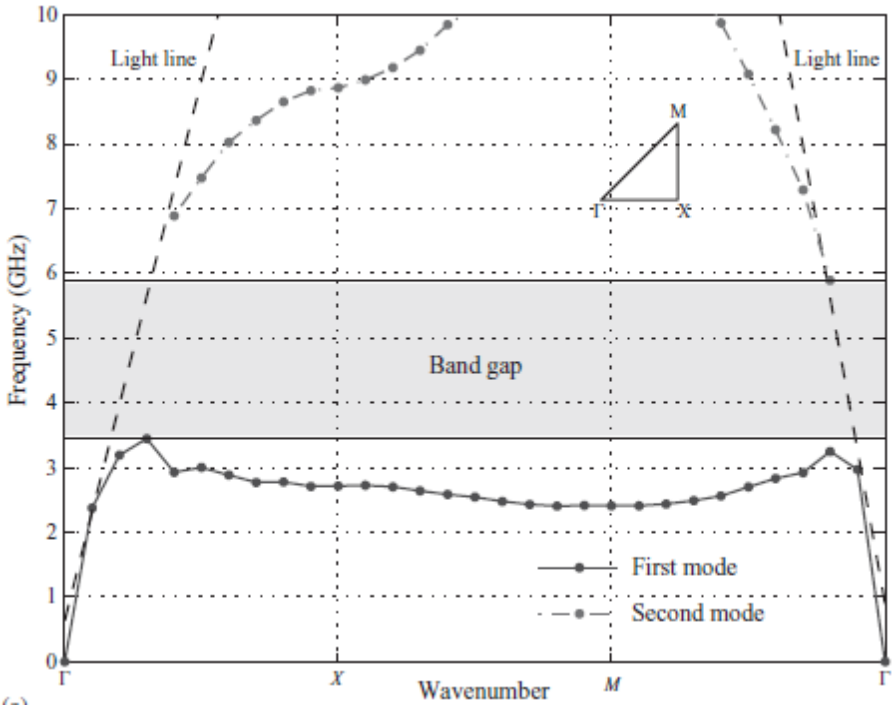

Figure 1.6: Surface wave band gap for two-dimensional and three-dimensional EBG structures. (with permission)

Another term that is also used interchangeably for EBG structures is metamaterials [10, 11, 12, 13, 14]. The prefix meta, means "beyond" in Greek, has been used to describe EBG materials because they have uncommon properties in their band gap, as they reflect incident electric fields without phase reversal at the frequency of resonance in band gap. Some other terms that have been used to describe EBG materials include double negative (DNG) materials, which have negative permittivity and negative permeability, and Left-handed (LH) materials, inside which the electric-field direction, magnetic-field direction, and propagation direction satisfy a left-hand relation, high-impedance surfaces, artificial magnetic conductor (AMC), negative refractive-index materials, magneto materials, soft and hard materials. It should be noted that some of the names used to describe EBG structures are related. Double negative materials have left-handed properties and possess a negative refractive index. A corrugated surface can behave like a soft surface in one direction (along the corrugations) and hard in the other direction (through the corrugations).

One dimensional periodic structures can behave like a left handed material in one frequency band and behave like an EBG structure in another frequency band. So, a periodic structure can behave as one material in one frequency band and as another in another frequency band, so it is not that easy to easily classify metamaterials. Due to their unique band-gap electrical properties, EBG structures can be classified as a special type of metamaterials. In the band gap, EBG structures have a high surface impedance and at the resonance frequency they behave like an artificial magnetic conductor, as they have an infinite surface impedance and reflects an incident wave with a 0^o reflection phase. EBG structures have high surface impedance for both TE and TM waves, they behave like hard structures in their band gap (by suppressing surface waves) and soft surfaces in frequencies away from band gap (by supporting surface waves). EBG structures are important for improving the performance of an antenna in number of scenarios, and they analysis design and applications with antennas are important.

1.3 Analysis

Various methods have been proposed to analyze EBG structures, by analyzing EBG's unit cell and using appropriate boundary conditions at the walls of the unit cell. The proposed methods can be broadly put into four categories:

1) Lumped-element circuit modeling
2) Transmission-line modeling
3) Computational-electromagnetic modeling
4) Using existing full-wave solver packages for modeling

Lumped-element circuit modeling is the simplest and quickest way to analyze EBG structures, but it is also the least accurate. This modeling is carried out by modeling an EBG structure as a tank circuit with capacitance and inductance represented as shown in Figure 1.7 [7]. The values of capacitance and inductance of the EBG structure is determined by its geometric parameters.

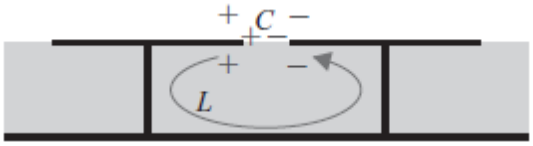

Figure 1.7: Capacitance and inductance of the EBG structure in lumped-element circuit modeling. (with permission)

Transmission-line modeling is another way of analyzing EBG structures, it is more accurate than lumped-element circuit modeling, but less accurate than computational-electromagnetic modeling. Transmission-line model consists of a transmission line that is periodically loaded by a series impedance [16], as shown in Figure 1.8.

In the transmission-line model, Z_P is the impedance of the periodic element and X_C is the coupling capacitance between adjacent patches in the EBG structure. Transmission line analysis provides surface-wave propagation details (dispersion curve), from which the band gap can be identified. The accuracy of this analysis depends on accurately finding the values of Z_P and X_C. Usually closed form equations are used for them and they are found to be not very accurate. Thanks to rapid progress in computational electromagnetic techniques various computational methods have developed for EBG analysis, this analysis is very accurate, but very time consuming, as Maxwell's equations need to be solved inside the unit cell by applying appropriate boundary conditions on unit cell walls. For FDTD, Yee's cell is used in meshing the unit cell. Figure 1.9 shows the setup used to analyze EBG structures using FDTD. Using existing full wave solver packages to analyze EBG structures is pretty straight forward and time consuming, and also it is very expensive to buy

a license of the software. Some of the existing solver packages that can accomplish the task include HFSS, FEKO, CST etc.

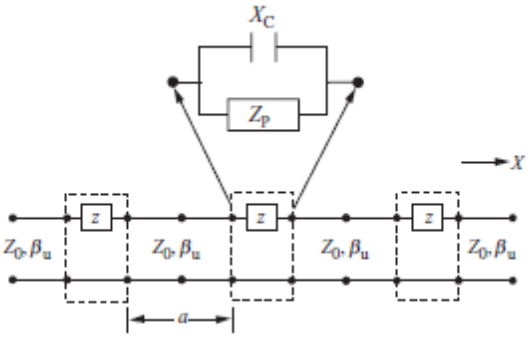

Figure 1.8: Transmission line model of EBG structures. (with permission)

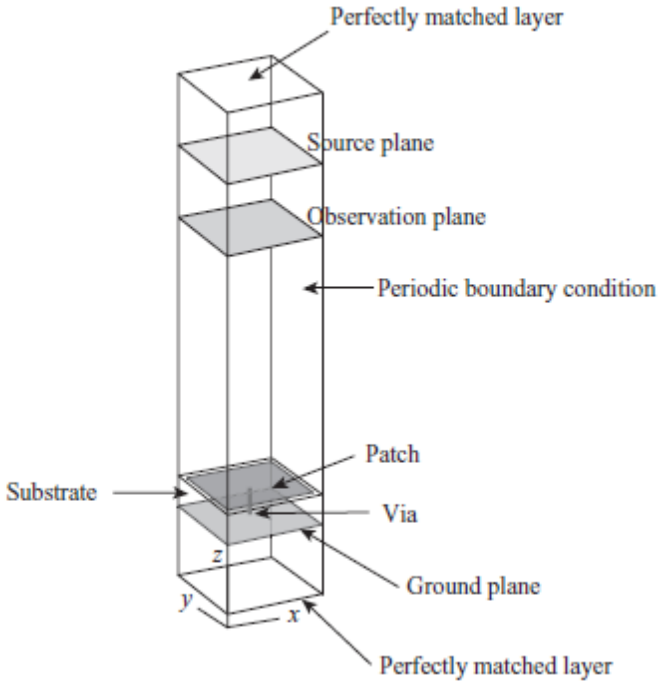

Figure 1.9: Setup used to analyze EBG structures using FDTD method. (with permission)

One of the advantages of using existing full wave solvers is that they can solve EBG structure configurations accurately and the other advantage is that the results allow the extraction of the properties of EBG structure (surface impedance, reflection phase, dispersion diagram).

1.4 Uses of EBG Structures in Antenna Engineering Applications

Unusual electrical properties of EBG structures have led to many applications in antenna engineering. These applications include:

1) Surface Wave Suppression on Conducting Planes: Surface waves are generally created over dielectric coated surfaces; such is the case of a microstrip antenna the couples energy into the dielectric slab guide. Surface waves can also be created on a periodic structure without dielectric, due to periodic coupling. When an antenna is placed close to a ground plane, it couples energy into the ground plane. When this happens, the overall efficiency of the antenna decreases. To avoid this from happening, EBG structures can be used as isolation barrier between the antenna and ground plane [18, 19, 20, 21], by placing the EBG structure between antenna and ground plane. In the EBG's band gap, EBG's surface behave like a high impedance surface, and this help decouple the antenna from the ground plane which helps increase the radiation efficiency of the antenna. Surface wave suppression is also useful in an antenna array, when the coupling between adjacent antennas is enough, it will affect the performance of the antenna array by introducing blind scan angles. This can be cured by placing EBG structures between antenna elements, as shown in Figure 1.10, EBG structures will suppress coupling between adjacent antennas by suppressing surface waves [22], in doing so blind scan angles are eliminated. Another application where the surface wave suppression of EBG structures is useful is when a surface is required to pass a certain band and reject another band. This suppression can be accomplished by designing EBG structure band-gap to fall in the frequency band where rejection is required and make the pass band fall outside the band gap of the EBG.

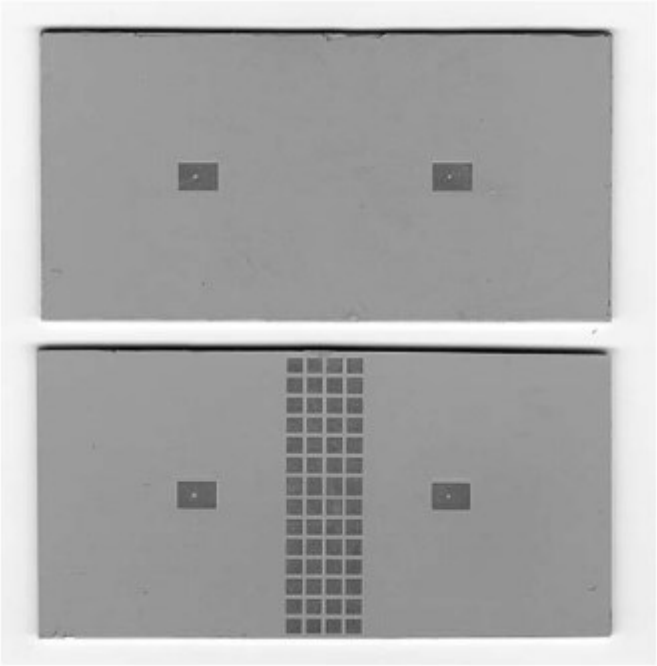

Figure 1.10: EBG structure placed between two patch antennas to eliminate mutual coupling. (with permission)

2) Low profile antenna design: Low profile antenna design can be achieved by using EBG structures underneath wire antennas to obtain low profile and high gain [23, 24, 25, 26, 27], as shown in Figure 1.11. Usually high gain is achieved by mounting wire antennas perpendicular to the conducting ground plane, this makes the antenna high-profile, to make it low profile the antenna can be mounted parallel to the EBG structure. Due to the AMC behavior of the EBG structure in its band gap, backward radiated energy is reflected in phase with respect to forward radiated energy, enhancing the gain of the antenna while maintaining a low profile.

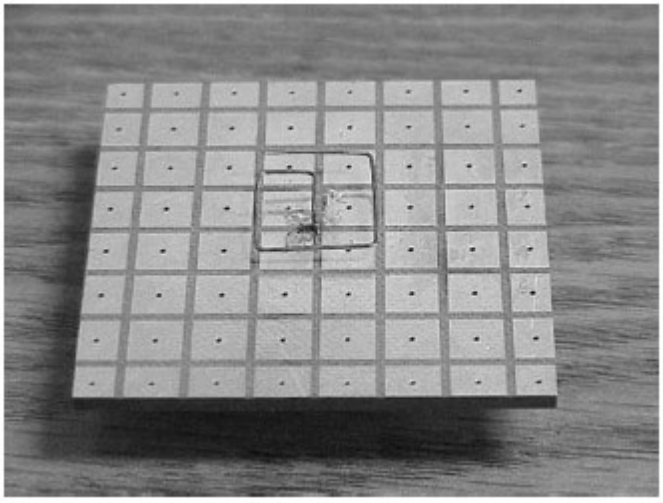

Figure 1.11: EBG structure used to design a low profile wire antenna. (with permission)

3) Improving the Gain of Antennas: When a high gain antenna is required, EBG structures can be used to obtain higher gain than if the antenna was operating without the EBG structure[28, 29, 30, 31]. One such example is a resonator antenna, where 19 dBi of gain is obtained from a small patch antenna by using an EBG structure above it to create a resonator antenna with high gain, as shown in Figure 1.12 [28].

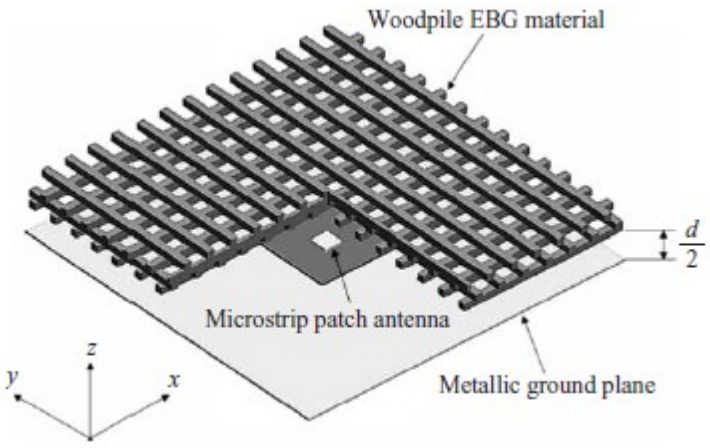

Figure 1.12: High gain resonator antenna achieved by using EBG structure with a patch antenna. (with permission)

4) Filtering & phase shifting

Band gap of EBG can be designed to behave like a band stop filter, while frequencies away from band gap behave like pass band of the filter. Periodic nature of EBG structures can be used to electrically steering an antenna array.

5) Frequency Selective Surfaces (FSS)

In a communication system that operates at multiple bands, EBG structures (FSS layers) can be used to separate bands. Consider an example of a satellite ground system that operates in L, S and C bands using the same optics. Using FSS layers on sub-reflector L and S bands can be separated into a feed placed at prime location of the optics, while C band can be separated into a feed placed in cassegrain position, as shown in Figure1.13. Figure1.14 shows EBG layer stack up that is designed to accomplish separation of bands. In this application L and S bands are transmitted through FSS layers and C band is reflected onto the mail reflector. Figures 1.15 and 1.16 show transmission and reflection of L/S and C bands through EBG layers respectively, for both TE and TM incident waves at different incident angles.

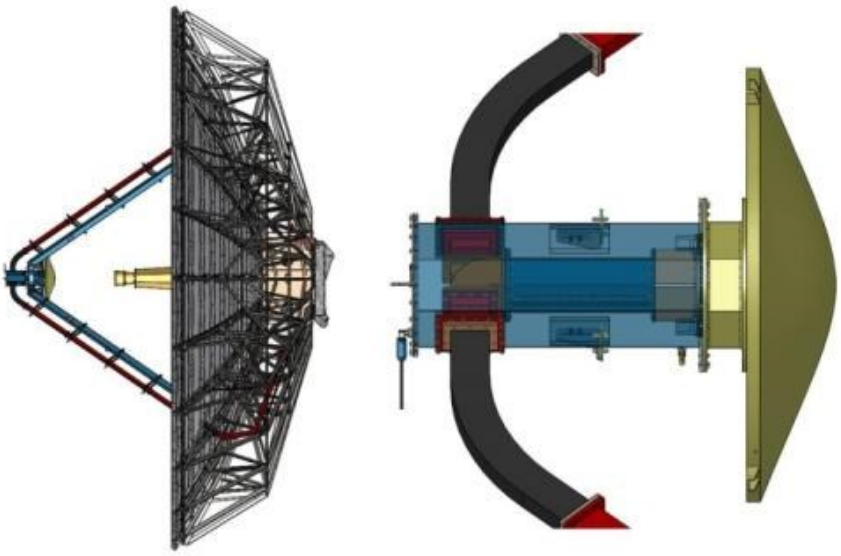

Figure 1.13: EBG application (FSS) in a multiband communication system. (with permission)

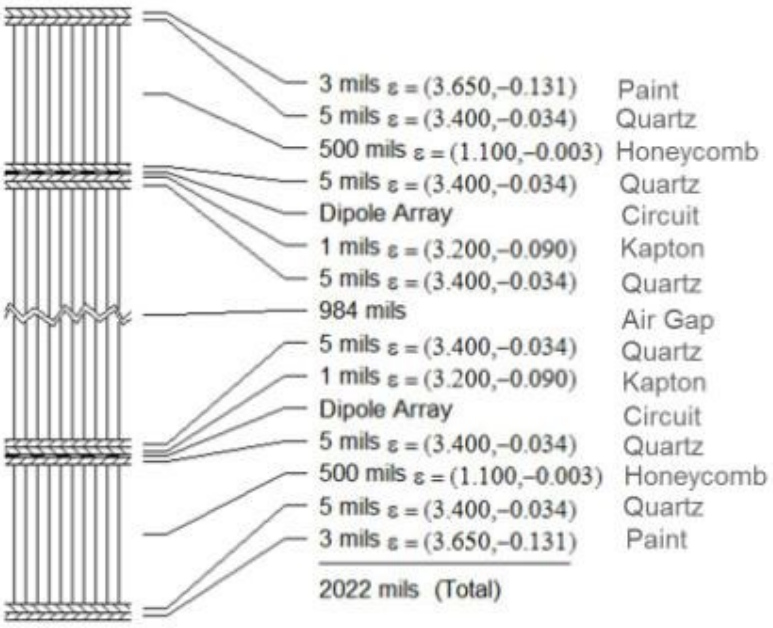

Figure 1.14: EBG layer stack up for frequency selective operation.(with permission)

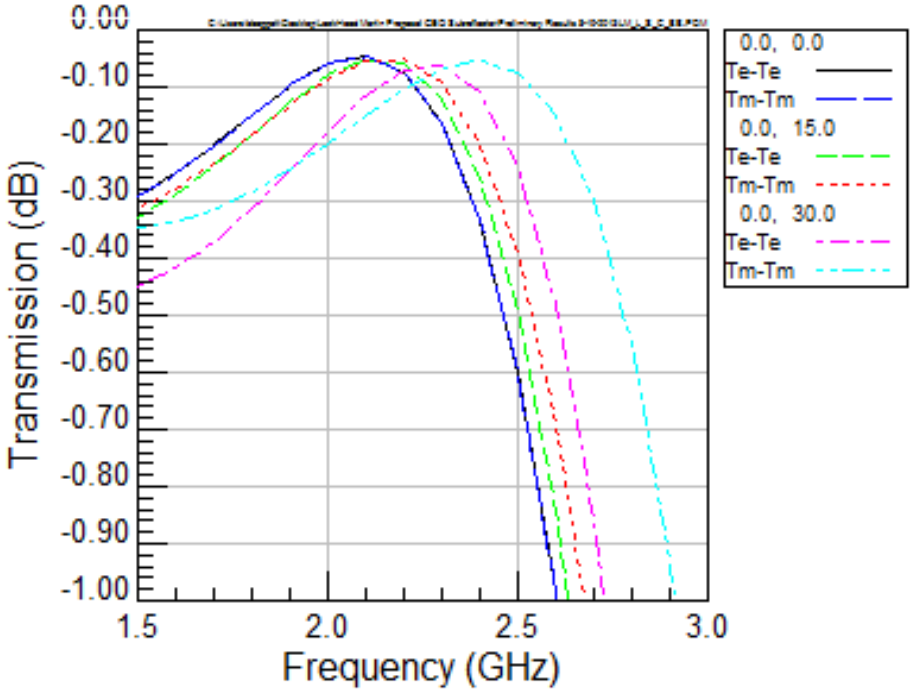

Figure 1.15: Transmission loss of L and S bands through FSS sub-reflector for TE and TM waves incident at different incidence angles.(with permission)

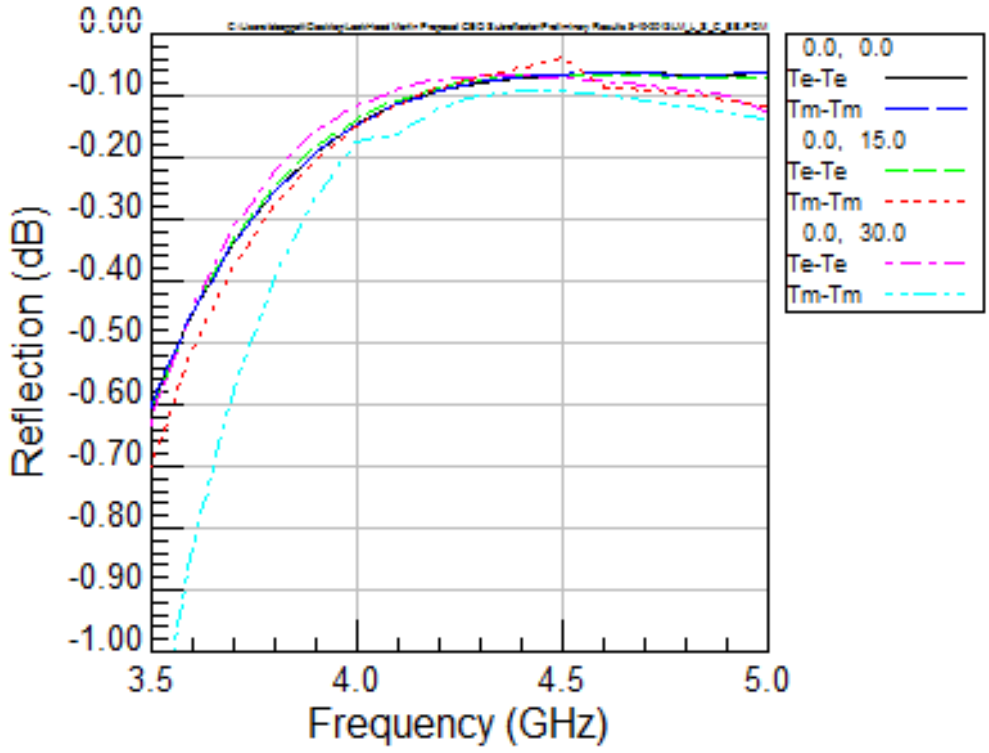

Figure 1.16: Reflection loss of C band from FSS sub-reflector for TE and TM waves incident at different incidence angles. (with permission)

1.5 Organization of the Dissertation

The rest of the dissertation shows the effects of a back cavity on antenna performance and what can be done to stop the degradation from the presence of a back cavity on antenna performance. Uniform EBG structures are explored in greater detail and their applications to antennas looked at in greater detail. The analysis of EBG structures is established from a couple of different principles, along with the necessary conditions required to operate in EBG band-gap derived. The bandwidth of EBG structures derived and the analysis in this dissertation is compared with published results and full-wave electromagnetic simulations. Wideband stacked EBG structures are introduced and their applications to suitable antennas explored. One such application is fabricated and performance improvement of the antenna is measured and compared with full-wave simulations and expected EBG performance. Wideband, progressive EBG structures are introduced and the applications with suitable antennas are explored. A special case of wideband progressive EBG structures, called uniform height progressive EBG structures with and without

vias, is introduced and its application to a spiral antenna explored. A prototype design is fabricated and performance improvement of the antenna is measured and compared with full-wave simulations and expected EBG performance. Fabrication of EBG structures is explored and measurement techniques for the built prototypes explored.

2 EFFECTSOF BACK CAVITIESON BROADBAND ANTENNAS

Broadband antennas have many applications in airborne and communication systems [24, 25, 26, 27]. Sinuous and spiral antennas, being broadband with constant beam width, low axial ratio, constant input impedance level and compact size, are good candidates in modern communication systems. Sinuous antennas, first conceived by DuHamel [28], perform like spiral antennas, but unlike spiral antennas, sinuous antennas are dual circular polarized. Spiral and sinuous antennas are usually cavity backed for unidirectional radiation[29], but the reflections from the cavity might degrade the performance of the antenna. Most often, the cavity used is a lossy cavity to absorb the back radiation, but that degrades the efficiency of the antenna by 50 percent. Recently much research has been done on metamaterials for the use in the cavity for increasing the efficiency of the antenna while not degrading its performance.

Like spiral antennas, different types of sinuous antennas can be formed by varying the growth rate (constant growth vs. logarithmic growth), sweep angle and number of arms. Each of these types has some benefits over the other. For example, four arm constant growth sinuous antennas are self-complimentary, and thus have constant input impedance level throughout frequencies [30]. Shown in Figure 2.1 are two sinuous antennas, one with faster rate of growth than the other. Each arm of the sinuous antenna is formed by rotating the curve formed by using the equation 2-1.

$$\phi(r) = (-1)^p \alpha_p \sin\left[\frac{\pi \ln\left(\frac{r}{R_p}\right)}{\ln(\tau_p)}\right] \tag{2-1}$$

Where r is the distance from origin, r_p is the radius of the p^{th} sector, τ_p is the radius growth rate (usually less than 1) and α_F is the sweep angle.

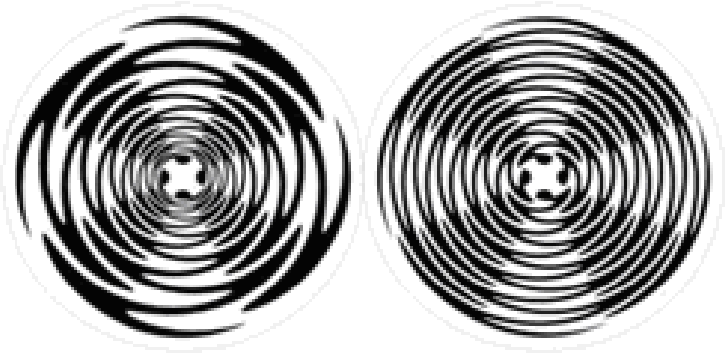

Figure 2.1: Typical four-arm sinuous antennas with different growth rates that are linear and logarithmic. (with permission)

The bandwidth of the sinuous antenna is limited by its physical size. Lower frequencies radiate from the outer turns of the antenna, while the higher frequencies radiate from the inner turns. The lowest frequency of operation is approximately where the length of the outermost turn is half a wavelength, and the highest frequency of operation is approximately where the length of the innermost turn is approximately half a wavelength.

2.1 Effects of Back Cavity

A 13 turn sinuous antenna, with and without a back cavity is simulated using FEKO [31], which employs the method of moments (MoM). Shown in Figure 2.2, is the meshed model of the sinuous antenna with and without a back cavity under consideration. Each arm of the antenna has 13 turns, and each turn is swept 180 degrees. The outer radius of the antenna is chosen as 1 inch, to accommodate the lowest frequency of 2 GHz, and the inner radius of the antenna is chosen as 0.075 inches to accommodate the highest frequency of 18 GHz. The back cavity depth is chosen to be 0.9 inches, which is roughly one wave length at the center of the band of interest. Figure 2.3 shows a comparison of the simulated input impedance of the sinuous antenna, with and without the back cavity from 2 GHz to 18 GHz. Figure 2.4 shows the simulated return loss comparison of the sinuous antenna, with and without the back cavity, when feeding with a balun of constant 188 ohm impedance.

From Figure 2.3, it is evident that the back cavity made the impedance level not flat, compared to the case of not having the back cavity. A reason it may be the difficulty in matching the sinuous

antenna with the back cavity. This is evident from Figure 2.4, without the back cavity, the return loss of the antenna is better than 10 dB throughout the band, but due to the reflections from the back cavity, the reflected power back into the input port increases, thus making the return loss worse.

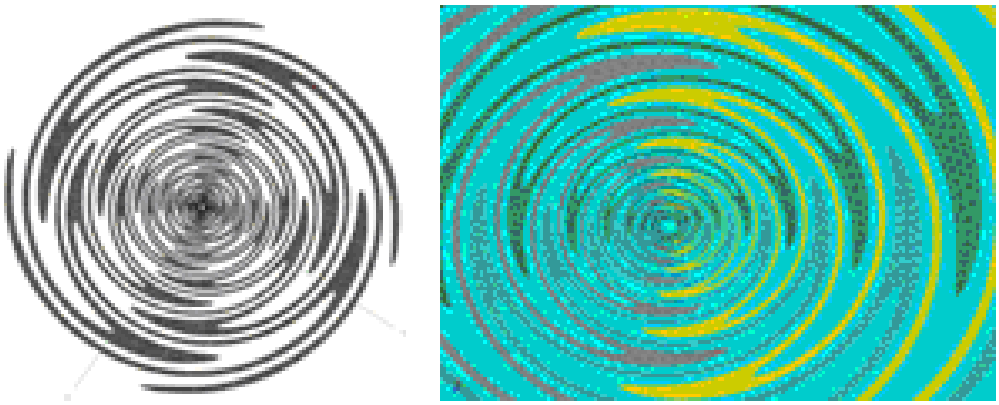

Figure 2.2: Meshed FEKO model of the four-arm sinuous antenna, with and without back cavity. Input is applied between two opposite arms.

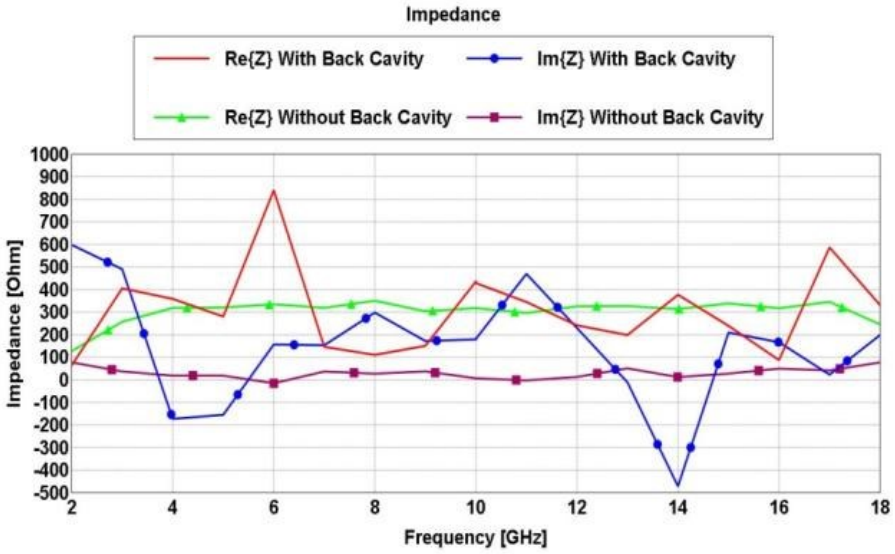

Figure 2.3: Input impedance comparison of the sinuous antenna, with and without, lossless back cavity.

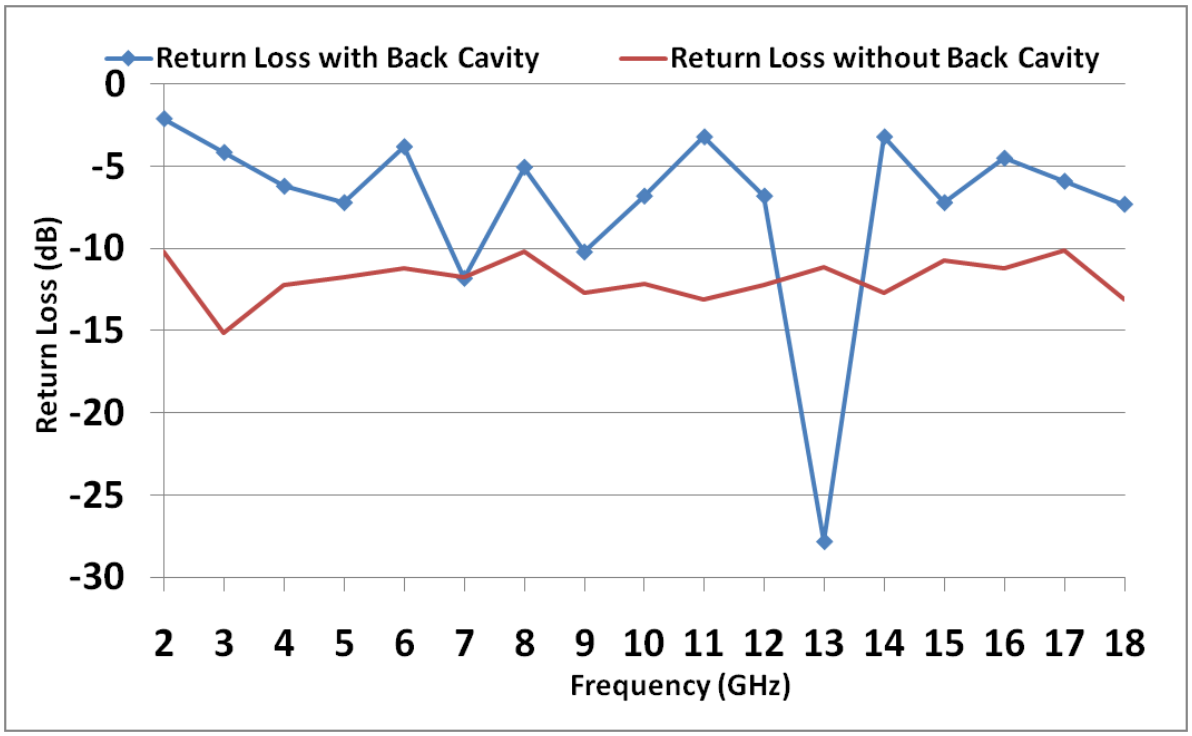

Figure 2.4: Return loss comparison of the sinuous antenna, with and without, lossless back cavity, using a 188 ohm reference impedance.

The four-arm sinuous antenna exhibits good axial ratio performance. Figure 2.5 shows the simulated boresight axial ratio comparison of the sinuous antenna with and without back cavity. The axial ratio at different angles over a broad frequency band of 2-18 GHz is shown in Figure 2.6 and Figure 2.7 for the antenna with and without the back cavity.

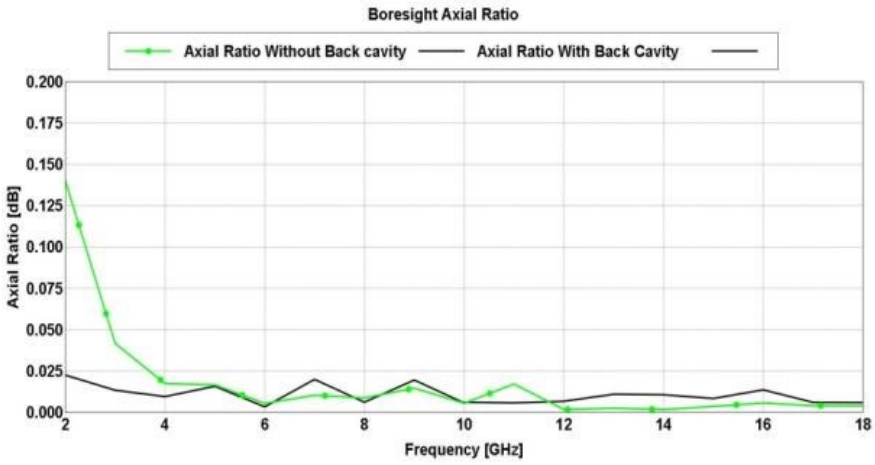

Figure 2.5: Axial ratio comparison of the sinuous antenna, with and without, lossless back cavity.

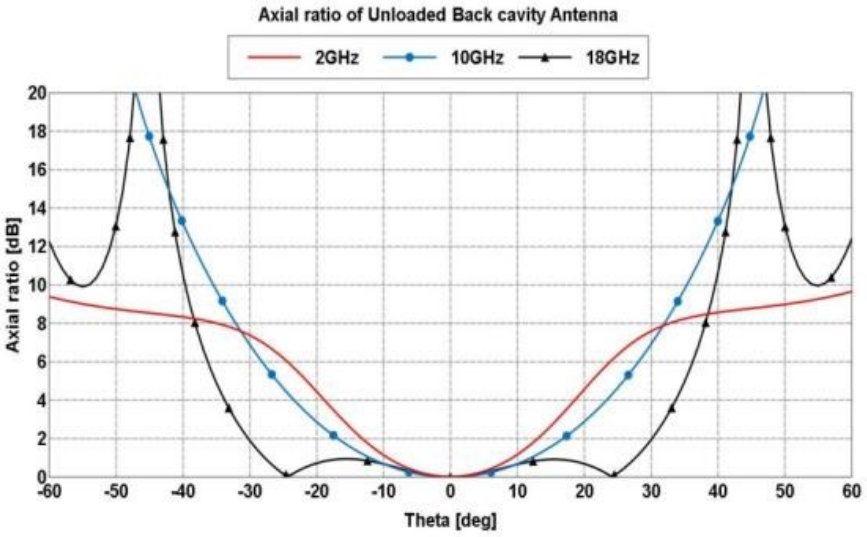

Figure 2.6: Axial ratio of the sinuous antenna with the lossless back cavity.

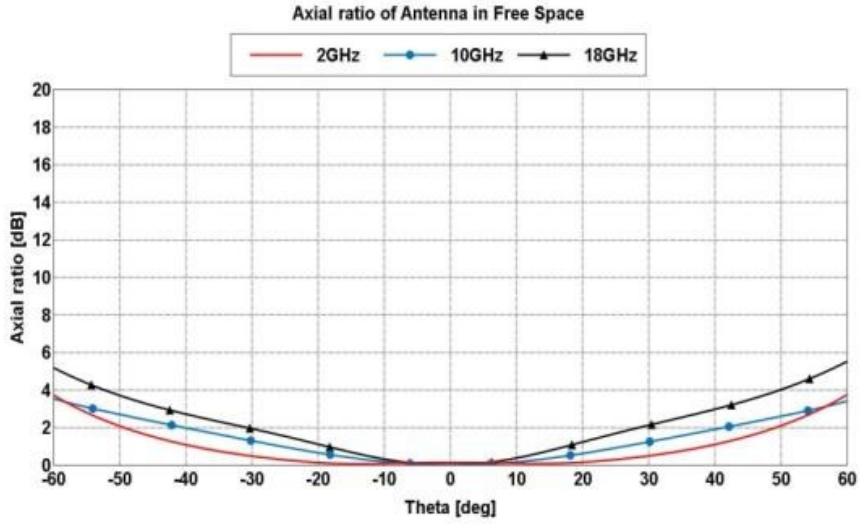

Figure 2.7: Axial ratio of the sinuous antenna without the back cavity.

From Figure 2.5, we see that the boresight axial ratio is not affected by the addition of the back cavity, but from Figure 2.6, it is evident that the off axis axial ratio is greatly affected. The reflections from the cavity, depending on the frequency, may not add in phase with the front radiated power, thus causes degradation of the off axis axial ratio of the antenna.

The comparison of the radiation patterns is shown in Figures 2.8 and 2.9. The radiation patterns of the sinuous antenna are plotted with and without the back cavity over the frequency band of 2 GHz to 18 GHz.

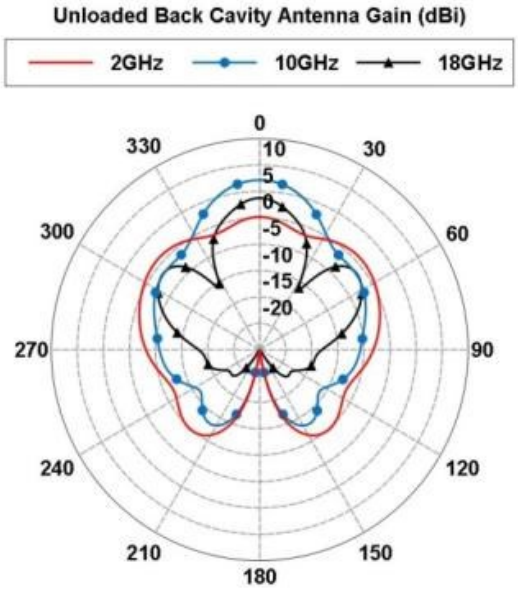

Figure 2.8: Gain pattern of the sinuous antennawith the lossless back cavity.

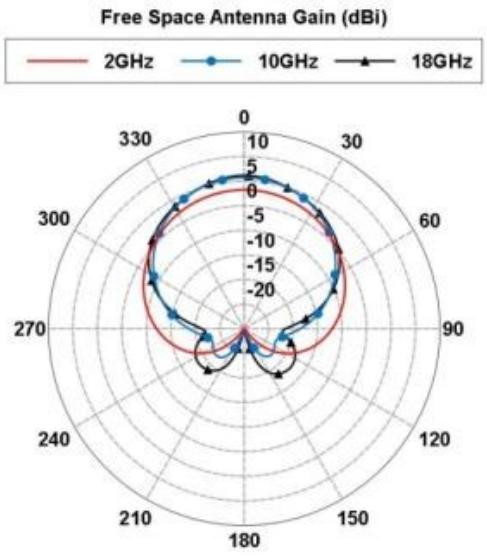

Figure 2.9: Gain pattern of the sinuous antenna without the back cavity.

From Figure 2.8, it can be seen that the 3 dB beam width of the antenna is not constant when a back cavity is added, compared with the absence of the back cavity. The reflections from the back

cavity, when added in-phase, with the front radiation gives higher gain than the bi-directional antenna, but when the reflections are out of phase compared to the front radiation, we see degradation in the gain. The reflections add in-phase when the depth of cavity is an odd multiple of quarter wavelength at the operating frequency, which gives a total additional phase of multiples of full wavelengths (multiples of 360 degrees) thus adding in phase with the forward radiating wave. The reflections from the back cavity subtract from the forward wave when the depth of the cavity is an even multiple of quarter wavelength at the operating frequency, which gives the reflected wave a total additional phase of odd multiples of 180 degrees, which is opposing to the phase of the forward travelling wave.

2.2 Optimized Lossy Back Cavities

As illustrated, in the presence of the back cavity, the reflections from the cavity, depending on the frequency, might not add in phase with the front radiated energy, thus degrading the performance of the antenna. One way to stop this from happening is to absorb the back radiated power by loading the back cavity with absorbers [32] as shown in Figure 2.10, and the other way to counter this is to reflect backward radiated energy in phase with respect to forward radiated energy, to add constructively. The cavity is loaded with three different absorbers with different thicknesses. The optimization is carried by keeping the total cavity depth fixed at 0.9 inches, while optimizing the thicknesses and electrical properties of the absorbers using FEKO to achieve a goal of axial ratio better than 0.2 dB at the boresight and a gain better than 3 dB, while maintaining off-axis axial ratio less than 2 dB in the 30 degree scan on the either side of the boresight. The results from the optimization show the top layer, closer to the antenna, is 0.29 inches thick with relative permittivity of 1.4 and loss tangent of 0.225. The middle layer is 0.155 inches thick with relative permittivity of 1.59 and loss tangent of 0.62. The bottom layer, closer to the back short, is 0.3 inches thick with relative permittivity of 2.66 and loss tangent of 1.6. The optimization was performed on a quad core machine and it required 8.2 GBytes of memory and 44.8 hours of optimization. The FEKO recommended mesh size of $\lambda/12$ at 18 GHz was chosen during meshing. The three layer absorbers can be custom ordered from Emerson & Cuming [33] from the eccostock and eccosorb series absorbers. The fabrication of the optimized antenna would not be hard, as the dimensions of the antenna are easily realizable and the absorbers can be obtained. The performance of the optimized antenna is verified by comparing the FEKO results (method of

moments) with the results from HFSS [34] (finite element method). The HFSS simulation required 4.7 GBytes of memory and 18 hours of run time. Figures 2.11 and 2.12 show the gain pattern and off-axis axial ratio, respectively, of the optimized lossy loaded back cavity model. Figures 2.13 and 2.14 show the respective boresight axial ratio and boresight gain comparison of the optimized antenna. Figures 2.15 through 2.17 show the gain pattern comparison of the optimized antenna at 2 GHz, 10 GHz and 18 GHz respectively. While Figures 2.18 through 2.20show the axial ratio pattern comparison of the optimized antenna at 2 GHz, 10 GHz and 18 GHz respectively.

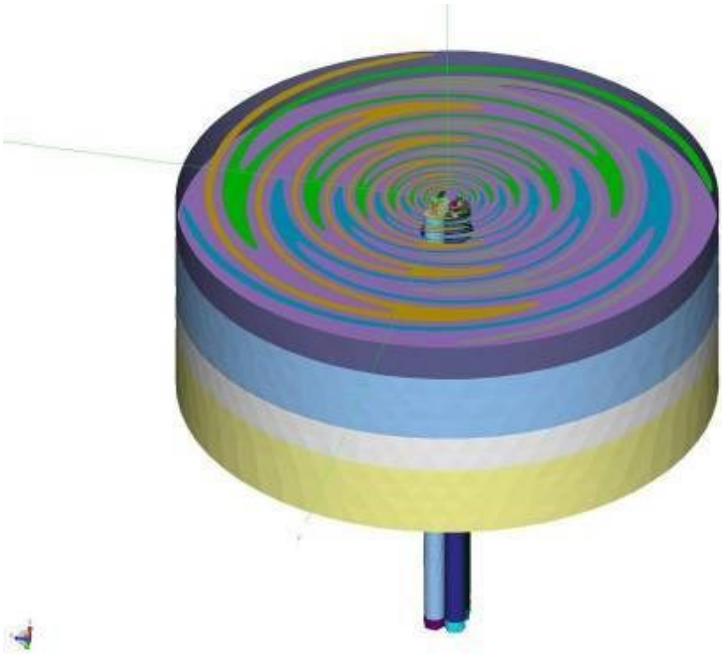

Figure 2.10: Emerson and Cumming ECCOSORB AN absorbers loaded in back cavity.

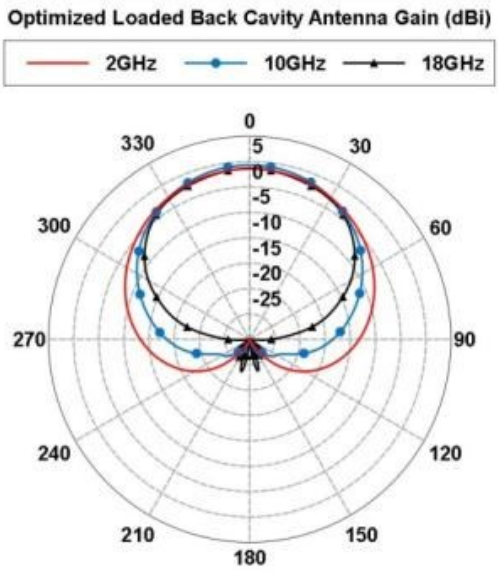

Figure 2.11: Gain pattern of the optimized sinuous antenna.

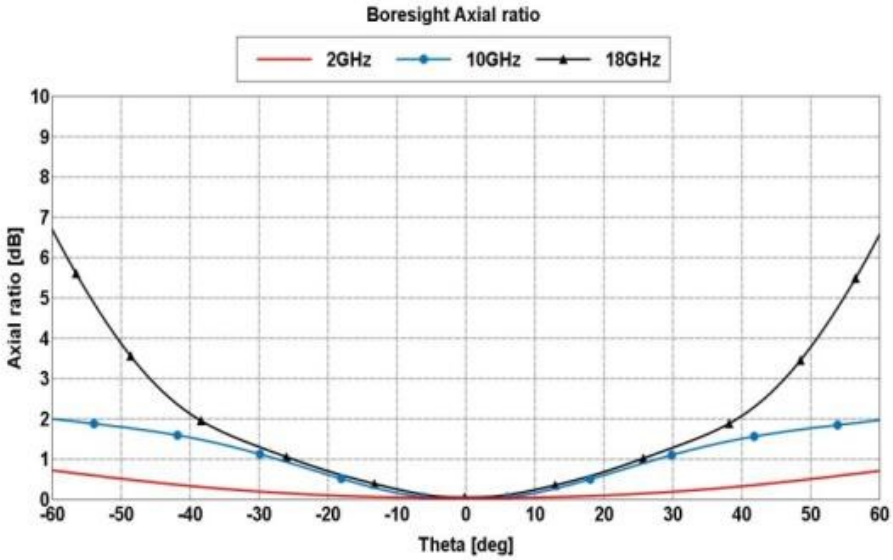

Figure 2.12: Off-Axis Axial Ratio of the optimized sinuous antenna.

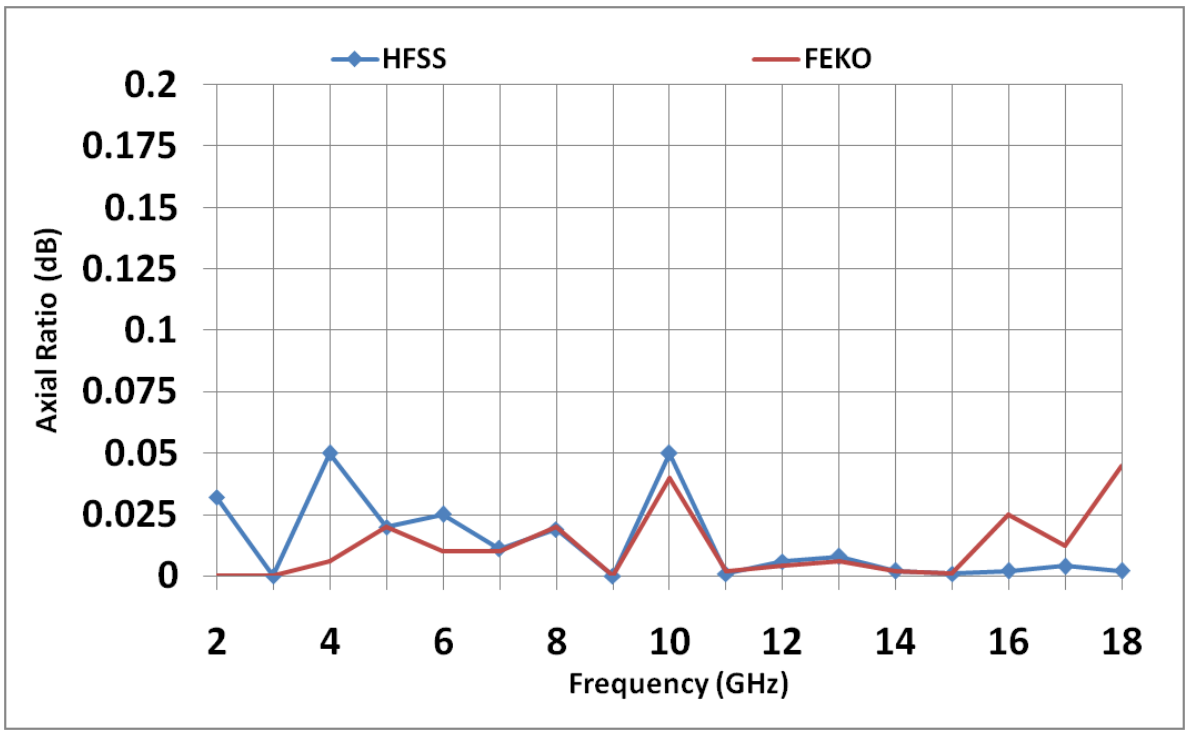

Figure 2.13: Boresight Axial Ratio comparison of the optimized sinuous antenna.

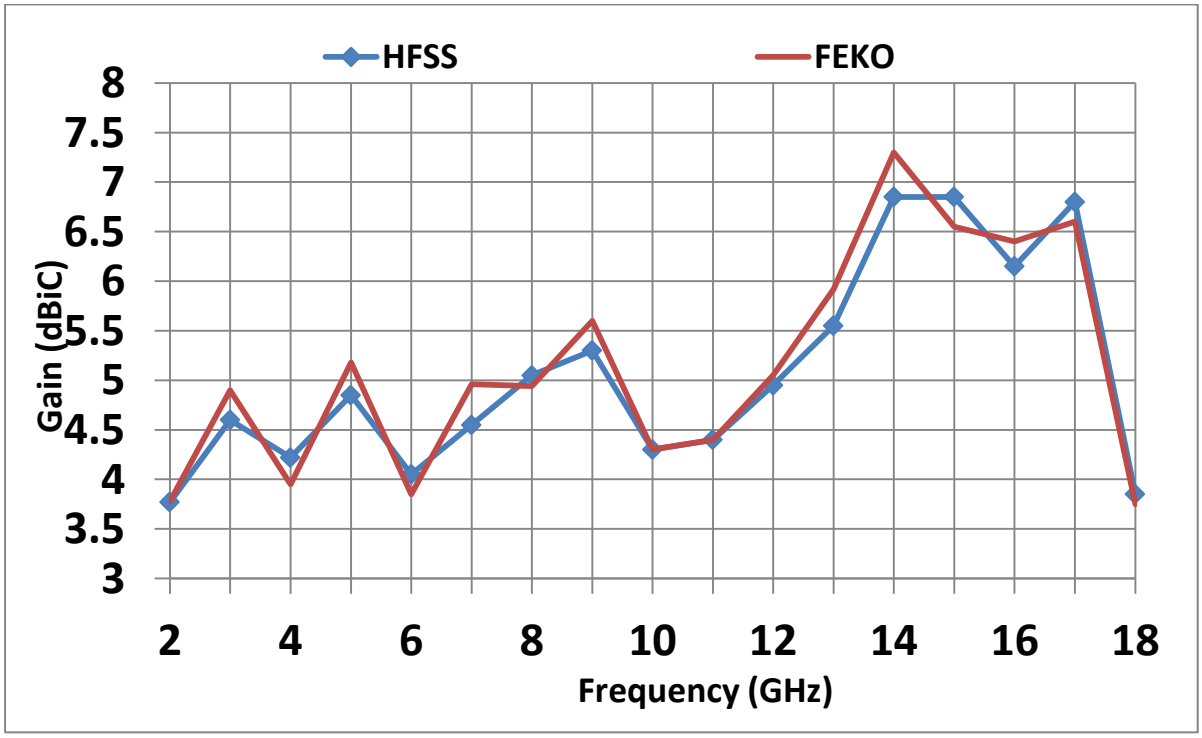

Figure 2.14: Boresight Gain comparison of the optimized sinuous antenna.

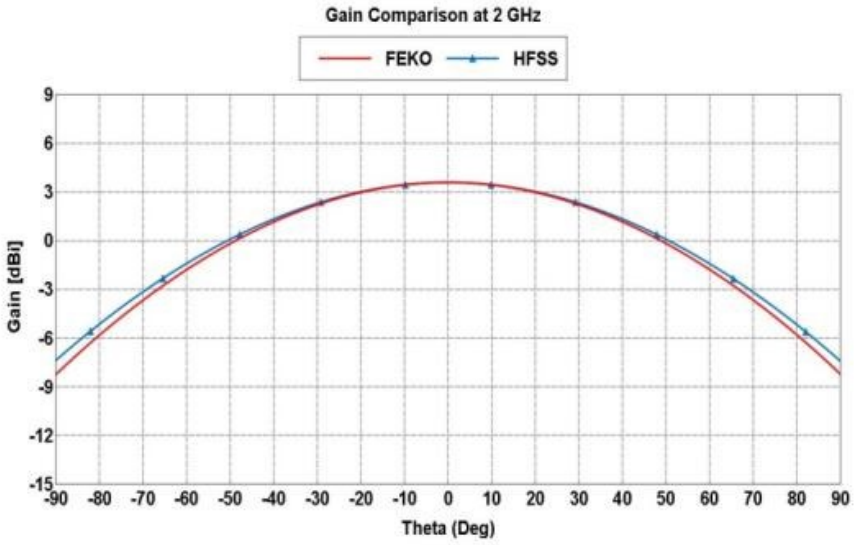

Figure 2.15: Gain comparison of the optimized sinuous antenna at 2 GHz.

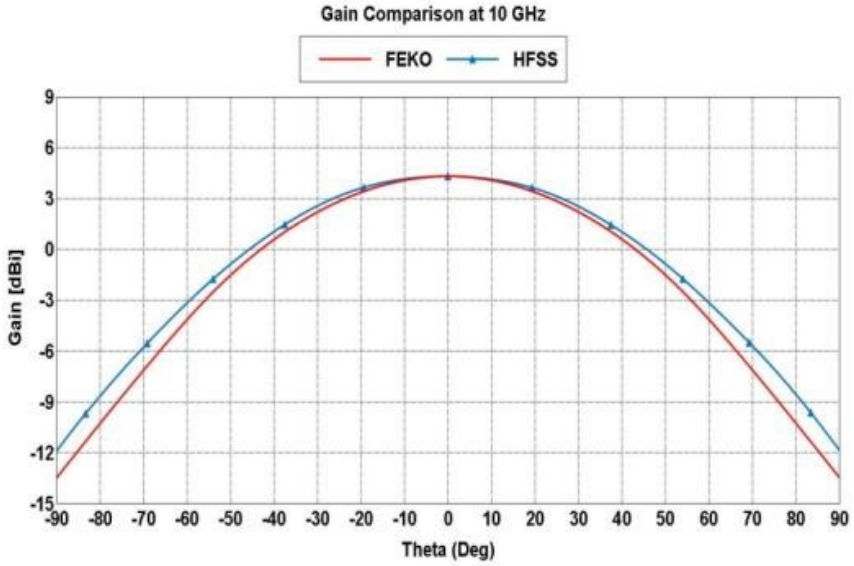

Figure 2.16: Gain comparison of the optimized sinuous antenna at 10 GHz.

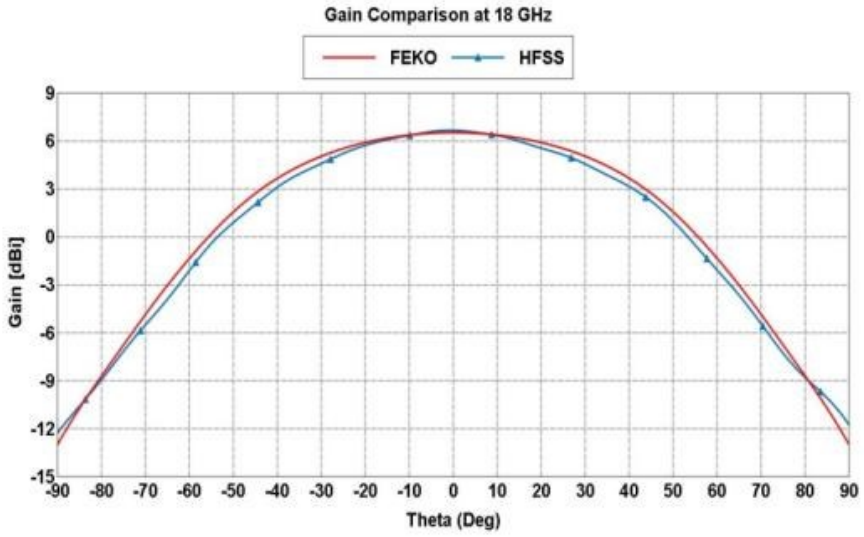

Figure 2.17: Gain comparison of the optimized sinuous antenna at 18 GHz.

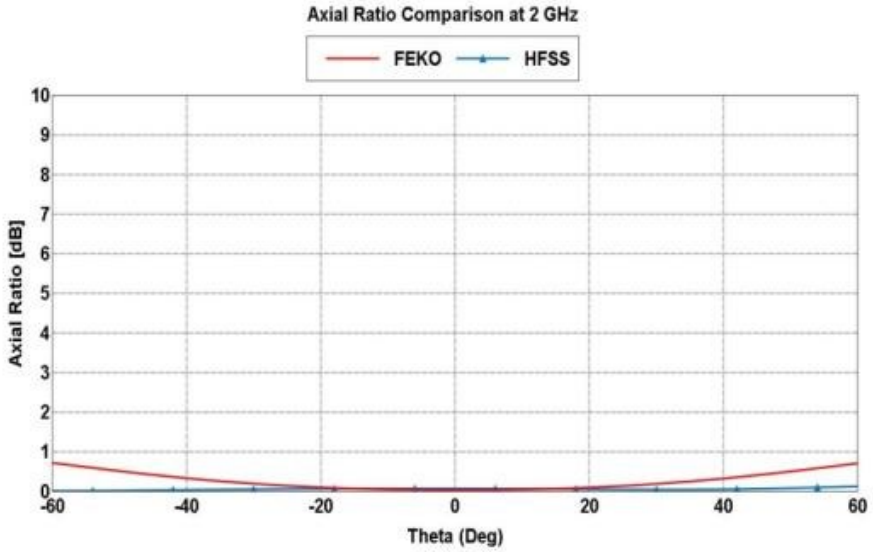

Figure 2.18: Axial Ratio comparison of the optimized sinuous antenna at 2 GHz.

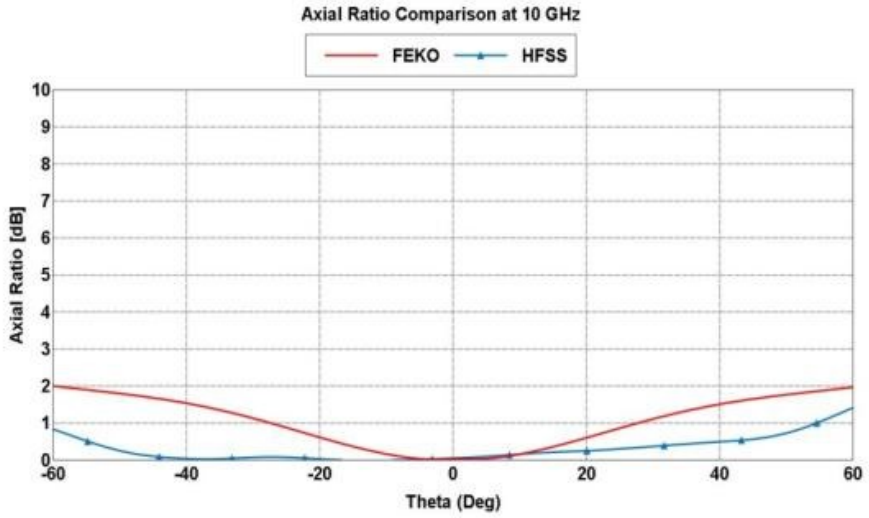

Figure 2.19: Axial Ratio comparison of the optimized sinuous antenna at 10 GHz.

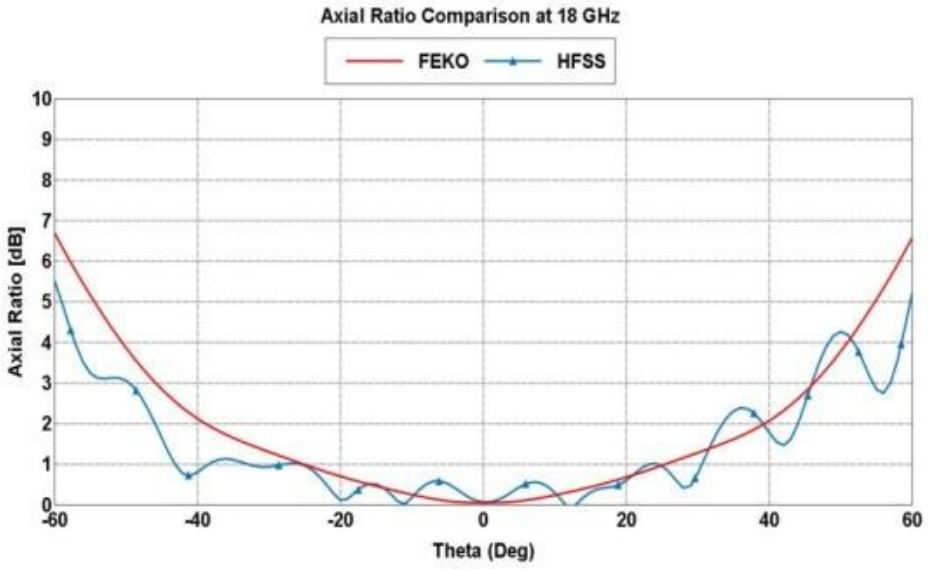

Figure 2.20: Axial Ratio comparison of the optimized sinuous antenna at 18 GHz.

Figures 2.11 through 2.20show that adding the absorbers in the back cavity has improved the performance of the antenna, compared to unloaded cavity case, by absorbing the back radiated energy and thus preventing it to interfere with the forward radiated energy. The off-axis axial ratio of the antenna is greatly improved by loading the back cavity with three layers of absorbers. Variations between HFSS and FEKO results are due to differences in meshed models, HFSS

employs adaptive meshing which increases the density of mesh cells where the fields change between adaptive passes, while FEKO uniformly meshes the entire structure. Another reason could be that HFSS uses radiation boundary condition to compute far-field patterns and axial ratio, which are sensitive to the matching at the radiation boundary, while FEKO does not use radiation boundary to compute far-field patterns and axial ratio. This section showed that a broadband lossy cavity can be designed without degrading the performance of the antenna.

It is evident from this exercise that the back cavity affects the performance of the sinuous antenna. Due to the reflections from the back cavity the input impedance of the antenna is not at a constant level, thus making it hard to match the antenna with a constant impedance source. It is also evident that the off-axis axial ratio and the gain pattern are adversely affected by the presence of the back cavity, due to the fact that the reflections from the back cavity might, or might not, add in-phase with the forward propagating wave depending on the frequency. We have also presented a way to improve the performance of the sinuous antenna by loading the back cavity with absorbers. The absorbers in the back cavity help absorb the back radiated energy and thus leaving the front radiating energy uninterrupted. Absorbers in the back cavity decrease the efficiency of the antenna by 50%, this can be prevented by adding electromagnetic band gap structures in the cavity. EBGs reflect the backward radiation in phase, which adds constructively with forward radiation and improving the efficiency of the antenna.

3 ELECTROMAGNETIC BAND GAP (EBG) STRUCTUTES

Electromagnetic band gap (EBG) structures, are mushroom like structures, have high surface impedance [35], which can be used when mounting an antenna close to a ground plane [36]. At their resonant frequency, EBG structures behave like perfect magnetic conductor (PMC) and reflect electric field, parallel to the EBG surface, with a reflection-phase of 0^o. This makes EBG structures a perfect candidate to employ to increase forward gain of antennas by decreasing backward radiation, provided the bandwidth of EBG structure is equal to or greater than the bandwidth of the antenna used [37, 38]; in their band gap they do not support surface waves. Mushroom-like EBG structures proposed by Sievenpiper [15] are compact in size, have low loss and can be integrated into an antenna [39, 40].

Reflection amplitude and phase describes electrical properties of a surface in the frequency band of interest. It specifies the amount of energy that is reflected along with the phase of the reflection at a given frequency. Electric filed that is parallel to perfect electric conductor, with normal incidence will have a reflection magnitude of 1 and reflection-phase of 180^0 because boundary condition dictates the total tangential component on electric field on perfect electric conductors should be zero. Electric filed that is parallel to perfect magnetic conductor, with normal incidence will have a reflection magnitude of 1 and reflection-phase of 0^0 because boundary condition dictates the total tangential component on magnetic field on perfect magnetic conductors should be zero. In both the cases reflection magnitude is unity, but the reflection-phase is different.

Structures can be classified based on reflection phases for the same reflection magnitude. EBG structures can be designed to have a reflection-phase of 0^o for a specific frequency, which make EBGs to behave like magnetic conductor; hence the name artificial magnetic conductor (AMC) is sometimes used to describe EBGs. Band gap of EBG structures is defined as the band of frequencies where the reflection-phase from EBG surface is between 90^o and -90^o. EBG structures are equivalent to a tank circuit with capacitance represented by the gap between the patches and the inductance represented by the distance between the patches and the ground plane. EBG structures are usually compact and have low loss and can be easily integrated with antennas, but operate over narrow band of frequencies. Bandwidth of EBG structures can be increased by

cascading EBG layers, which resonate close to one another, vertically in multiple layers or progressively in one layer.

3.1 Uniform EBG Structures

Mushroom-like uniform EBG structures, as shown in Figure3.1 are proposed by Sievenpiper, Uniform EBG structures consist of metal patches that are separated by some gap, while the patches may or may not be connected to the ground plane by vias. Uniform EBG structures are equivalent to a resonant tank circuit, with capacitance represented by the gap between the metal patches and inductance represented by the distance between the patches and the ground plane. The resonant frequency of the EBG structure is defined as the frequency where the susceptance of the tank circuit is zero, at this frequency the surface impedance of EBG structures becomes infinity, thus not supporting surface waves and behaves like a magnetic conductor, and reflects electromagnetic energy without a phase reversal. The bandwidth of the EBG structure is defined as the band of frequencies where the reflection-phase from the EBG structure is between $+90^0$ and -90^0as shown in Figure 3.2. Reflection-phase of the EBG structure is calculated by using a plane wave incidence and calculating the phase of the received signal in the boresight in far field, and then comparing it with a known reflection-phase (e.g. PEC plate). Equations 3-1 through 3-5 give the surface impedance, resonance frequency, inductance, capacitance and the bandwidth, respectively, of a uniform EBG structure.

$$Z_s = \frac{j\omega L}{1 - \left(\frac{\omega}{\omega_0}\right)^2} \tag{3-1}$$

$$\omega_0 = \frac{1}{\sqrt{LC}} \tag{3-2}$$

$$L = \mu_0 t \tag{3-3}$$

$$C = \frac{W\varepsilon_0\left(1+\varepsilon_r\right)}{\pi}\cosh^{-1}\left(\frac{W+g}{g}\right) \tag{3-4}$$

$$BW = \frac{1}{120\pi}\sqrt{\frac{L}{C}} \tag{3-5}$$

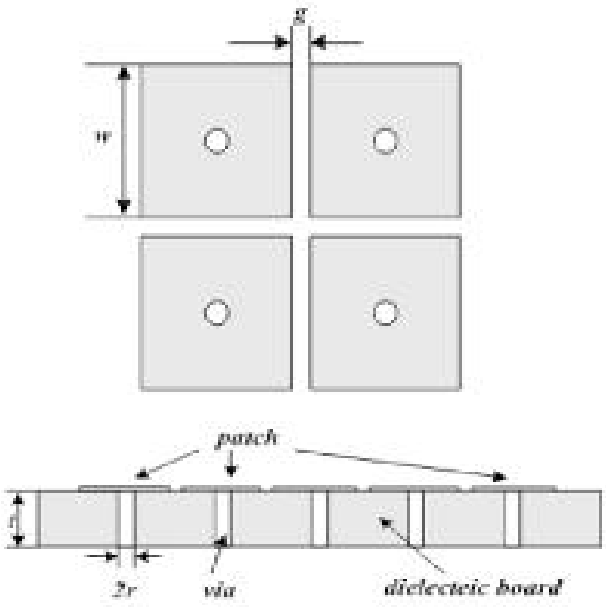

Figure 3.1: Uniform EBG Structure.

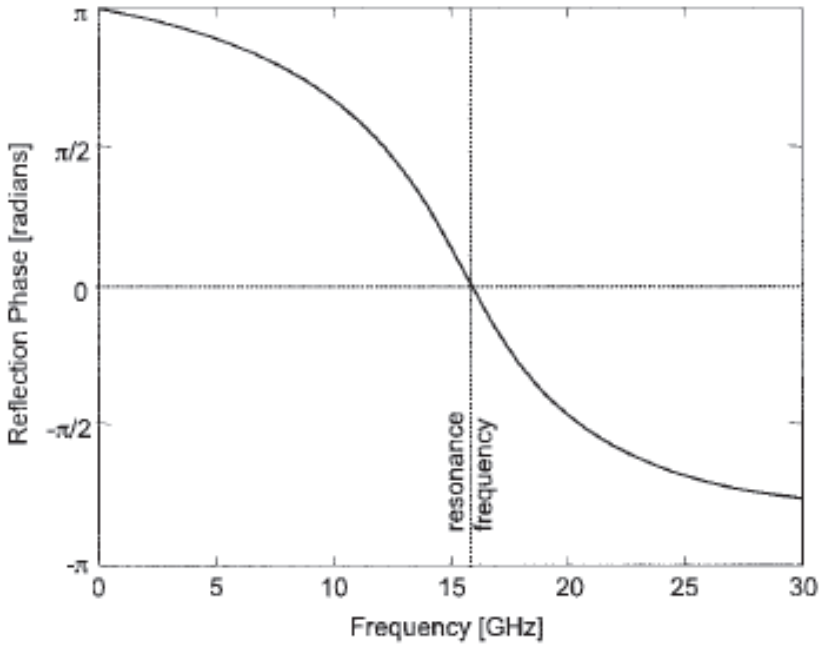

Figure 3.2: Uniform EBG Reflection Phase.

3.2 Analysis of periodic structures

Uniform EBG structures are periodic in two dimensions, which makes analysis of periodic structures a useful way to analyze EBG structures [2, 3]. Assume a periodic structure formed by periodically loading a lossless transmission, line of characteristic impendence Z_0,with a shunt element as shown in Figure 3.3.

Let V_n and I_n be Voltage and current at the left node of the unit cell, and V_{n+1} and I_{n+1} be voltage and current at the right node of the unit cell. Using ABCD matrix we have

$$\begin{bmatrix} V_n \\ I_n \end{bmatrix} = \begin{bmatrix} A & B \\ C & D \end{bmatrix} \begin{bmatrix} V_{n+1} \\ I_{n+1} \end{bmatrix} \tag{3-6}$$

where A,B,C,D are matrix parameters of the unit cell. The unit cell consists of a transmission line of length *l/2*, followed by a shunt element 'X' followed by transmission line of length *l/2*.Using ABCD parameters of transmission line and shunt element, unit cell ABCD parameters are computed as follows

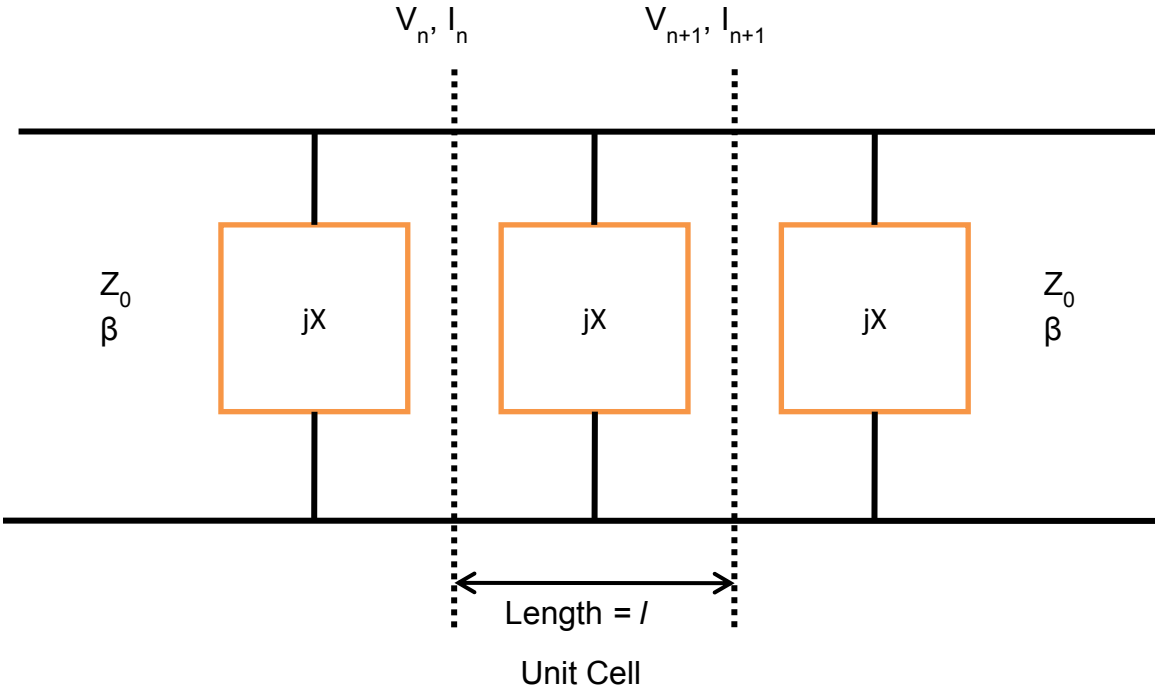

Figure 3.3: Periodic structure formed by loading a transmission line.

$$\begin{bmatrix} A & B \\ C & D \end{bmatrix} = \begin{bmatrix} \cosh\left(\frac{\gamma l}{2}\right) & Z_0 \sinh\left(\frac{\gamma l}{2}\right) \\ \left(\frac{1}{Z_0}\right)\sinh\left(\frac{\gamma l}{2}\right) & \cosh\left(\frac{\gamma l}{2}\right) \end{bmatrix} \begin{bmatrix} 1 & 0 \\ \frac{1}{jX} & 1 \end{bmatrix} \begin{bmatrix} \cosh\left(\frac{\gamma l}{2}\right) & Z_0 \sinh\left(\frac{\gamma l}{2}\right) \\ \left(\frac{1}{Z_0}\right)\sinh\left(\frac{\gamma l}{2}\right) & \cosh\left(\frac{\gamma l}{2}\right) \end{bmatrix} \quad (3\text{-}7)$$

The outer matrices represent the transmission-line segments on the two sides of the center element. Multiplying we obtain

$$\begin{bmatrix} A & B \\ C & D \end{bmatrix} = \begin{bmatrix} \cosh(\gamma l) - \mathrm{j}\frac{Z_0}{2\mathrm{X}}\sinh(\gamma l) & Z_0 \sinh\left(\frac{\gamma l}{2}\right) - \mathrm{j}\frac{{Z_0}^2}{\mathrm{X}}\sinh^2\left(\frac{\gamma l}{2}\right) \\ \left(\frac{1}{Z_0}\right)\sinh(\gamma l) - \frac{j}{X}\cosh^2\left(\frac{\gamma l}{2}\right) & \cosh(\gamma l) - \mathrm{j}\frac{Z_0}{2\mathrm{X}}\sinh(\gamma l) \end{bmatrix} \quad (3\text{-}8)$$

Note that since $AD - BC = 1$, the result proves the reciprocity of the network. The quantity $\gamma = \alpha + j\beta$ is the propagation constant of the transmission line. When γ is real, the propagation through the transmission line is attenuated.

Due to periodicity in the structure

$$V_n = V_{n+1}e^{\gamma_X l} \quad (3\text{-}9)$$

$$I_n = I_{n+1}e^{\gamma_X l} \quad (3\text{-}10)$$

Where$\gamma_X = \alpha_X + j\beta_X$ in the unit cell. Substituting equations 3-18,and 3-19 in equation 3-6 we get

$$\begin{bmatrix} V_{n+1}e^{\gamma_X l} \\ I_{n+1}e^{\gamma_X l} \end{bmatrix} = \begin{bmatrix} A & B \\ C & D \end{bmatrix} \begin{bmatrix} V_{n+1} \\ I_{n+1} \end{bmatrix} \quad (3\text{-}11)$$

Solving for γ_X that may be complex, gives

$$cosh(\gamma_X l) = \frac{A+D}{2} \quad (3\text{-}12)$$

The above equation can be used to find attenuation and phase constants of the periodic structure. When the phase constant is plotted with respect to frequency, band gaps of the periodic structure are the bands of frequencies where the phase constant does not exist. Surface wave suppression occurs in the band where γ_X is real.

4 ANALYSIS OF EBG STRUCTURES

There are a number of ways that can be employed to analyze EBG structures. Lumped element circuit modeling is the simplest and quickest way of analyzing EBG structures, while not most accurate, while full-wave, 3D electromagnetic analysis is the most laborious and time consuming, while being very accurate. Transmission line analysis is pretty accurate, while not laborious and time consuming. Both circuit analysis and transmission line analysis are carried out and compared with 3D electromagnetic analysis. 2-D periodic boundary conditions are used in unit cell in transmission line analysis and 3D computational analysis to capture periodic EBG structure.

Computational electromagnetic methods can be used to accurately analyze EBG structures; they include frequency domain solvers (e.g, Method of Moments [MoM] and Finite Element Method [FEM]) and time domain solvers (e.g, Finite Difference-Time Domain [FDTD]). One of the advantages of the computational EM methods is that they can be used to accurately analyze any EBG configuration for band gaps, surface impedance and surface propagation characteristics simultaneously.

Accurate analysis of EBG structures involves solving Maxwell's equations in a periodic medium. Different techniques exist that characterize and predict the performance of EBG structures. Some of the frequently discussed methods are:

1) Plane wave/Spherical wave expansion

Maxwell's equations in generalized eigenvalue form are solved using plane/spherical wave expansions. Plane wave/special wave expansion techniques are used in converting Maxwell's equations into an eigenvalue problem and solved. Since this method is easier to understand and implement, the plane wave/spherical wave expansion technique is widely used. When the EBG structure becomes complicated, many plane/spherical waves are needed to accurately analyze the structure.

2) Transfer Matrix Method

A boundary value problem is solved at every layer at every frequency to get a scattering transfer matrix for each individual layer, and then the matrices are cascaded to get the overall scattering transfer matrix, from which transmission and reflection characteristics are obtained.

3) Computational Electromagnetic Methods

Existing full wave frequency and time domain solvers (HFSS, FEKO, CST etc..) can be used to model and simulate EBG structures to characterize their properties. 3D solvers can be used to setup EBG analysis by using plane wave incidence and using periodic boundary conditions (a pair of magnetic walls and electric walls) to solve accurately and faster, as shown in Figure 4.1. Solution setup frequency is usually selected as the highest frequency of analysis required, and a frequency sweep of required frequencies is selected. After the analysis, the excitation port needs to be de-embedded to the surface of the EBG structure to plot the reflection-phase at the surface of the EBG. Time domain solvers (e.g, Finite Difference Time Domain) can characterize complex EBG structures for broad range of frequencies quicker than a frequency domain solver. EBG structures are meshed in FDTD using Yee's cell and using perfectly matched layers (PML). This approach usually only solves the unit cell of the EBG and uses periodic boundary conditions to solve for the entire EBG structure and extract surface characteristic (impedance, reflection phase, wave number etc..) of the EBG structures.

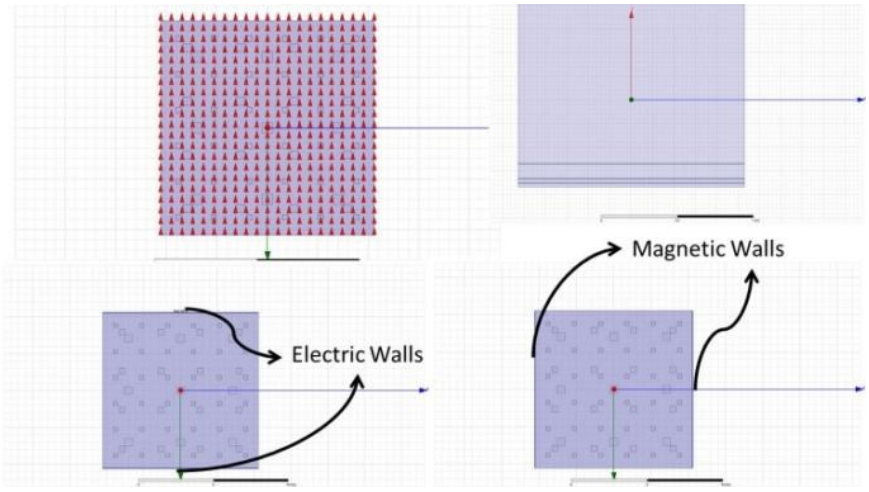

Figure 4.1: Setup of multiple layer EBG structure in HFSS.

4.1 Image Theory Analysis of EBG Structures

Parallel antenna currents near a surface have an equivalent image current in free space, as noted in image theory. The image current is out of phase with respect to antenna currents when the surface is an electric conductor, and in phase with respect to antenna currents when the surface is magnetic conductor. Figure 4.2 shows antenna currents and image currents along with a surface. Maximum efficiency of an antenna occurs when image currents are in phase, and of same magnitude, with antenna currents that are parallel to a surface. This occurs when surface impedance is equal to infinity. If the surface is an EBG structure, the band-gap is found by solving for 50% efficiency of the antenna, which occurs when the impedance of the surface is equal to the medium impedance in which antenna is present. 50% efficiency occurs for an antenna in free space when $|Z_s| = \eta_o$, where Z_s is surface impedance and η_o is free space impedance.

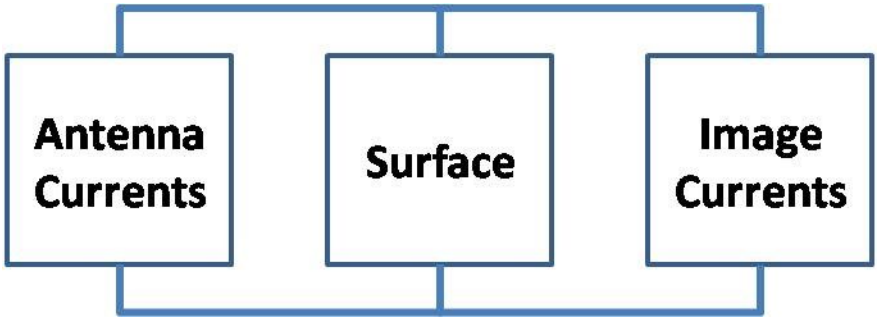

Figure 4.2: Antenna currents and image currents near a surface.

For an EBG structure, which will be explained in the next section, Z_s is equivalent to a tank circuit. The bandwidth of EBG structures can be calculated by equating the surface impedance magnitude to η_o as follows:

$$Z_s = \frac{j\omega L}{(1-\omega^2 LC)} \tag{4-1}$$

$$\left|\frac{j\omega L}{(1-\omega^2 LC)}\right| = \eta_0 \tag{4-2}$$

Case 1:

$$\frac{\omega_1 L}{(1-\omega_1{}^2 LC)} = -\eta_0 \tag{4-3}$$

$$\omega_1 L = -\eta_0 + \eta_0 \omega_1{}^2 LC \tag{4-4}$$

Case 2:

$$\frac{\omega_2 L}{(1-\omega_2{}^2 LC)} = \eta_0 \tag{4-5}$$

$$\omega_2 L = \eta_0 - \eta_0 \omega_2{}^2 LC \tag{4-6}$$

Adding equation 4-4 and equation 4-6, we get

$$(\omega_1 + \omega_2)L = \eta_0 LC(\omega_1^2 - \omega_2^2) \tag{4-7}$$

$$(\omega_1 - \omega_2) = \frac{1}{\eta_0 C} \tag{4-8}$$

to give a bandwidth of

$$\text{Bandwidth} = \frac{\omega_1 - \omega_2}{\omega_0} \quad ; \quad \omega_0 = \frac{1}{\sqrt{LC}} \tag{4-9}$$

or

$$\text{Bandwidth} = \left(\frac{1}{\eta_0 C}\right)\left(\sqrt{LC}\right) = \frac{1}{\eta_0}\sqrt{\frac{L}{C}} \tag{4-10}$$

4.2 Circuit Analysis of EBG Structures

Assuming a plane wave incidence and using circuit analysis, the reflection-phase of the EBG structure can be found [41]. Transmission line theory is used to find the complex reflection coefficient from the EBG surface and then the reflection-phase is found. The reflection coefficient from a load Z_L in a transmission line with a characteristic impedance of Z_0 is given by:

$$\Gamma = \frac{Z_L - Z_0}{Z_L + Z_0} \tag{4-11}$$

The reflection coefficient from a perfect electric conductor (PEC) is -1. The reflection coefficient from a perfect magnetic conductor (PMC) is +1.

In both the cases the magnitude is the same, but the phase is different. So, to accurately analyze the reflection phase, we need to come up with an approach that does not change the magnitude of the reflection with frequency change, but changes the reflection-phase with frequency. How can this be done when the reflection coefficient has difference of impedances in the numerator and

sum of the impedances in the denominator? A complex number and its complex conjugate have the same magnitude. Free space has a real impedance, so the EBG structure needs to be modeled as a purely-imaginary surface impedance. This is a good approximation as EBG structures have low loss, which implies the real part of the surface impedance is very small compared to imaginary part. This analysis assumes the EBG structure is lossless. Let Zs be the surface impedance of the EBG structure. The reflection coefficient and the reflection-phase can be calculated as:

$$Z_s = jX \tag{4-12}$$

$$\Gamma = \frac{Z_s - \eta_0}{Z_s + \eta_0} \tag{4-13}$$

$$\Gamma = \frac{jX - \eta_0}{jX + \eta_0} \tag{4-14}$$

$$\left|\Gamma\right| = 1 \tag{4-15}$$

$$\angle\Gamma = \pi - 2\tan^{-1}\left(\frac{x}{\eta_0}\right) \tag{4-16}$$

The bandwidth of EBG structure is defined as the band where the reflection-phase is between +90° to -90°. Using this condition in the above equation 4-16 we can find the required conditions on the surface impedance.

$$-90° \leq \angle\Gamma \leq +90^{\circ} \tag{4-17}$$

$$X \geq \eta_0 \text{ or } X \leq \eta_0 \tag{4-18}$$

The required conditions to operate in the bandwidth of EBG structure is $X \geq \eta_0$ or $X \leq \eta_0$. Figure 4.3 shows the relationship between surface impedance and the reflection phase.

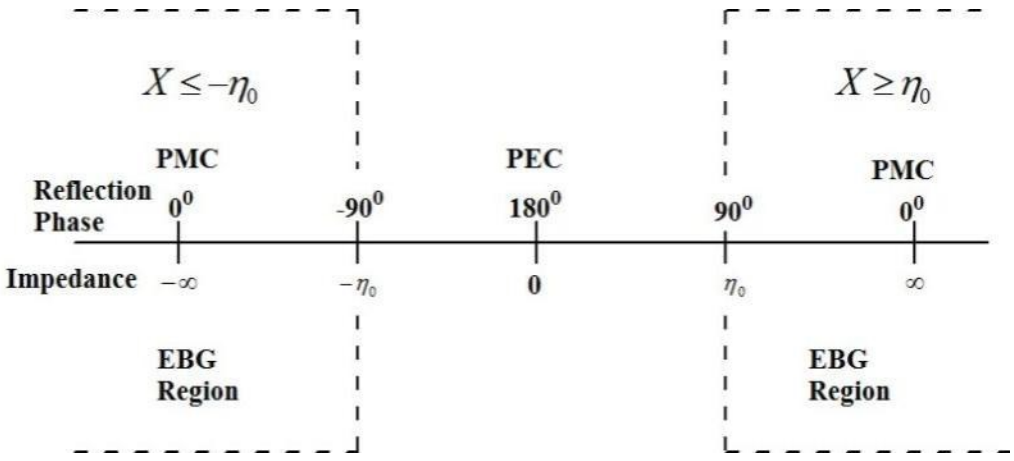

Figure 4.3: Relationship between surface impedance and reflection-phase of EBG structure.

The band edges of the EBG structure, as shown in Figure 4-3, are where the reflection-phase is $+90^{\circ}$ (where the surface impedance is equal to η_0) and -90° (where the surface impedance is equal to $-\eta_0$). In (4-10) we found the bandwidth to be given by

$$\text{Bandwidth} = \left(\frac{1}{\eta_0 C}\right)\left(\sqrt{LC}\right) = \frac{1}{\eta_0}\sqrt{\frac{L}{C}} \tag{4-10}$$

We see that above equation for bandwidth agrees with the reported bandwidth of EBG in different papers and books, hence validating this analysis. Using this analysis the reflection-phase is found using Matlab [42] and compared with the published results in the book [15] which were obtained using finite difference-time domain (FDTD and periodic boundary conditions for the case where patch width is 3 mm, gap between the patches is 0.5 mm, via height is 1 mm and the relative permittivity of the board is 2.20. Figure 4.4 shows the comparison of the effect of the patch width on the reflection phase, computed using circuit analysis in this study and computational EM method FDTD, while Figure 4.5 shows the comparison of the effect of the gap width on the reflection phase, computed using circuit analysis in this study and computational EM method FDTD.

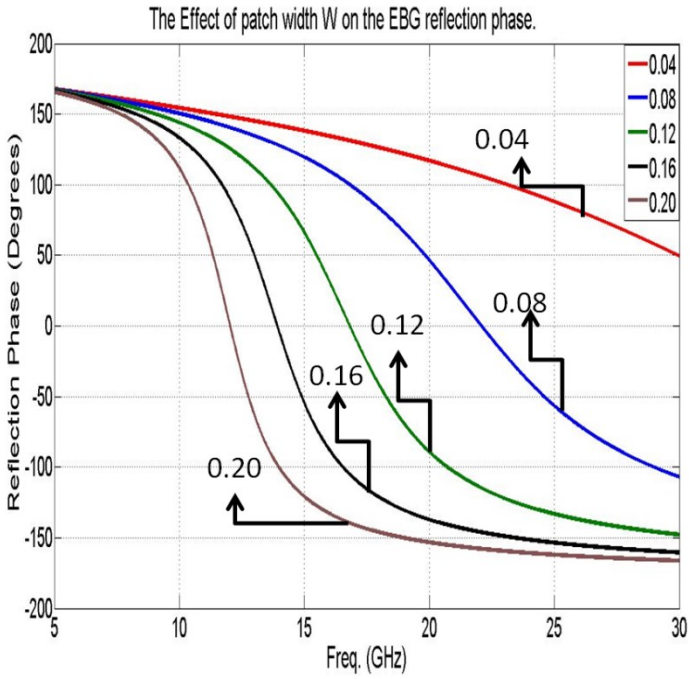

(a)

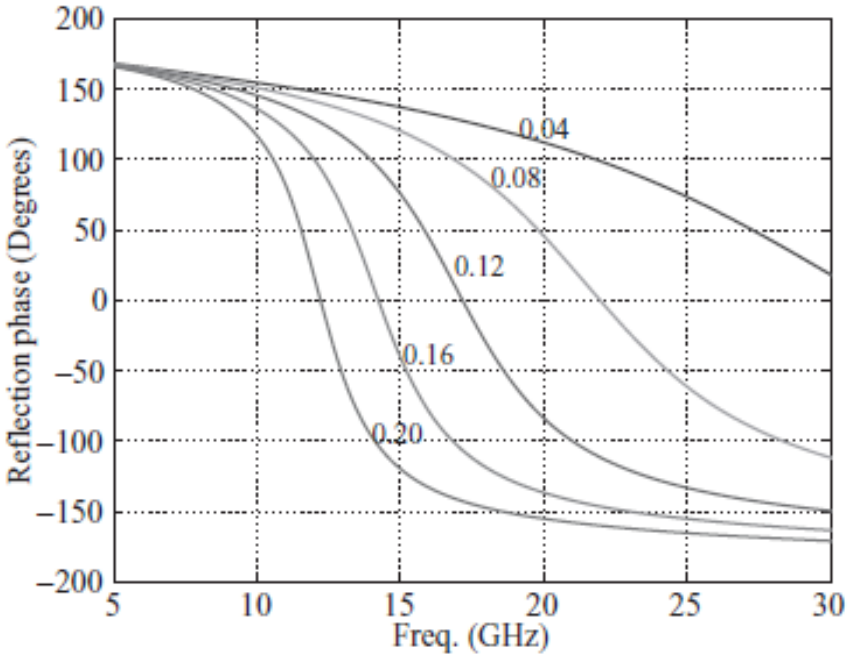

(b)

Figure 4.4: Comparison of the effect of the patch width on the reflection phase(a) calculated and (b) taken from reference. (with permission)

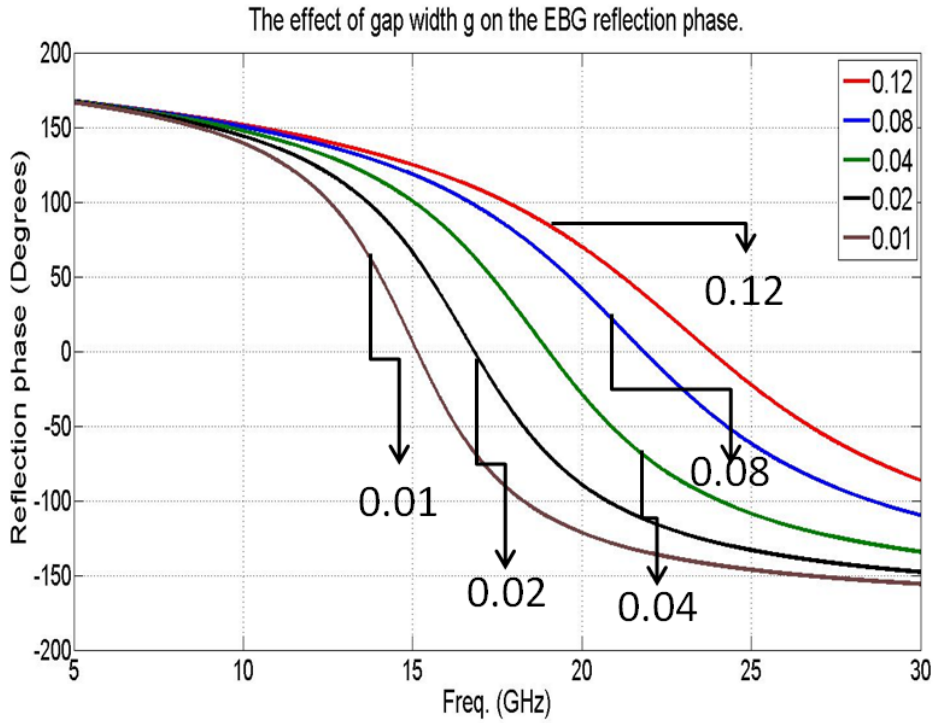

(a)

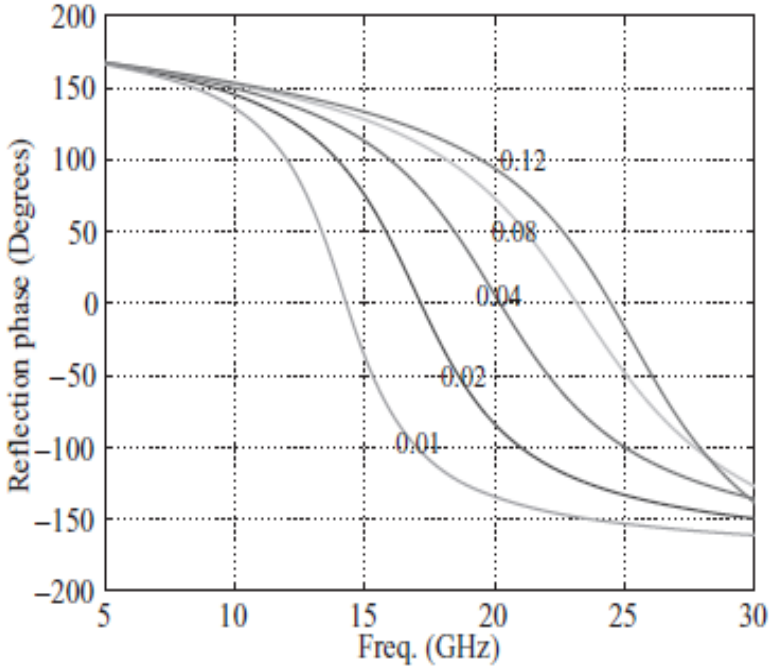

(b)

Figure 4.5: Comparison of the effect of the gap width on the reflection phase(a) calculated and (b) taken from reference. (with permission)

Figure 4.6 shows the comparison of the effect of the substrate height on the reflection phase, computed using circuit analysis in this study and computational EM method FDTD, while Figure 4.7 shows the comparison of the effect of the substrate permittivity on the reflection phase, computed using circuit analysis in this study and computational EM method FDTD. Figures 4.4 through 4.7 show good agreement and validates this analysis.

From Figure 4.4 it is evident that when patch width increases, the resonant frequency of EBG moves lower and the bandwidth decreases, because increasing patch width decreases patch gap which in turn increases the capacitance. Resonance frequency is inversely proportional to the square root of capacitance, so increasing patch width decreases the resonance frequency of the EBG structure. Bandwidth of EBG structure is inversely proportional to the square root of capacitance, so increasing patch width decreases the bandwidth of the EBG structure.

From Figure 4.5 it is evident that when patch gap increases, the resonant frequency of EBG moves higher and the bandwidth increases, because increasing patch gap decreases the capacitance. Resonance frequency is inversely proportional to the square root of capacitance, so increasing patch gap increases the resonance frequency of the EBG structure. Bandwidth of EBG structure is inversely proportional to the square root of capacitance, so increasing patch gap increases the bandwidth of the EBG structure.

From Figure 4.6 it is evident that when substrate height increases, the resonant frequency of EBG moves lower and the bandwidth increases, because increasing substrate height increases the inductance. Resonance frequency is inversely proportional to the square root of inductance, so increasing substrate height results in lower resonance frequency of the EBG structure. Bandwidth of EBG structure is directly proportional to the square root of inductance, so increasing substrate height increases the bandwidth of the EBG structure.

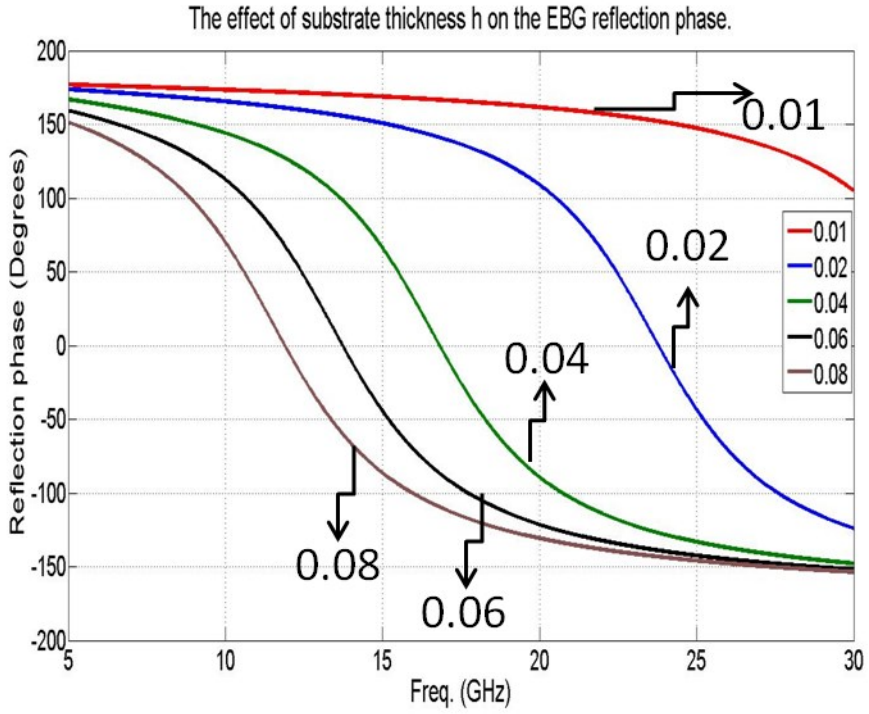

(a)

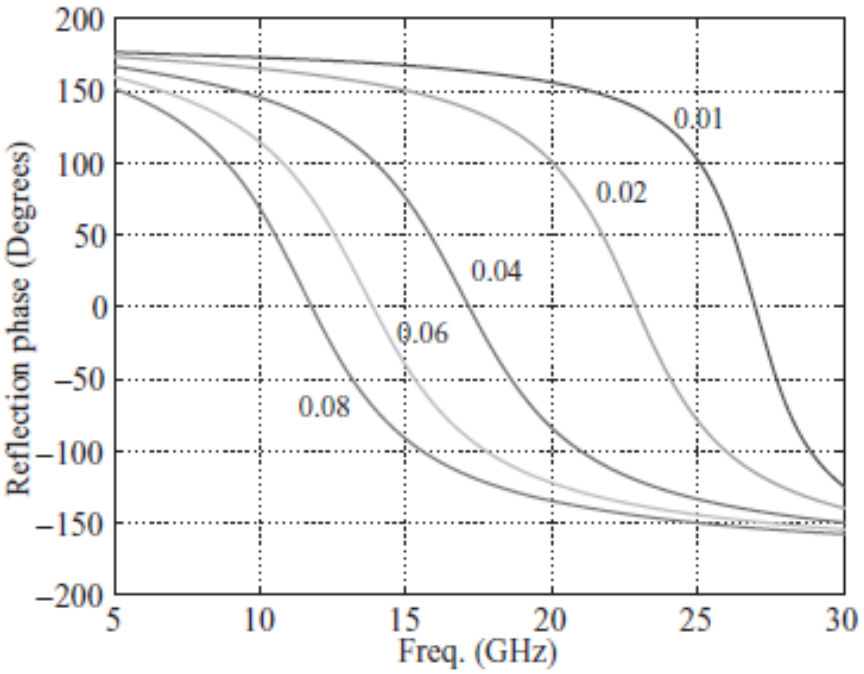

(b)

Figure 4.6: Comparison of the effect of substrate height on the reflection phase(a) calculated and (b) taken from reference. (with permission)

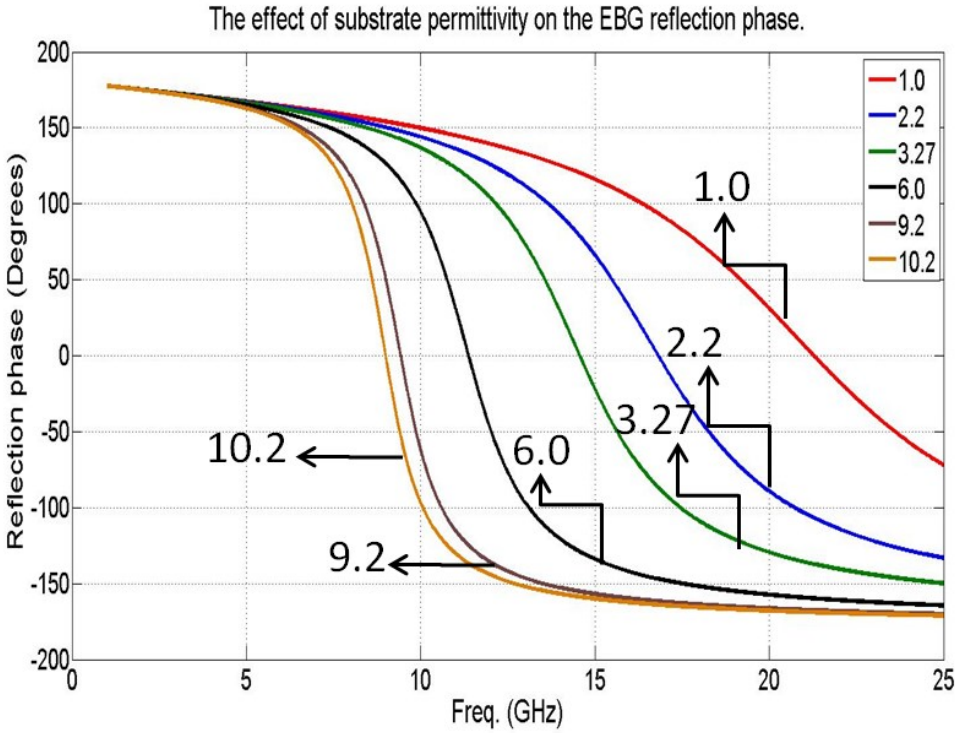

(a)

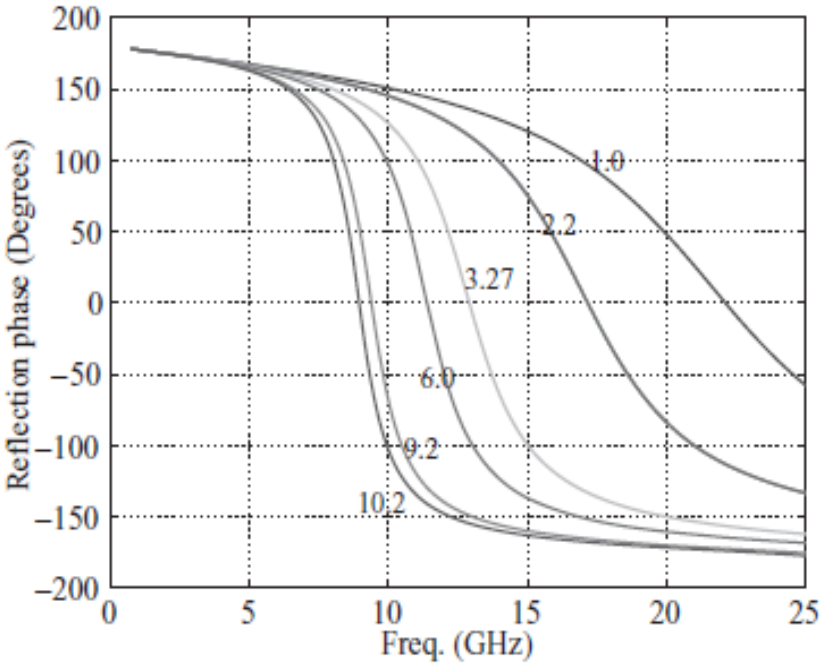

(b)

Figure 4.7: Comparison of the effect of the substrate permittivity on the reflection phase(a) calculated and (b) taken from reference. (with permission)

From Figure 4.7 it is evident that when substrate permittivity increases, the resonant frequency of EBG moves lower and the bandwidth decreases, because increasing substrate permittivity increases the capacitance. Resonance frequency is inversely proportional to the square root of capacitance, so increasing substrate permittivity results in lower resonance frequency of the EBG structure. Bandwidth of EBG structure is inversely proportional to the square root of capacitance, so increasing substrate permittivity decreases the bandwidth of the EBG structure. This section showed the analysis and characterization of EBG structures using circuit theory, and the required conditions for a desired range of reflection-phase are calculated using a closed-form equation approach and the results are compared with the published results and they agree very well.

EBG surface impedance has been modeled as purely imaginary impedance, which can be realized by a short-circuited or open-circuited transmission line of finite length. A transmission line backed by a load Z_L, as shown in Figure 4.8, it's input impedance seen at a distance '*l*' away from load is [23]:

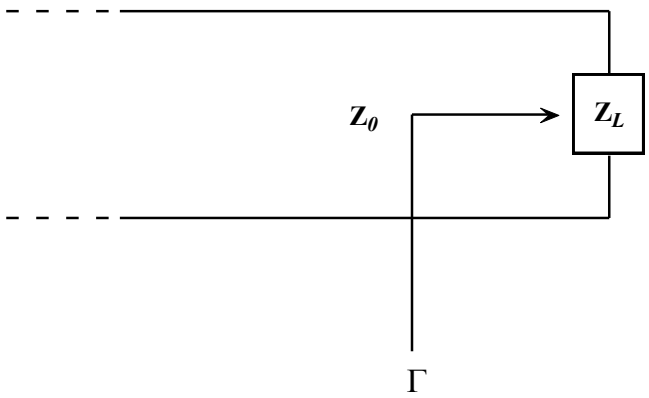

Figure 4.8: Transmission line model of a medium backed by a load Z_L.

$$Z_{in} = Z_0 \left(\frac{Z_L + jZ_0 tan\beta l}{Z_0 + jZ_L tan\beta l}\right) \quad (4\text{-}19)$$

A. Short Circuited Load Condition

When

$$Z_L = 0 \Rightarrow Z_{in} = Z_0 \left(\frac{jZ_0 tan\beta l}{Z_0}\right) \quad (4\text{-}20)$$

$$Z_{in} = jZ_0 tan\beta l \tag{4-21}$$

Z_{in} is purely imaginary, reflection coefficient with free space is

$$\Gamma = \frac{Z_{in} - \eta_0}{Z_{in} + \eta_0} \tag{4-22}$$

$$\Gamma = \frac{jZ_0 tan\beta l - \eta_0}{jZ_0 tan\beta l + \eta_0} \tag{4-23}$$

$$|\Gamma| = \left|\frac{jZ_0 tan\beta l - \eta_0}{jZ_0 tan\beta l + \eta_0}\right| = 1 \tag{4-24}$$

$$\lfloor\Gamma = \left[\pi - tan^{-1}\left(\frac{Z_0 tan\beta l}{\eta_0}\right)\right] - tan^{-1}\left(\frac{Z_0 tan\beta l}{\eta_0}\right) \tag{4-25}$$

$$\lfloor\Gamma = \left[\pi - 2\, tan^{-1}\left(\frac{Z_0 tan\beta l}{\eta_0}\right)\right] \tag{4-26}$$

Bandwidth of $\lfloor\Gamma$ between $-\frac{\pi}{2}$ and $\frac{\pi}{2}$ is

$$-\frac{\pi}{2} \leq \pi - 2\, tan^{-1}\left(\frac{Z_0 tan\beta l}{\eta_0}\right) \leq \frac{\pi}{2} \tag{4-27}$$

$$-\frac{3\pi}{2} \leq -2\, tan^{-1}\left(\frac{Z_0 tan\beta l}{\eta_0}\right) \leq -\frac{\pi}{2} \tag{4-28}$$

$$\frac{3\pi}{4} \geq tan^{-1}\left(\frac{Z_0 tan\beta l}{\eta_0}\right) \geq -\frac{\pi}{4} \tag{4-29}$$

$$-1 \geq \left(\frac{Z_0 tan\beta l}{\eta_0}\right) \geq 1 \tag{4-30}$$

$$-\eta_0 \geq Z_0 tan\beta l \geq \eta_0 \tag{4-31}$$

$$\text{i. e, } \; tan\beta l \geq \eta_0/Z_0 \quad \text{or} \quad tan\,\beta l \leq -\eta_0/Z_0 \tag{4-32}$$

The common solution ($\lfloor\Gamma = 0$)occurs when $tan\beta l = \infty$this happens when $\beta l = \frac{\pi}{2}$(or)$l = \frac{\lambda}{4}$. This result is the reason antennas are mounted quarter wave away from conducting planes to get maximum possible gain.

Open Circuit Load Condition

When $Z_L = \infty \Rightarrow \frac{1}{Z_L} = 0$

$$Z_{in} = Z_0\left(\frac{1 + j\frac{Z_0}{Z_L} tan\beta l}{\frac{Z_0}{Z_L} + jtan\beta l}\right) = \frac{Z_0}{jtan\beta l} \tag{4-33}$$

$$Z_{in} = -jZ_0 cot\beta l \tag{4-34}$$

Z_{in} is purely imaginary reflection coefficient with free space is

$$\Gamma = \frac{-jZ_0 cot\beta l - \eta_0}{-jZ_0 cot\beta l + \eta_0} = \frac{Z_0 cot\beta l - j\eta_0}{Z_0 cot\beta l + j\eta_0} \tag{4-35}$$

$$|\Gamma| = 1 \tag{4-36}$$

$$\lfloor\Gamma = -tan^{-1}\left(\frac{\eta_0}{Z_0 cot\beta l}\right) - tan^{-1}\left(\frac{\eta_0}{Z_0 cot\beta l}\right) \tag{4-37}$$

$$\lfloor\Gamma = -2tan^{-1}\left(\frac{\eta_0 tan\beta l}{Z_0}\right) \tag{4-38}$$

the bandwidth of $\lfloor\Gamma$ between $-\frac{\pi}{2}$ and $\frac{\pi}{2}$ is

$$-\frac{\pi}{2} \leq -2tan^{-1}\left(\frac{\eta_0 tan\beta l}{Z_0}\right) \leq \frac{\pi}{2} \tag{4-39}$$

$$\frac{\pi}{4} \geq tan^{-1}\left(\frac{\eta_0 tan\beta l}{Z_0}\right) \geq -\frac{\pi}{4} \tag{4-40}$$

$$1 \geq \frac{\eta_0 tan\beta l}{Z_0} \geq -1 \tag{4-41}$$

$$\frac{Z_0}{\eta_0} \geq tan\beta l \geq -\frac{Z_0}{\eta_0} \tag{4-42}$$

i.e.,

$$tan\beta l \leq \frac{Z_0}{\eta_0} \;;\; tan\beta l \geq -\frac{Z_0}{\eta_0} \tag{4-43}$$

The common solution ($\lfloor\Gamma = 0$) occurs when $tan\beta l = 0$, which occurs when $\beta l = 0$ (or) $l = 0$. This result is why antennas are mounted right on top of perfect magnetic conductors to obtain maximum possible gain.

4.3 Transmission Line Analysis of EBG Structures

Assuming a plane wave incidence on the EBG structure, a unit cell can be formed by choosing a smallest cell that repeats itself in two dimensions to form the entire EBG structure. The boundaries of the unit cell are perfect electric walls, for the walls that are perpendicular to the electric field orientation of the plane wave, and perfect magnetic walls, for the walls that are parallel to the electric field orientation of the plane wave, as shown in Figure 4.9.

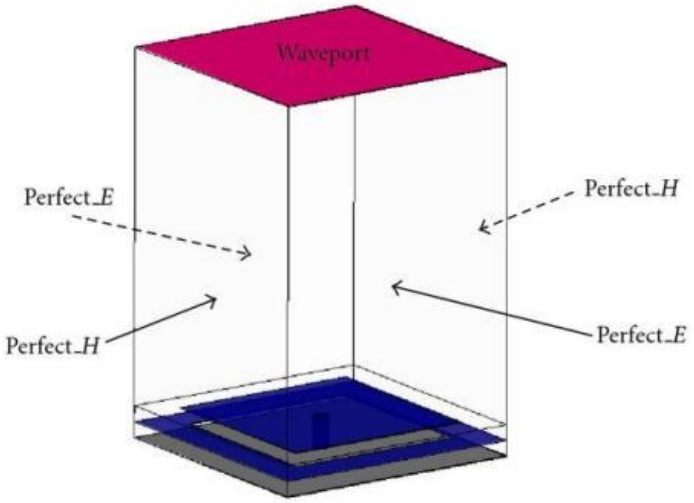

Figure 4.9: Boundary conditions of an EBG unit cell.

Circuit analysis of uniform EBG structures and the required conditions to stay in the EBG band, where the reflection-phase from EBG surface is between +90 degrees and -90 degrees is established in the previous section and this analysis adds in similar analysis and conditions required from transmission line analysis perspective [43]. In a uniform EBG structure, the transmission line analysis consists of a source/port with free space impedance of 377Ω, and two transmission line sections, one for the transmission line formed by the patch and the other for the transmission line formed by the via, with their corresponding lengths, and a back short at the end, to capture the ground plane, as shown in Figure 4.10.

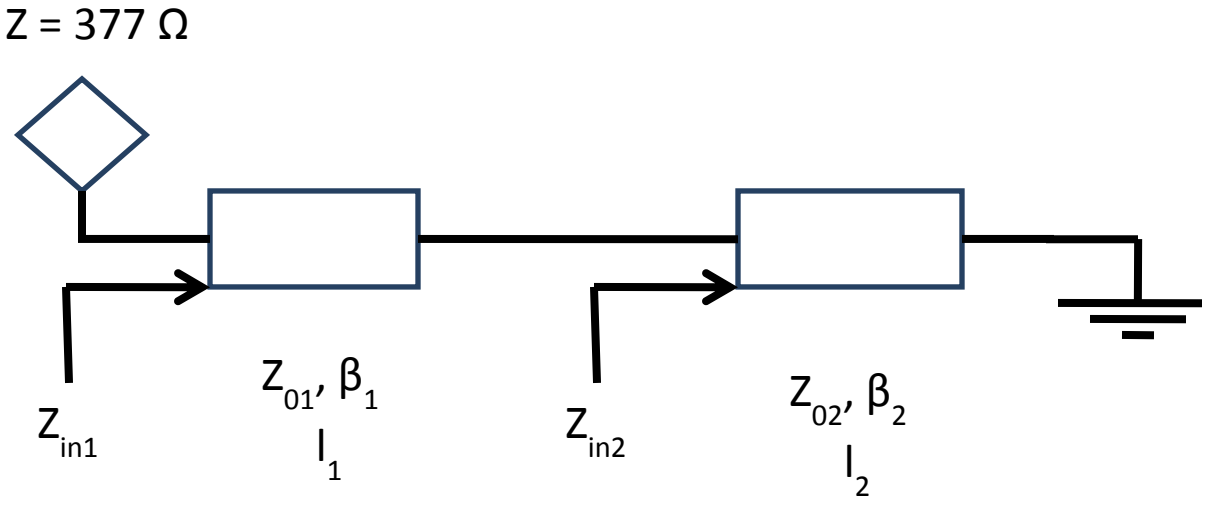

Figure 4.10: Transmission line model of uniform EBG structure.

The quantities Z_{01}, β_1 and l_1 are the impedance, phase constant and length of the transmission line formed by the EBG patch with the length equal to the thickness of the patch. Similarly, Z_{02}, β_2 and l_2 are the impedance, phase constant and length of the transmission line formed by the via section underneath the patch, with the length equal to the length/height of the via. Using the ABCD matrix for a transmission line, the Z_{in2}, as shown in Figure 4.10, is calculated as:

$$\begin{pmatrix} A_2 & B_2 \\ C_2 & D_2 \end{pmatrix} = \begin{pmatrix} cos\beta_2 l_2 & jZ_{02} sin\beta_2 l_2 \\ \dfrac{jsin\beta_2 l_2}{Z_{02}} & cos\beta_2 l_2 \end{pmatrix} \tag{4-44}$$

$$Z_{in2} = \frac{A_2 Z_{L2} + B_2}{C_2 Z_{L2} + D_2} = \frac{B_2}{D_2} (\text{since } Z_{L2} = 0) = jZ_{02} \tan \beta_2 l_2 \tag{4-45}$$

Similarly Z_{in1} can be calculated as follows, by using Z_{in2} as the load impedance Z_{L1} to the previous section.

$$\begin{pmatrix} A_1 & B_1 \\ C_1 & D_1 \end{pmatrix} = \begin{pmatrix} cos\beta_1 l_1 & jZ_{01} sin\beta_1 l_1 \\ \dfrac{jsin\beta_1 l_1}{Z_{01}} & cos\beta_1 l_1 \end{pmatrix} \tag{4-46}$$

$$Z_{in1} = \frac{A_1 Z_{L1} + B_1}{C_1 Z_{L1} + D_1}; Z_{L1} = Z_{in2} \tag{4-47}$$

$$Z_{in1} = \left\{ \frac{\left(cos(\beta_1 l_1) jZ_{02} \tan(\beta_2 l_2)\right) + \left(jZ_{01} sin(\beta_1 l_1)\right)}{\left(\dfrac{jsin(\beta_1 l_1) jZ_{02} \tan(\beta_2 l_2)}{Z_{01}}\right) + \left(cos(\beta_1 l_1)\right)} \right\} \tag{4-48}$$

$$Z_{in1} = \left\{ \frac{j\left(cos(\beta_1 l_1) Z_{02} \tan(\beta_2 l_2) + Z_{01} sin(\beta_1 l_1)\right)}{\left(\dfrac{-sin(\beta_1 l_1) Z_{02} \tan(\beta_2 l_2)}{Z_{01}}\right) + \left(cos(\beta_1 l_1)\right)} \right\} \tag{4-49}$$

Where Z_{in1} is the surface impedance of the uniform EBG structure. It can be seen from equation 4-49 that Z_{in1} is purely imaginary, which validates the assumption made earlier in the circuit analysis of the EBG structures. So, the reflection coefficient looking into the EBG from free space is calculated as follows

$$\Gamma = \frac{Z_{in1} - Z_s}{Z_{in1} + Z_s} \Rightarrow |\Gamma| = \left| \frac{jX - 377}{377 + jX} \right| = 1; Z_{in1} = jX \tag{4-50}$$

So, the magnitude of the reflection coefficient is always unity, while the phase of the reflection coefficient changes with frequency, as seen earlier in the circuit analysis of the EBG structures. The frequency of resonance of the EBG is defined as the frequency where the EBG surface acts like a perfect magnetic layer, which happens when Z_{in1} becomes infinite, or when the denominator of Z_{in1} becomes zero. So, the frequency of resonance of the EBG occurs at a frequency where equation 4-53 is satisfied.

$$Z_{in1} = \left\{ \frac{j\left(cos(\beta_1 l_1) Z_{02} \tan(\beta_2 l_2) + Z_{01} sin(\beta_1 l_1)\right)}{\left(\frac{-sin(\beta_1 l_1) Z_{02} \tan(\beta_2 l_2)}{Z_{01}}\right) + \left(cos(\beta_1 l_1)\right)} \right\} = \infty = 1/0 \tag{4-51}$$

$$cos(\beta_1 l_1) = \frac{Z_{02}}{Z_{01}} sin(\beta_1 l_1) \tan(\beta_2 l_2) \tag{4-52}$$

$$Z_{01} \cot \beta_1 l_1 = Z_{02} \tan \beta_2 l_2 \tag{4-53}$$

Similarly, the same type of analysis can be performed for stacked EBG layers, with each EBG layer represented by two transmission line sections as shown in Figure 4.10, and similar analysis can be performed to come up with the required condition for resonance frequency of the stacked EBG structures. Circuit and transmission line analysis of EBG structures, regular, progressive and stacked, is valid as long as the unit cell of EBG does not accommodate waveguide modes. It is recommended to ensure the EBG unit cell is electrically small. For stacked EBG structures the overall height of unit cell needs to be less than half wavelength to ensure the ground plane of the EBG is not transformed to its surface.

Impedances Z_{01} and Z_{02} are calculated with the help of perfect electric wall and perfect magnetic wall boundary conditions in the unit cell, as shown in Figure 4.9, which make the structure equivalent to three coupling lines in a stripline with perfect magnetic walls between the center line and its adjacent coupling lines, and electric walls formed by the enclosing top and bottom metal covers, as shown in Figure 4.11, which makes Z_{01} and Z_{02} as even-mode impedances of the center coupling line as noted in equations 4-54 and 4-55 [44].

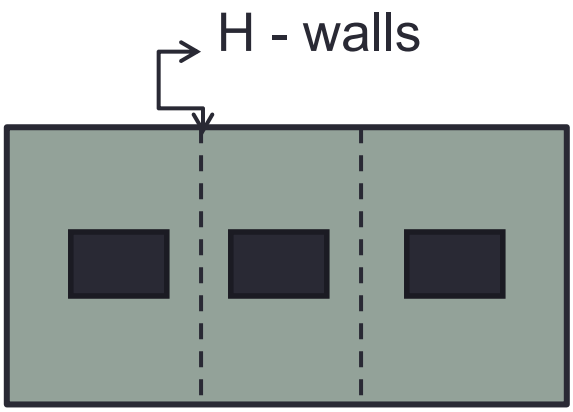

Even Mode

Figure 4.11: EBG unit cell equivalence with coupled lines in stripline.

$$Z_{01} = \frac{\left(94.15/\sqrt{\varepsilon_r}\right)}{\frac{w}{g} + \frac{2}{\pi} e^{\left(-0.56W/(w+g)\right)} \ln\left(1 + \tanh\left(\frac{g}{w+g}\right)\right)} \tag{4-54}$$

$$Z_{02} = \frac{\left(94.15/\sqrt{\varepsilon_r}\right)}{\frac{2r}{w+g-2r} + \frac{2}{\pi} e^{\left(-1.12r/(w+g)\right)} \ln\left(1 + \tanh\left(\frac{w+g-2r}{w+g}\right)\right)} \tag{4-55}$$

Where 'r' is the radius of the via.

A three layer stacked EBG structure is designed using this analysis and its reflection-phase performance is compared with HFSS simulation. Figure 4.12 and Figure 4.13 show the stacked EBG structure used in transmission line analysis, and its reflection-phase comparison using transmission line analysis and commercially available EM simulation tool HFSS [34] respectively. It can be seen in Figure 4.13 that the reflection phases agree very well, hence validating transmission line analysis.

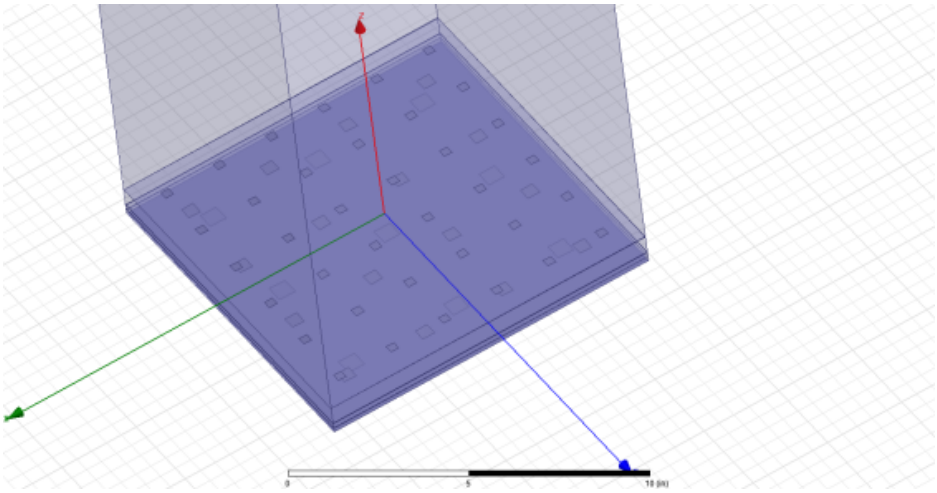

Figure 4.12: Three-layer stacked EBG used in the analysis.

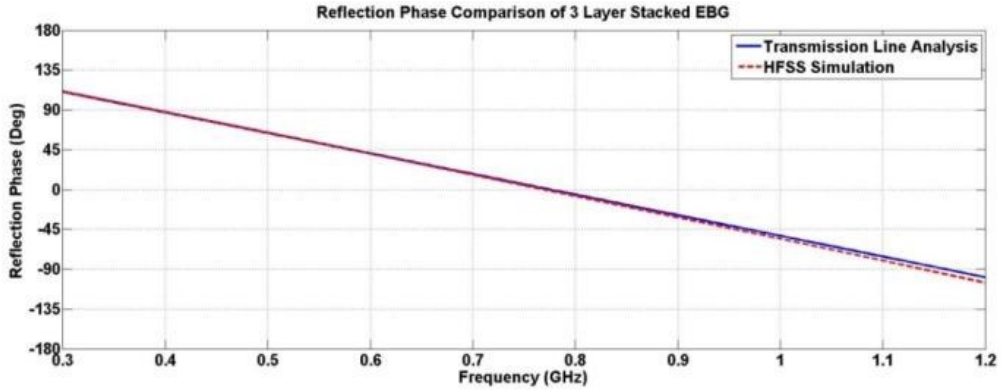

Figure 4.13: Reflection-phase comparison.

EBG structures are helpful when mounting an antenna near a ground plane [45, 46]; they are compact in size and have low loss [47]. The analysis and characterization of EBG structures using circuit and transmission line theories is established, circuit analysis yielded the required conditions for a desired range of reflection-phase and the results are compared with the published results and they agree very well. Transmission line analysis of EBG structures yielded the required condition for the resonance and the reflection-phase of the analysis is compared with the simulated phase and they agree very well.

5 STACKED EBG STRUCTURES

5.1 Introduction to Stacked EBG Structures

Stacked EBG structures are formed by stacking uniform EBG structures that resonate at frequencies close to each other [48, 49]. A sketch of the stacked EBG configuration is shown in Figure 5.1 along with its unit cell configuration. The dimensions of the stacked layers are functions of the corresponding resonance frequencies. Using FEKO, the reflection-phase of the stacked EBG is computed and, compared with the reflection-phase of a uniform EBG, show in Figure 5.2. The dimensions of the uniform EBG are selected such that it resonates at 0.8 GHz, and the dimensions of the 3 layer stacked EBG are selected such that the bottom layer resonates at 0.6 GHz, middle layer resonates at 0.85 GHz and top layer resonates at 1.05 GHz. From the slow phase change over a broader band, we can see that the stacked EBG has an octave bandwidth, and it has a wider bandwidth compared to uniform EBG.

The proposed stacked EBG structure is used with an UWB monopole antenna, as shown in Figure 5.3. The performance of the monopole antenna in free space is taken as a benchmark and is compared with the performance of the antenna near uniform EBG and the three layer stacked EBG. To better understand the effects of the antenna near a ground plane, the performance of the antenna on a ground plane is also used for the comparison purposes. Figure 5.4 shows the XY plane gain patterns of the monopole antenna in free space, while Figure 5.5 shows the XY plane gain patterns of the antenna on a PEC plate.

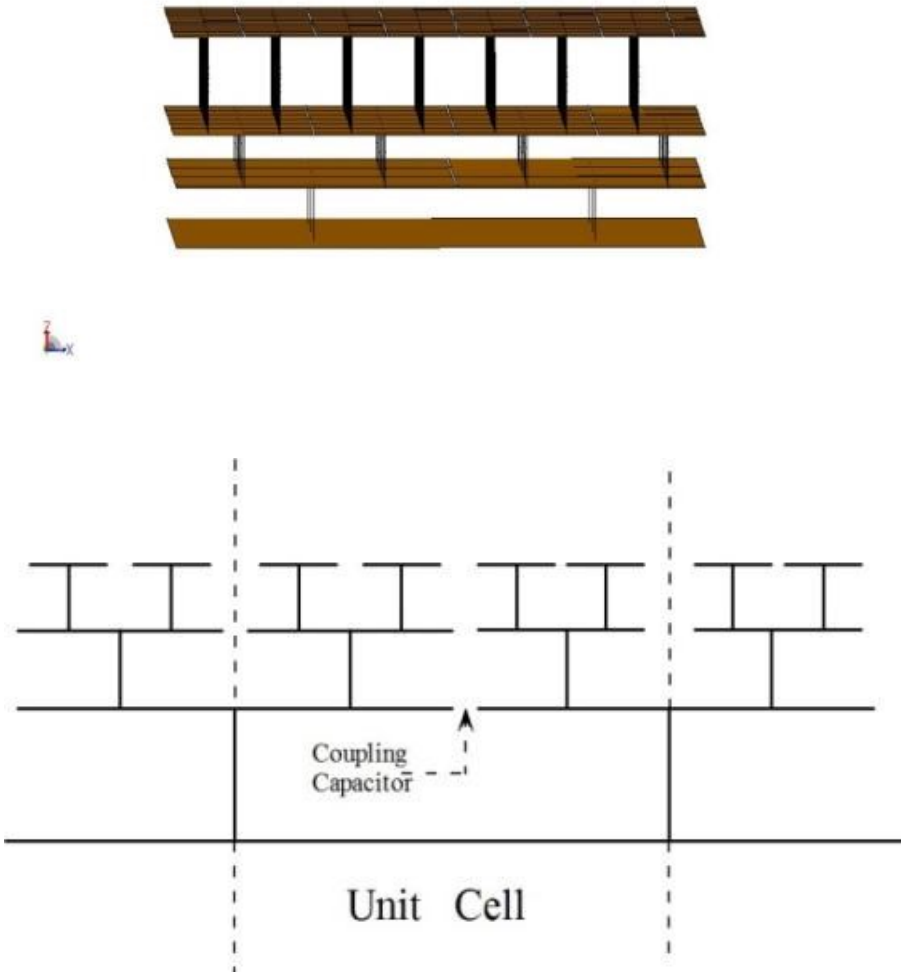

Figure 5.1: Three layer stacked EBG structure (top) and its unit cell (bottom).

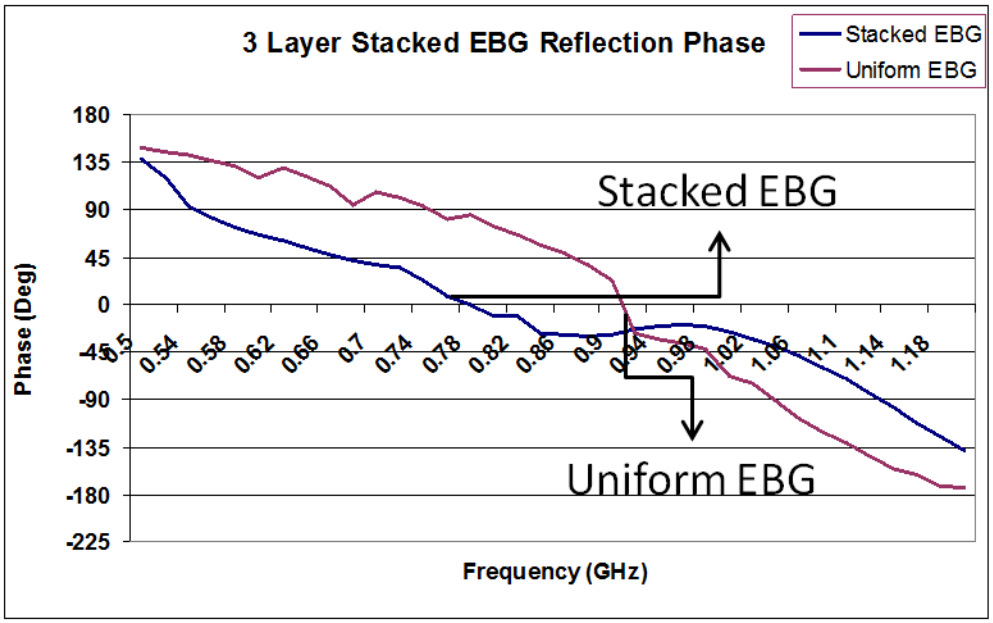

Figure 5.2: Reflection-phase Comparison.

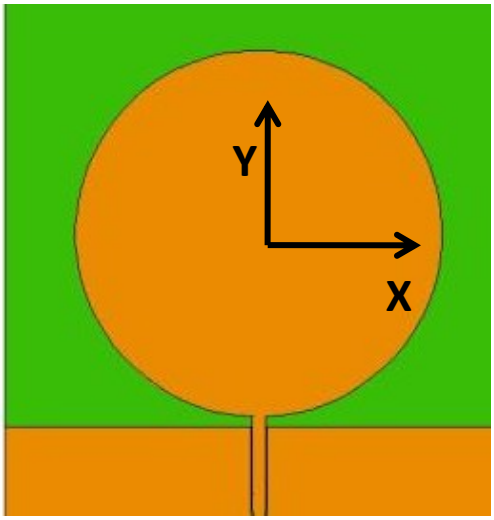

Figure 5.3: UWB antenna used with the 3 layer stacked EBG.

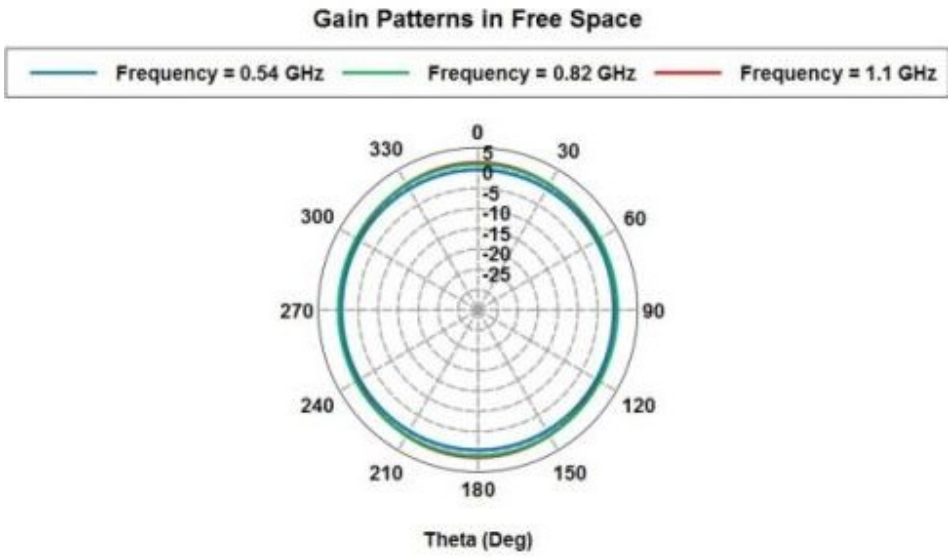

Figure 5.4: XY Plane Gain Patterns in Free Space.

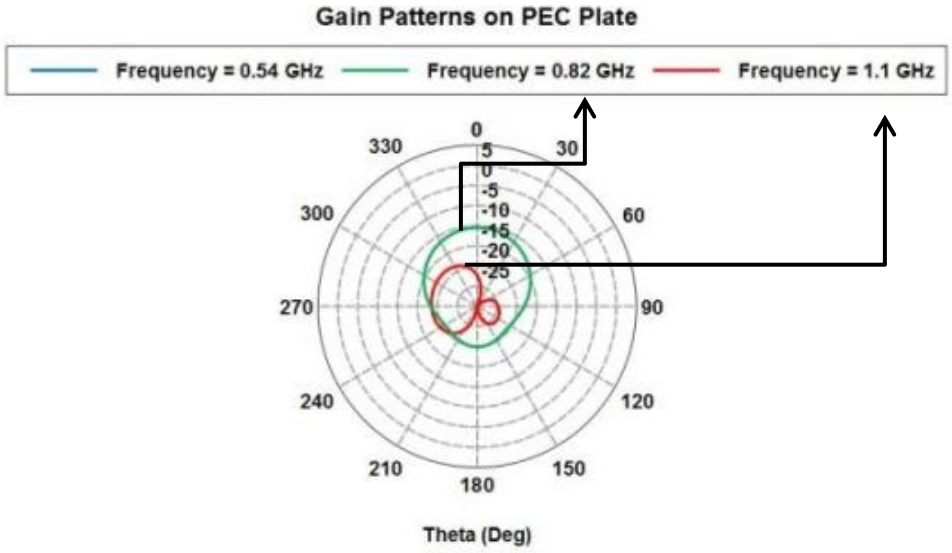

Figure 5.5: XY Plane Gain Patterns on PEC Plate.

Comparing Figures 5.4 and 5.5 it can be easily seen that the presence of a conducting plate has degraded the performance of the antenna, because the reflected wave from the PEC plate cancels the forward radiating wave and yields very low gain in boresight. Figure 5.6 shows XY plane gain patterns of the antenna near a uniform EBG structure, while Figure 5.7 shows XY plane gain patterns of the antenna near the threelayer stacked EBG structure. Comparing Figures 5.6 and 5.7 it can be seen that uniform EBG does not have the required bandwidth to cover the octave band of interest (550 MHz to 1100 MHz), a fact that is proved in Figure 5.2. It can be seen that the

stacked EBG has the required bandwidth to cover the octave bandwidth as shown in Figures 5.2 and 5.7.

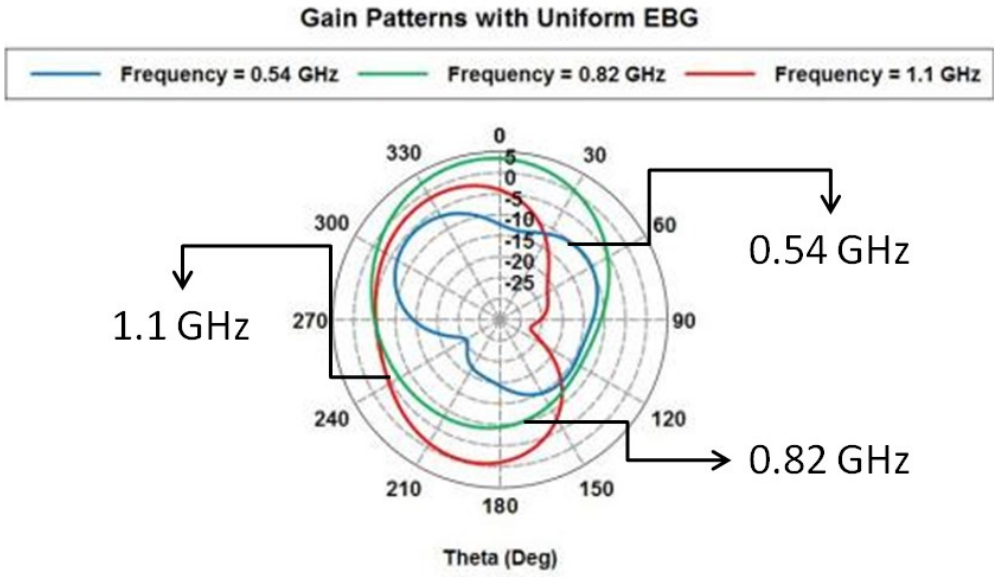

Figure 5.6: XY Plane Gain Patterns near Uniform EBG.

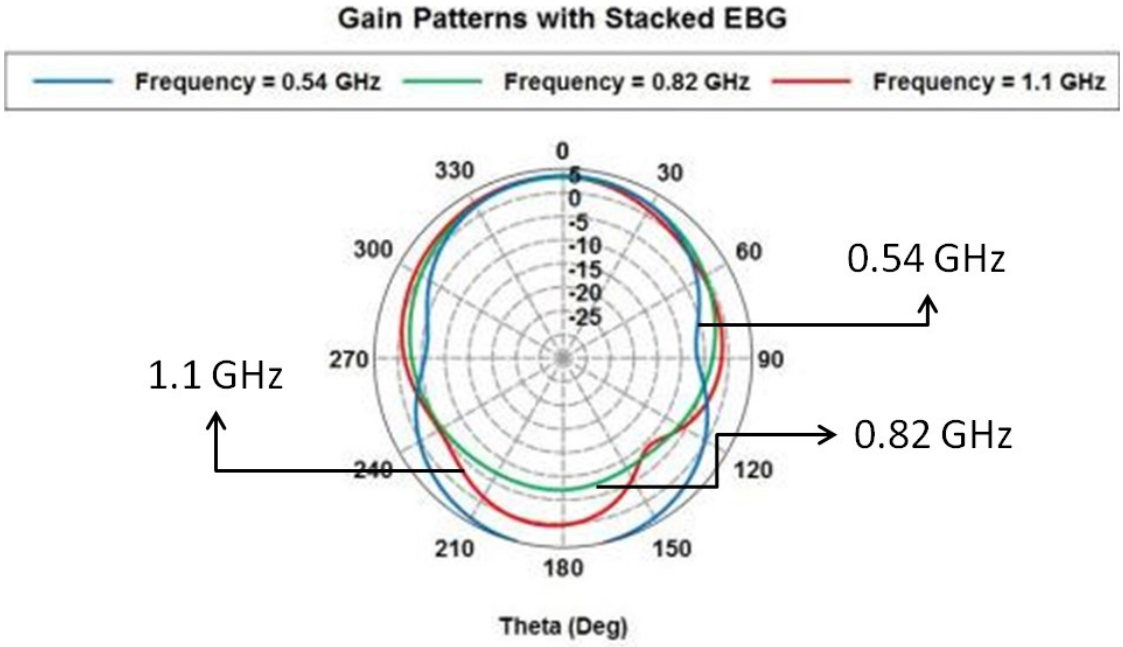

Figure 5.7: XY Plane Gain Patterns near Stacked EBG.

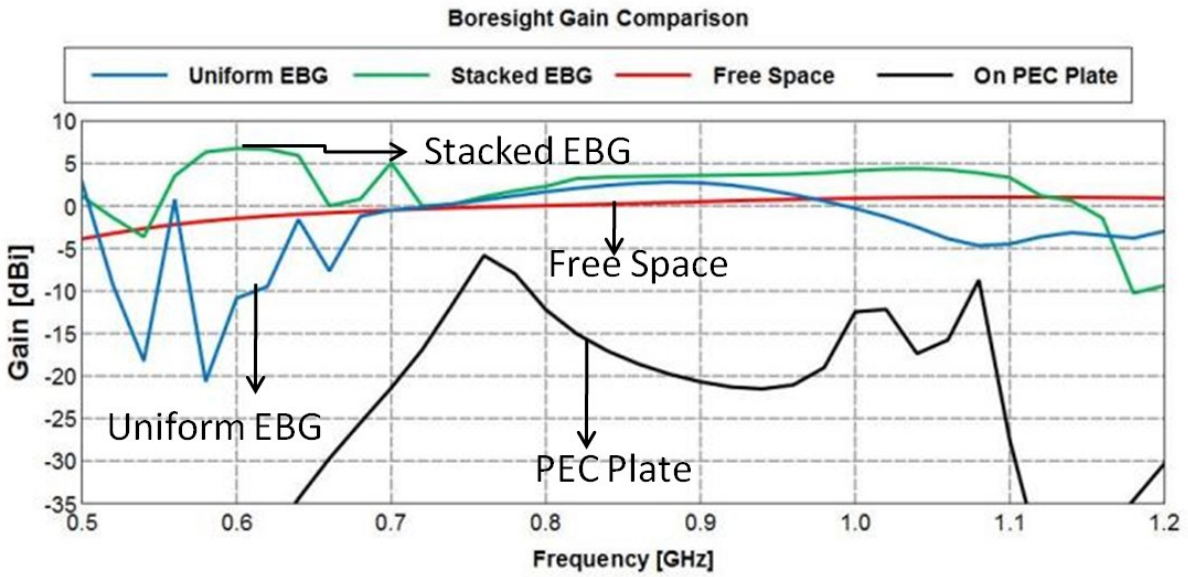

Figure 5.8: Boresight Gain Comparison of the antenna under different loading conditions.

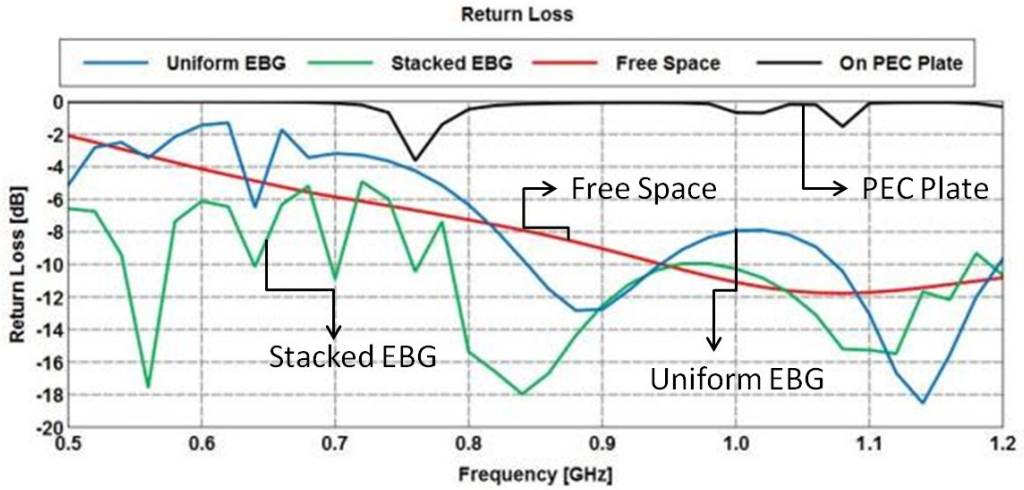

Figure 5.9: Return loss comparison of the antenna under different loading conditions with respect to a 50 ohm input.

Figure 5.8 compares the boresight gain, as shown in Figure 5.3, of the antenna under different loading conditions, while Figure 5.9 shows the return loss performance of the antenna under different loading conditions. It can be seen from Figures 5.8 and 5.9 that the stacked EBG has the required bandwidth, as its gain and return loss are better than free space case from 550 MHz to

1100 MHz, while the uniform EBG does not have the required bandwidth to cover the entire bandwidth.

5.2 Stacked EBG Application to UWB Antenna

Stacked EBG structure is formed by vertically stacking EBG layers, which operate over frequency bands close to one another. Stacked EBG structures resonate at the same place over different frequencies, so an antenna that resonates at the same place at different frequencies is best suited to work with stacked EBG structures. Figure 5.10 shows such an antenna, a UWB co-planer fed monopole antenna, and its boresight gain of the antenna.

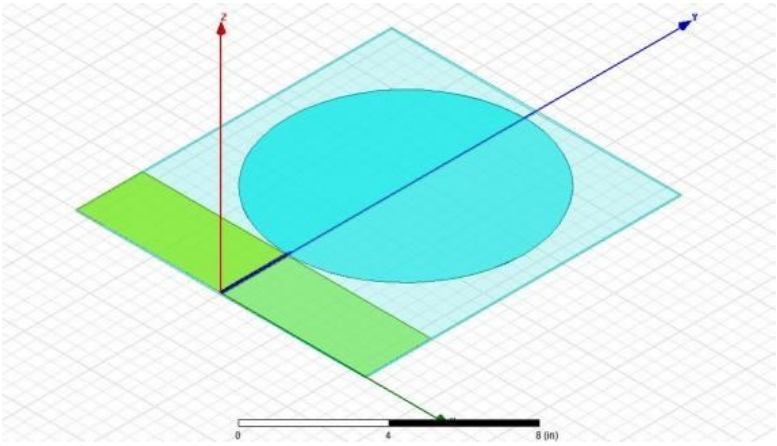

(a)

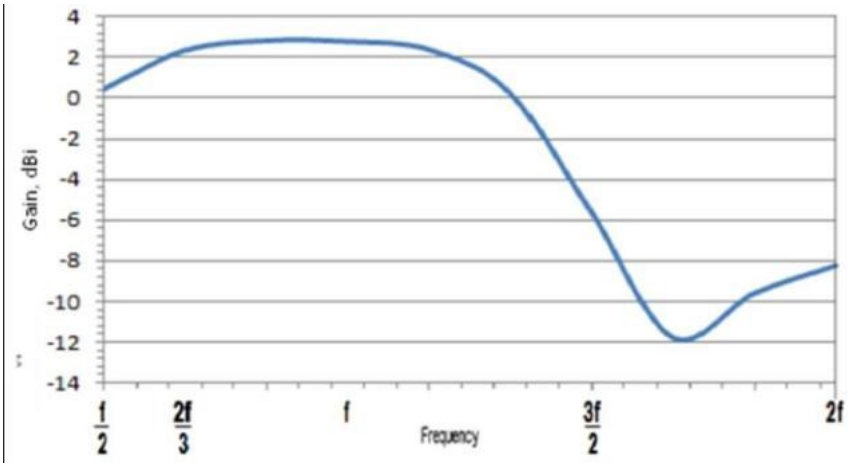

(b)

Figure 5.10: Circular Monopole UWB Antenna (a) and Gain Performance over 4:1 Frequency Band (b).

Figure 5.11 shows three layer stacked EBG and the UWB monopole antenna over it, which is designed to work together to increase the efficiency of the antenna.

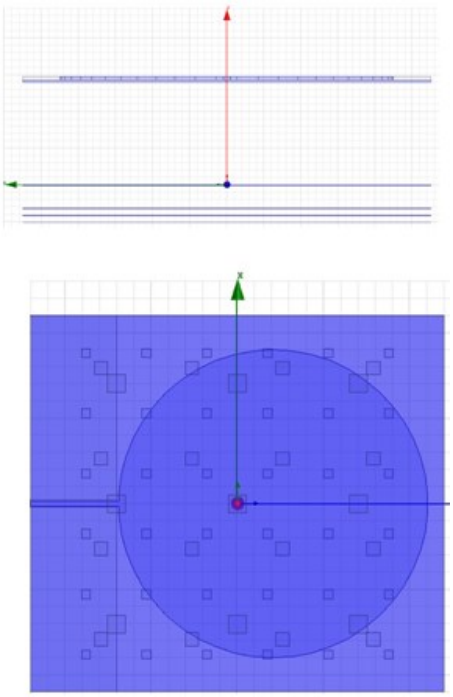

Figure 5.11: UWB antenna over three layer stacked EBG.

Three layer stacked EBG is designed to work over a 3:1 bandwidth, and is used with UWB antenna to enhance the boresight gain. The purpose of designing three layer stacked EBG is to work over broadband and get higher off-boresight gain for the UWB antenna compared to a comparable Vivaldi antenna. Figure 5.12 shows the simulated reflection-phase comparison of the three layer stacked, computed using transmission line analysis and commercially available EM simulation tool HFSS. Reflection phase agrees very well, validating transmission line analysis.

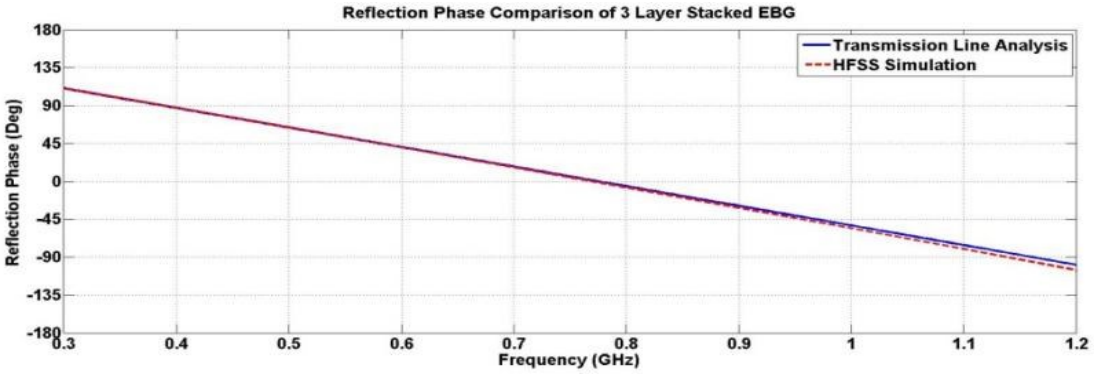

Figure 5.12: Reflection-phase comparison (notice good agreement).

Figures 5.13 and 5.14 compare simulated return loss and boresight gain of the antenna with and without three layer stacked EBG Structure. Maximum gain of the antenna with three layer stacked is achieved off-boresight, as shown in Figure 5.15.

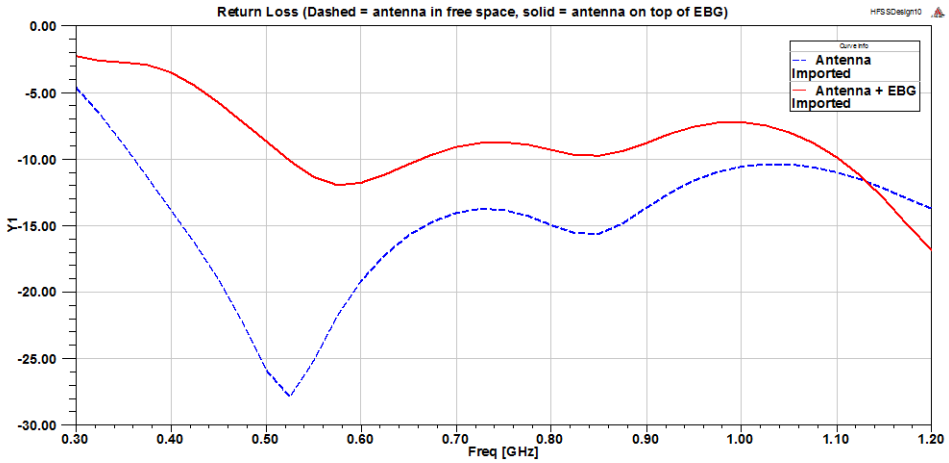

Figure 5.13: Return Loss of UWB Monopole in Free Space (dashed) and over 3-Layer EBG Structure (solid).

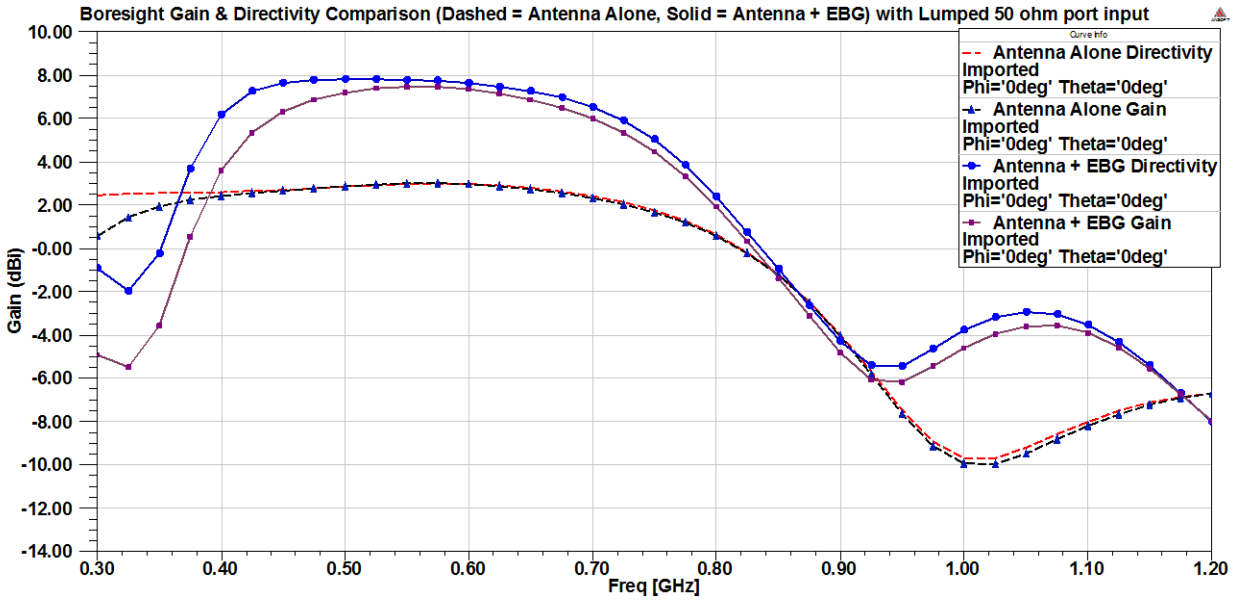

Figure 5.14: Realized Gain and Directivity at Broadside for Circular Monopole in Free Space (dashed red) and over 3-Layer EBG Structure (solid blue and grey).

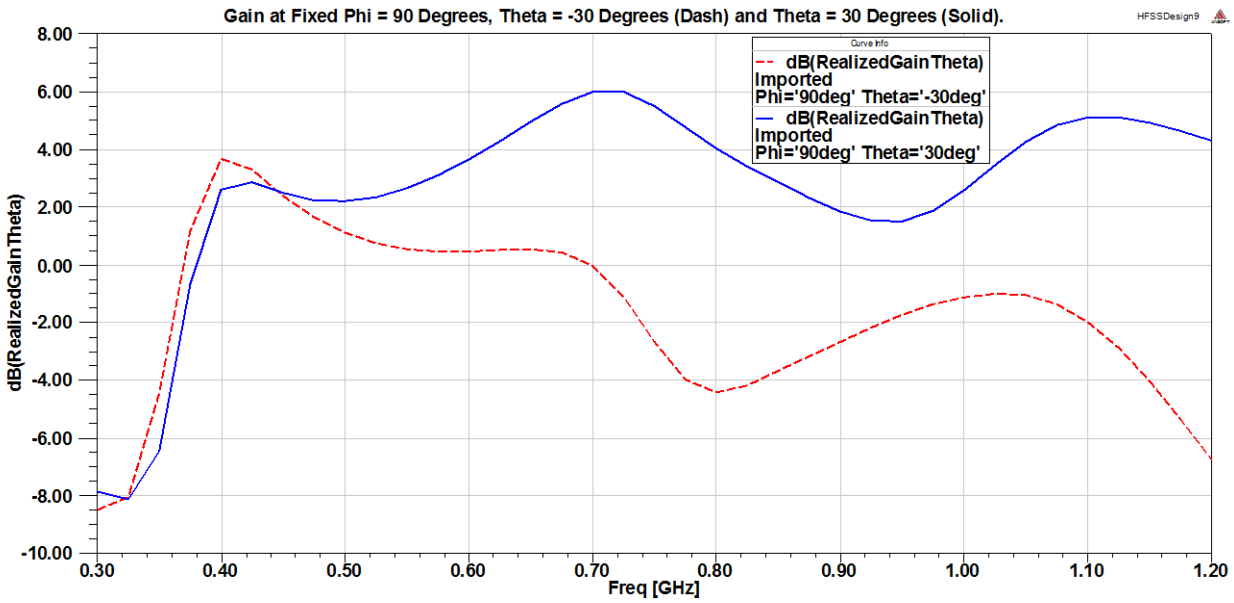

Figure 5.15: Realized Gain of Circular Monopole over 3-Layer EBG Structure at +30^{o} (solid) and -30^{o}(dash) Off Broadside.

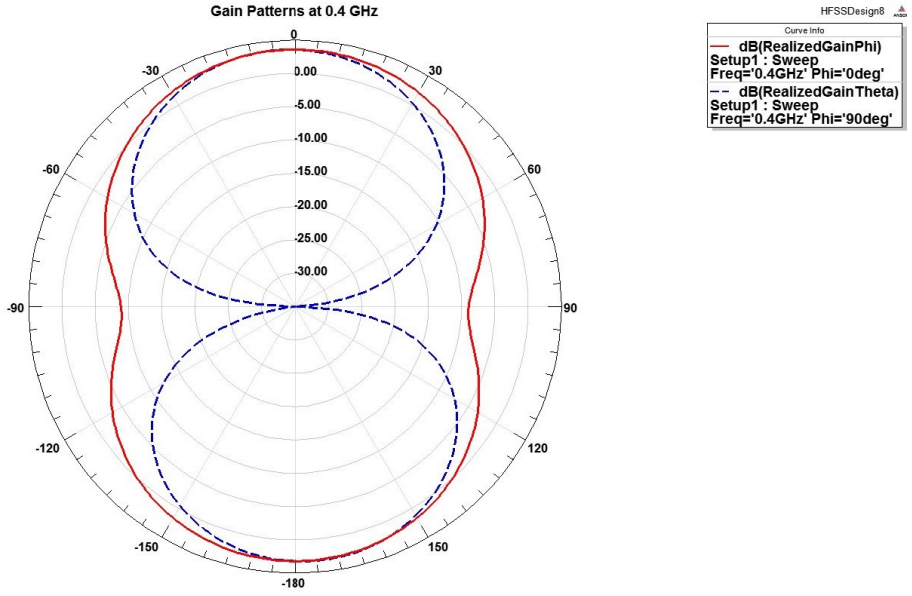

Figure 5.16: Gain patterns of Circular Monopole over 3-Layer EBG Structure at 0.4 GHz in E-plane (solid) and H-plane (dash).

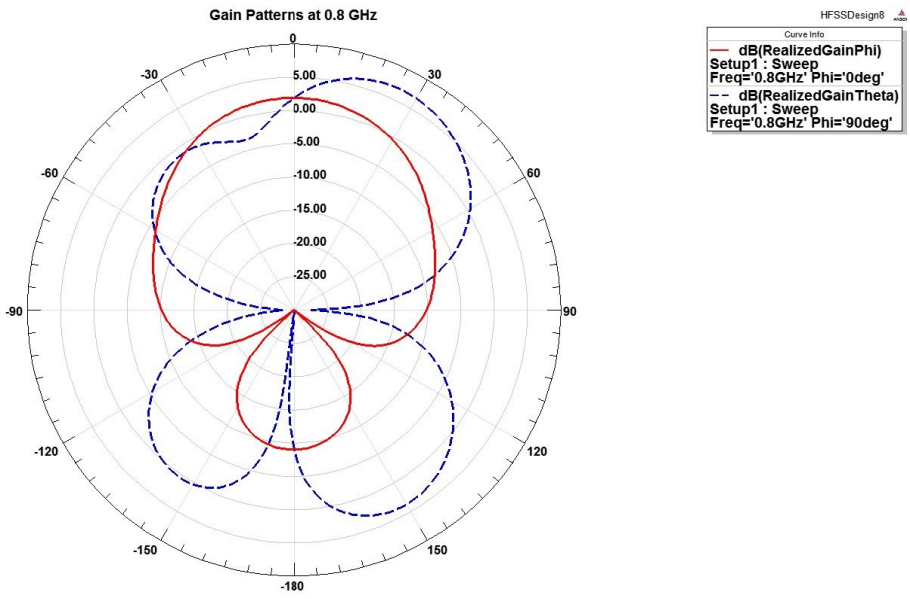

Figure 5.17: Gain patterns of Circular Monopole over 3-Layer EBG Structure at 0.8 GHz in E-plane (solid) and H-plane (dash).

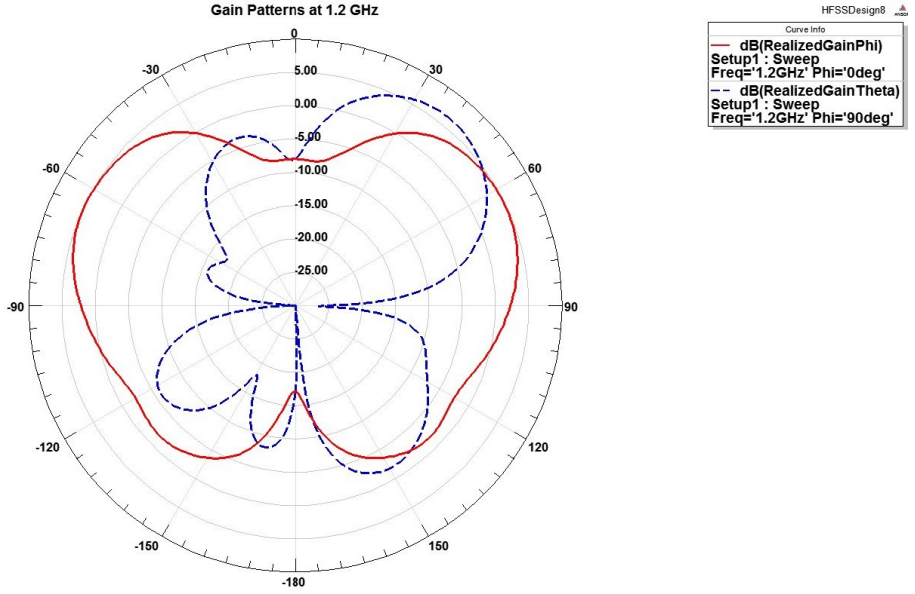

Figure 5.18: Gain patterns of Circular Monopole over 3-Layer EBG Structure at 1.2 GHz in E-plane (solid) and H-plane (dash).

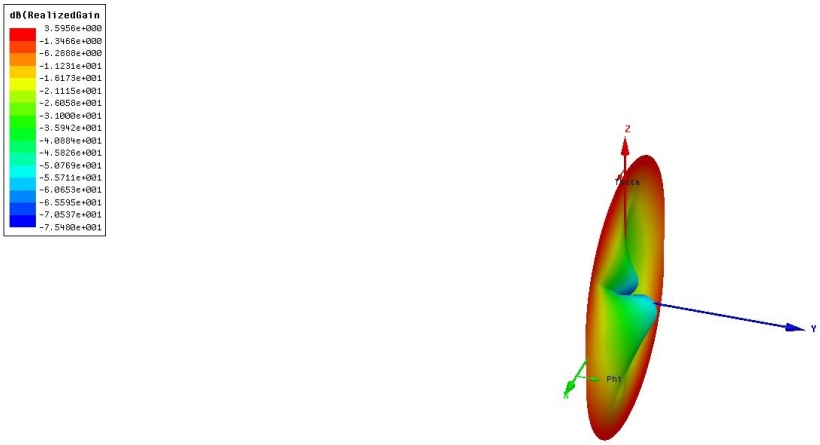

Figure 5.19: 3D Gain pattern of Circular Monopole over 3-Layer EBG Structure at 0.4 GHz.

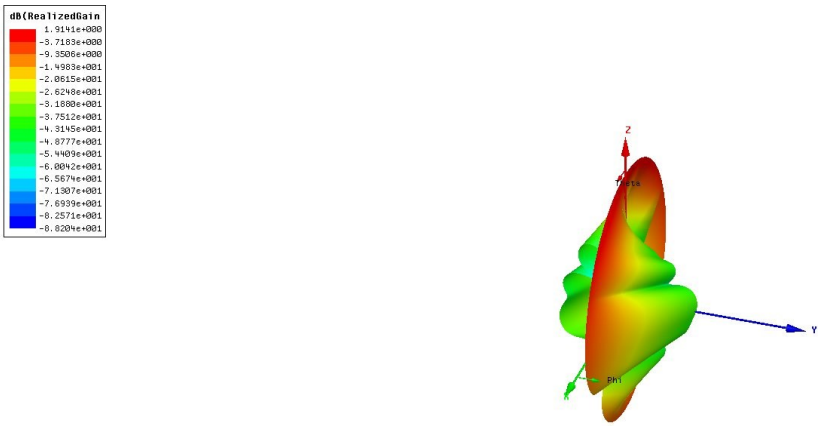

Figure 5.20: 3D Gain pattern of Circular Monopole over 3-Layer EBG Structure at 0.8 GHz.

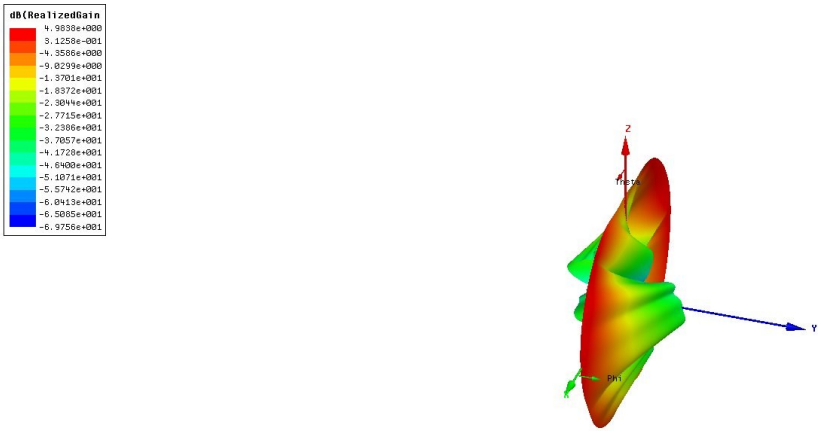

Figure 5.21: 3D Gain pattern of Circular Monopole over 3-Layer EBG Structure at 1.2 GHz.

Figures 5.16 through 5.18 show gain patterns of UWB antenna with 3 layer EBG at 0.4 GHz, 0.8 GHz and 1.2 GHz respectively, while Figures 5.19 through 5.21 show 3D patterns of UWB antenna with 3 layer EBG at 0.4 GHz, 0.8 GHz and 1.2 GHz respectively.FromFigures 5.16 through 5.21 it can be seen that gain patterns are symmetric in E-plane because both the antenna and 3 layer EBG is symmetric along that plane, while patterns are not symmetric in H-plane, because antenna is not symmetric along that plane. Figure 5.14 shows three layer stacked EBG helped in increasing the boresight gain of the UWB monopole antenna, showing the band gap of three layer stacked EBG structure is roughly from 2f/3 to 2f. This section introduced stacked EBG structure, a way to increase the bandwidth of an EBG structure by vertically cascading different size uniform EBGs that resonate close to each other in frequency. The performance of the stacked EBG is validated by using it with a UWB monopole antenna and showing the improvement in gain performance. Boresight and off-boresight gain performance improvements are noticed and a correlation between stacked EBG band-gap and improvement in antenna performance is noted.

6 PROGRESSIVE EBG STRUCTURES

6.1 Introduction to Progressive EBG Structures

A progressive EBG structure is formed by cascading several uniform EBG structures, which resonate close to each other, as shown in Figure 6.1. Progressive EBG structures have wider band gap compared to uniform EBG structures [50, 51]. To produce the same phase response over a broader band, a progressive EBG structure is proposed and it is formed by cascading uniform EBG structures that resonate at different bands. The progressive EBG results in a wider band gap compared to uniform EBG. Figure 6.2 shows the setup to compute reflection phase, while Figure 6.3 shows the reflection-phase comparison of the progressive EBG structure and uniform EBG structure. The phase response of the multiple-tier progressive EBG versus the uniform EBG is simulated using FEKO under two different incidence scenarios. In the first scenario, two horns act as the transmitting (incident) signal and the receiving (reflected) signal. The horns are at symmetric angles relative to the normal to the EBG plate. This arrangement was used in [50], and is shown in Figure 6.2 for the two EBG configurations.

The reflected phases relative to incident phases are plotted in Figure 6.3 for the multiple-tier uniform-EBG configuration tuned at 15 GHz, and the 3-band progressive EBG structurecomputed using commercially available EM simulation tool FEKO. The 3-band structure shows a broadband response for slow phase variation. The uniform EBG structure has a resonance frequency of 15 GHz, while the Progressive EBG structure has three resonances at 12 GHz, 15 GHz and 18 GHz. It can be seen that progressive EBG structure has wider band gap than uniform EBG structure.

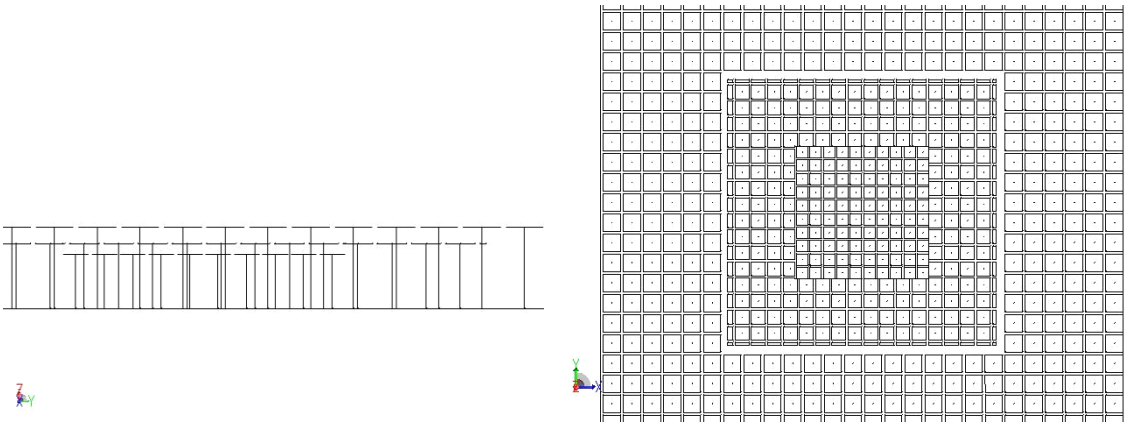

Figure 6.1: Progressive EBG structure.

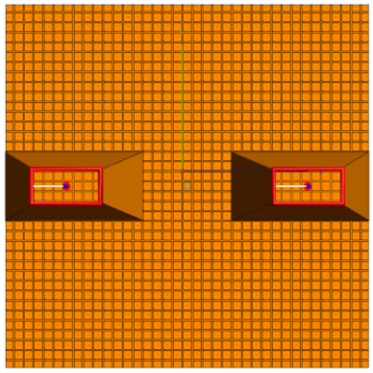

(a)

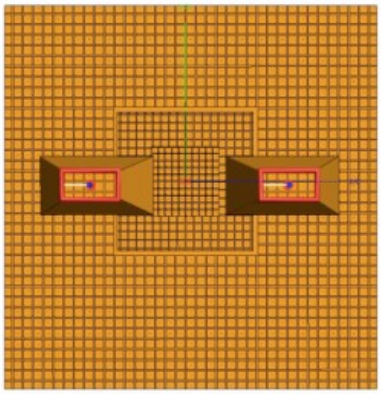

(b)

Figure 6.2: (a) Narrowband uniform EBG and (b) Broadband, 3-resonance progressive EBG structures. Transmit and receive horns are used to measure the phase response of the structure.

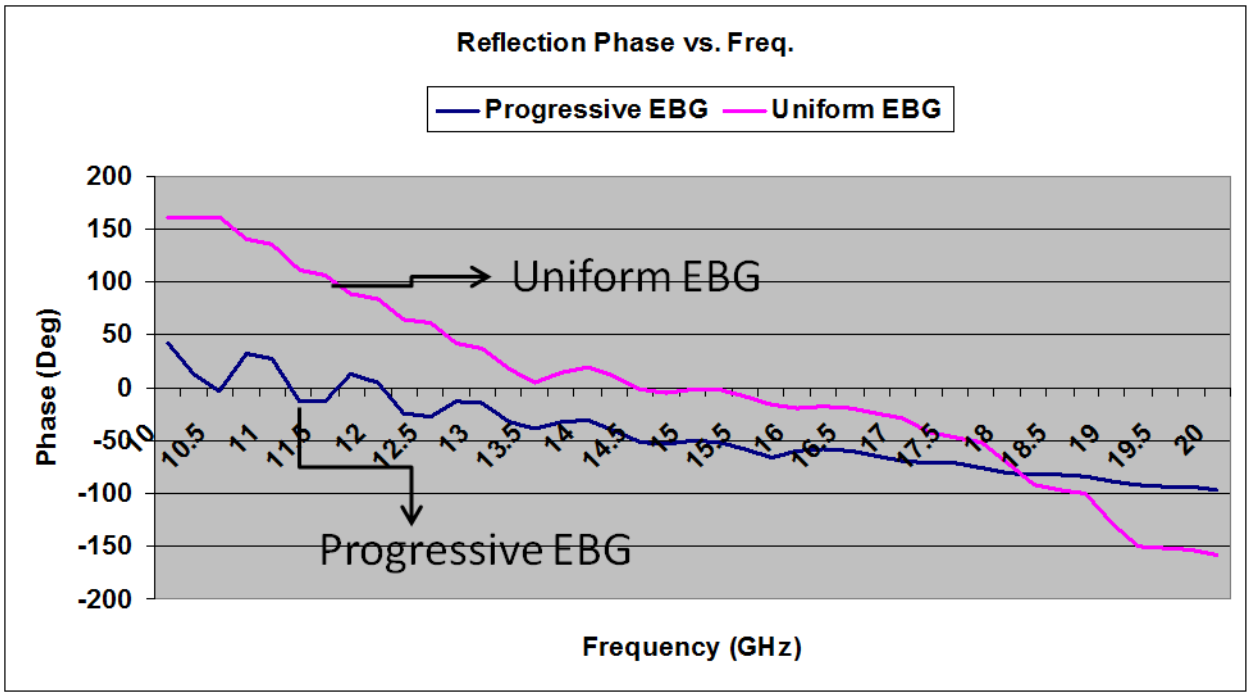

Figure 6.3: Reflection-phase Comparison.

In the second scenario, a plane wave is incident normal to the EBG plate, and the reflection-phase results for a broadband EBG versus 15-GHz and 12 GHZ uniform EBG platescomputed using commercially available EM simulation tool FEKO are shown in Figures 6.4 (a) and (b), respectively. The broadband operation of the progressive EBG is measured as the $\pm$ 90^{o} range of the reflection phase. This is apparent in Figure6.4(b), where the 12 GHz EBG has shown a bandwidth of less than 2 GHz (11-13 GHz) while the progressive EBG exhibits a bandwidth of 16 GHz (9-25 GHz).

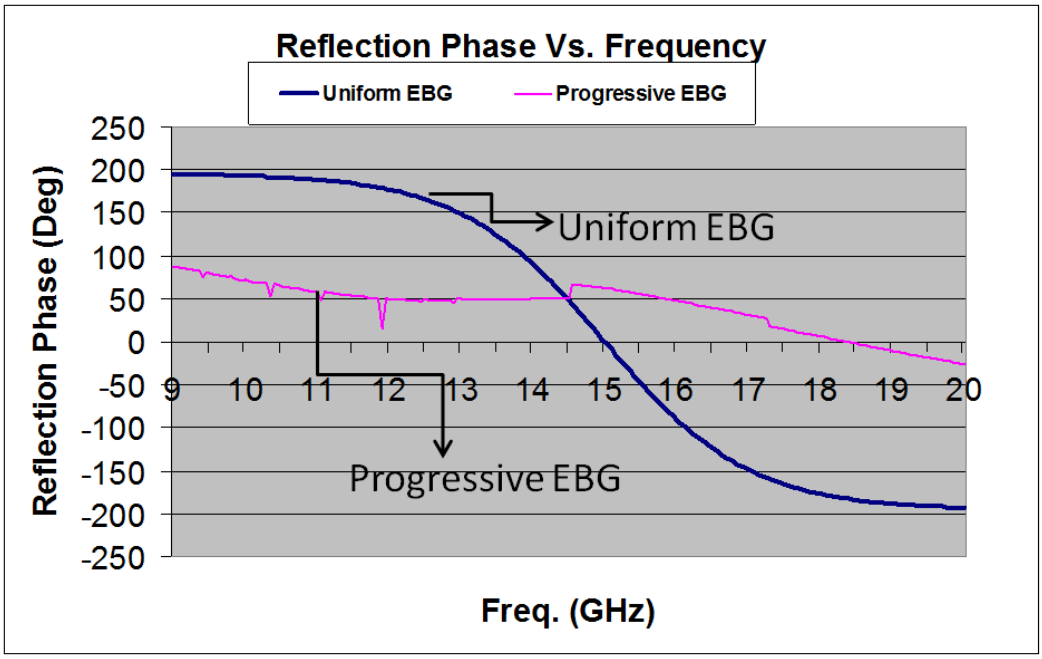

(a)

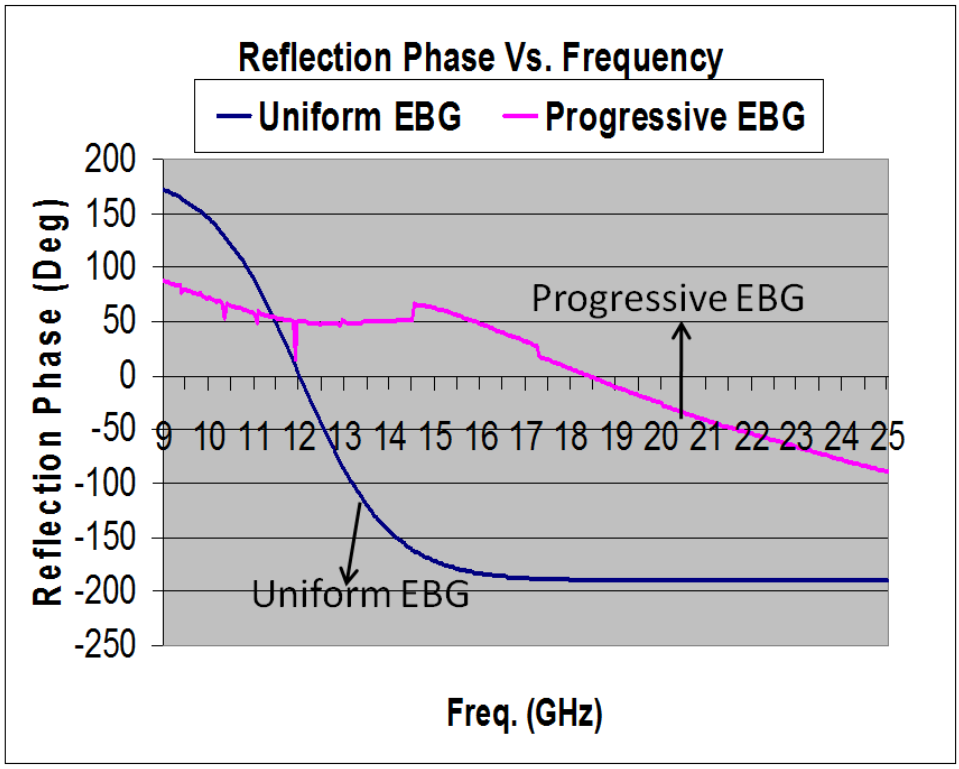

(b)

Figure 6.4: Normal incidence reflection-phase comparison of the 3-band (progressive) EBG against a 15-GHz uniform EBG (a) and a 12-GHz uniform EBG (b).

6.2 Progressive EBG application

The reflection-phase of the EBG structure is in the range of $\pm 90^{o}$, which produces addition of the incident and reflected signals in a quasi-constructive fashion. This is unlike the perfect electric conducting (PEC) surfaces, where the reflected signal is at 180^{O} in phase relative to the incident signal. This requires that patches and other radiators have to be elevated above the PEC plane such that reflected and incident waves do not cancel each other in the direction of radiation. Radiating elements can be placed at a small distance above the EBG surface, which results in reduction of the overall antenna size. An example is the wideband sinuous antenna that is backed by a cavity with absorbers to reduce the back lobe radiation. Using an EBG directly behind, or at a short distance from, the radiating sinuous element will reduce the cavity size and increase the gain in the forward direction. Simulation of the gain and axial ratio are presented in this section for a sinuous antenna in free space, and PEC (unloaded cavity), uniform EBG and progressive EBG backed sinuous antenna.

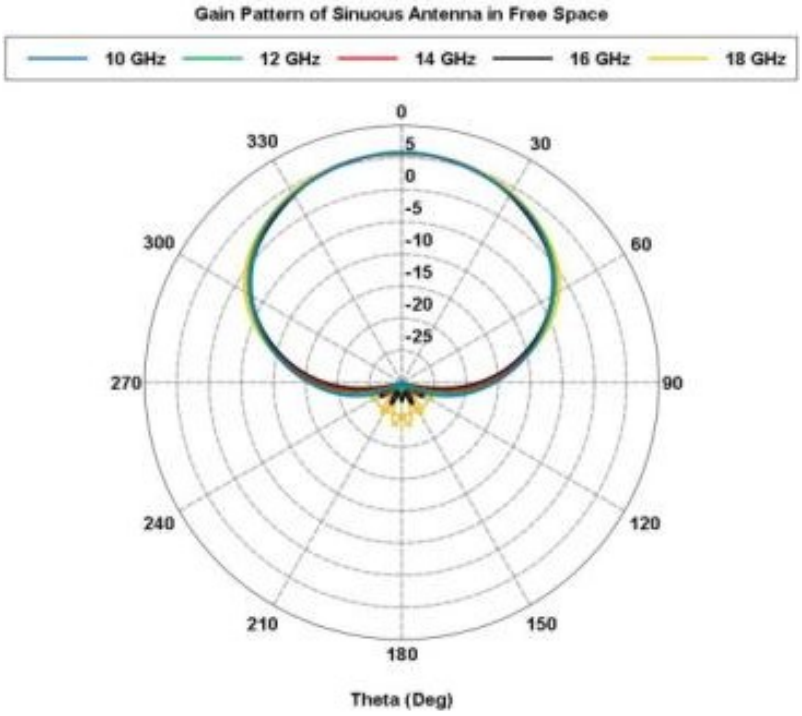

Figure 6.5: Gain patterns of antenna in Free Space.

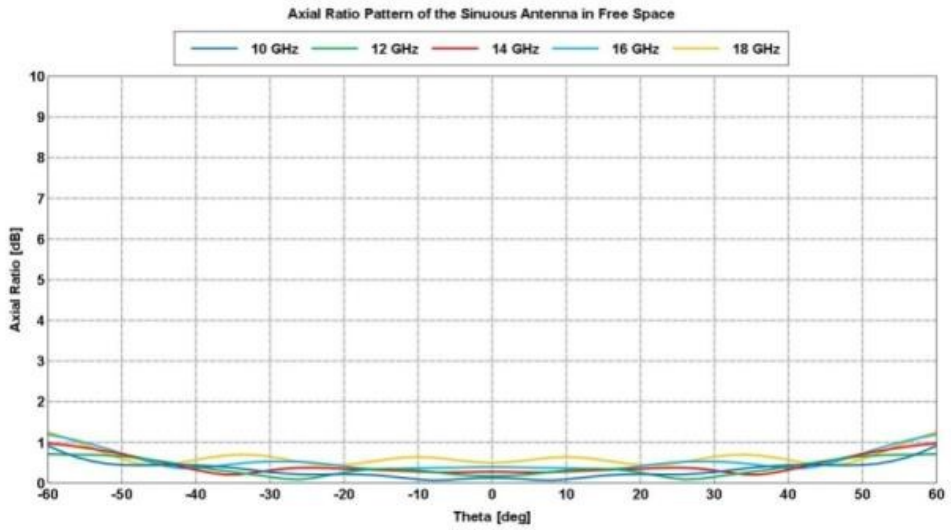

Figure 6.6: Axial ratio pattern of the antenna in free space.

Figure 6.5 and Figure 6.6 show the radiation pattern and axial ratio pattern of the sinuous antenna, respectively, in free space, while Figure 6.7 and Figure 6.8 show the radiation pattern and axial ratio pattern of the sinuous antenna, respectively, with an unloaded back cavity of 0.3 inches. Figure 6.9 and Figure 6.10 show the radiation pattern and axial ratio pattern of the sinuous antenna, respectively, with a uniform EBG loaded in the back cavity with a resonance at 12 GHz. Figure 6.11 and Figure 6.12 show the radiation pattern and axial ratio pattern of the sinuous antenna, respectively, with a progressive EBG loaded in the back cavity with resonances at 12 GHz, 15 GHz and 18 GHz.

Figure 6.13 shows the comparison of the boresight gain of the antenna under different loading conditions. It can be seen that the back cavity has a degrading effect on the performance of the antenna compared to the antenna in free space. The progressive EBG in the back cavity of the antenna exhibits better performance than a uniform EBG in the back cavity of the antenna.

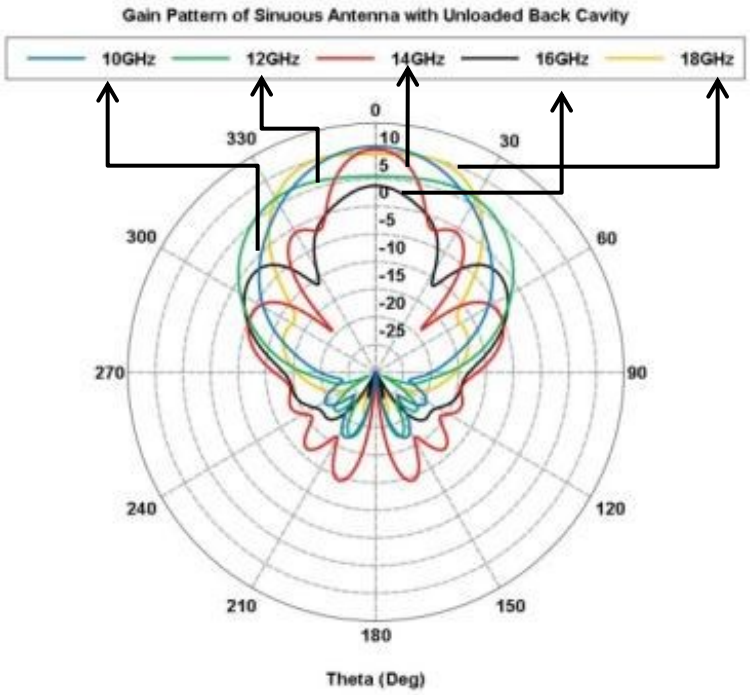

Figure 6.7: Gain pattern of the antenna with unloaded back cavity.

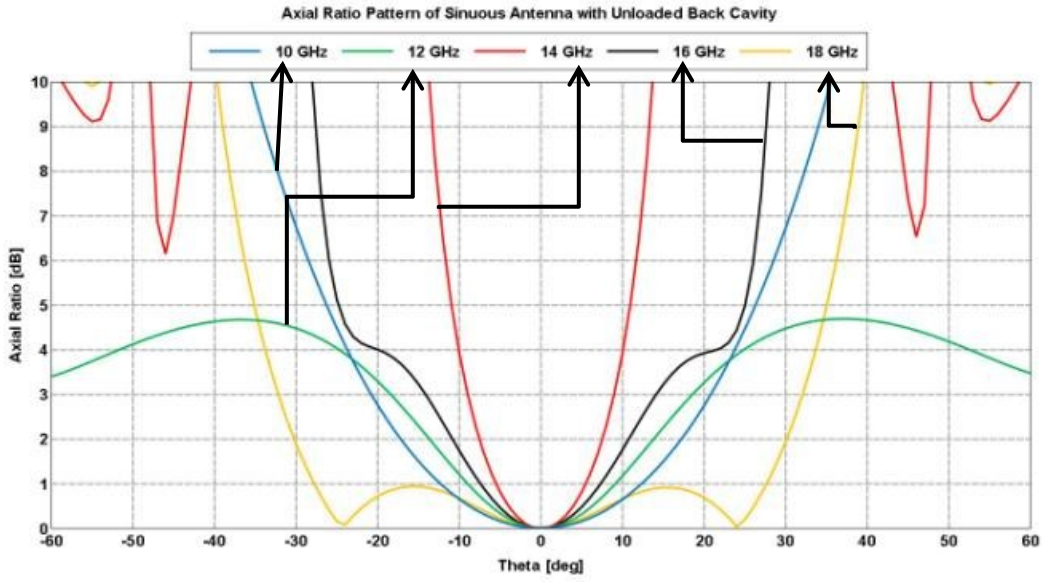

Figure 6.8: Axial Ratio pattern of the antenna with unloaded back cavity.

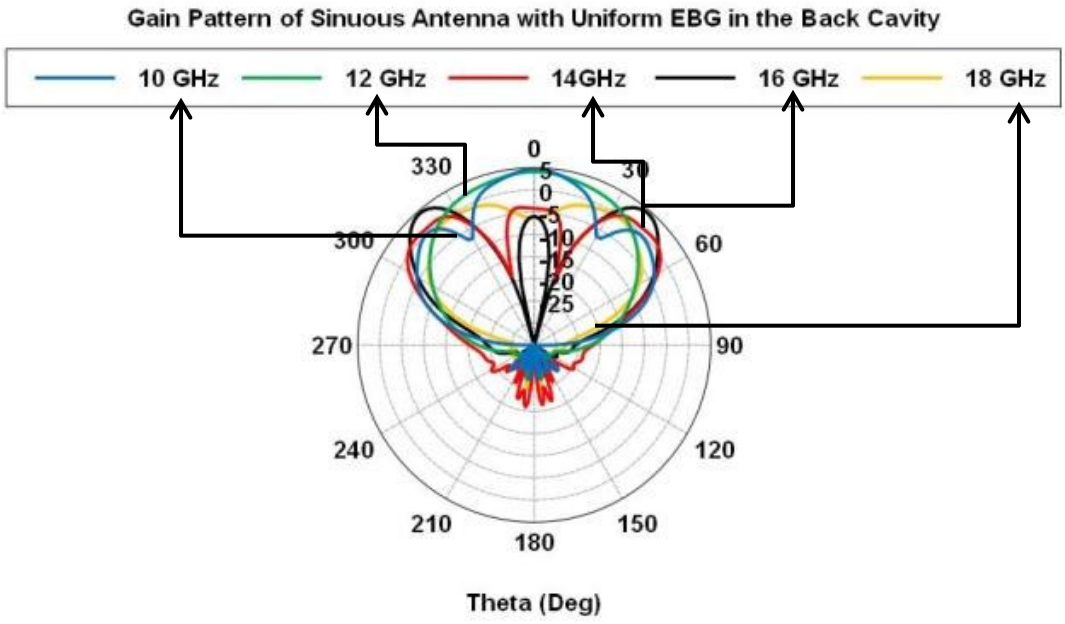

Figure 6.9: Gain pattern of the antenna with uniform EBG loaded back cavity.

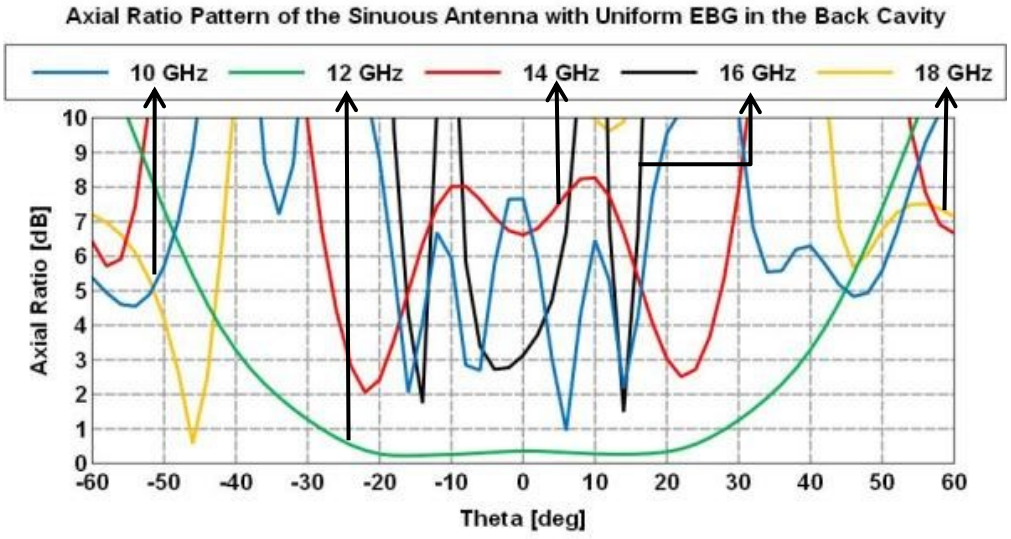

Figure 6.10: Axial Ratio pattern of the antenna with uniform EBG loaded back cavity.

Figure 6.7 and Figure 6.8, compared to Figure 6.5 and Figure 6.6, show that the unloaded back cavity degrades the performance of the sinuous antenna because the reflections from the back cavity might, or might not, add in phase with the forward propagating wave, depending on the frequency, and thus can degrade the performance of the antenna. Figure 6.9 and Figure 6.10 show that loading the cavity with uniform EBG has improved the performance of the antenna a bit, but

the uniform EBG does not have the required bandwidth to improve the performance of the antenna, since the uniform EBG has only one resonance at 12 GHz. Figure 6.11 and Figure 6.12 show that loading the cavity with the progressive EBG has improved the gain pattern of the antenna, and also improved the off-axis axial ratio. This is because the progressive EBG has enough bandwidth, due to multiple resonances, to cover the required bandwidth. Figure 6.13, compares boresight gain of the antenna under different loading conditions. Figure 6.13 shows that boresight gain of the sinuous antenna, with progressive EBG in the back cavity, is higher than with uniform EBG in the back cavity; and it is smoother when compared to unloaded back cavity case, and is higher compared to the antenna in free space case.

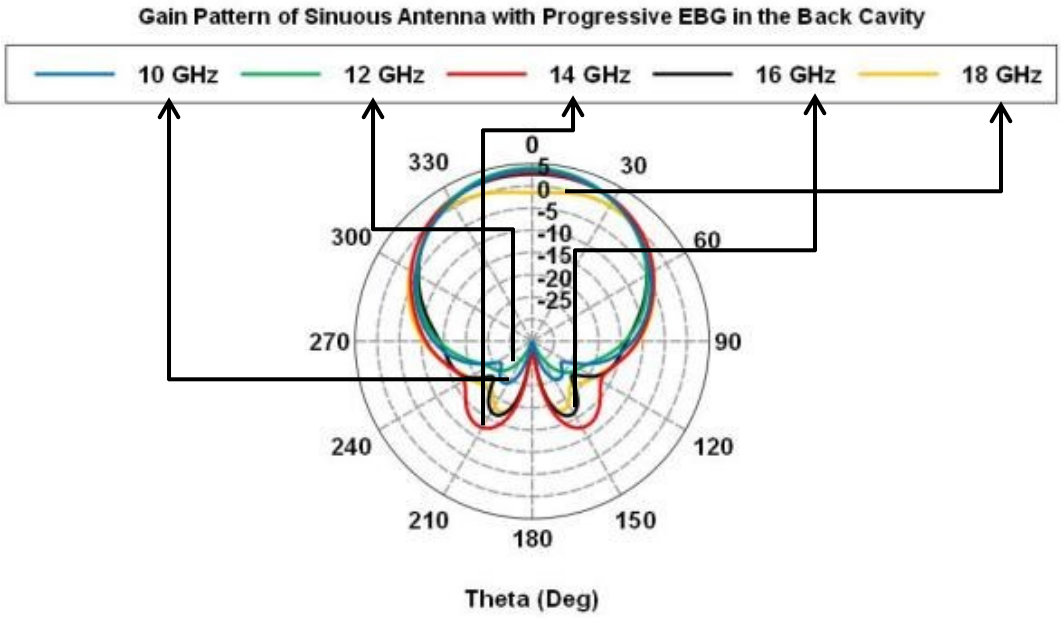

Figure 6.11: Gain pattern of the antenna with progressive EBG loaded back cavity.

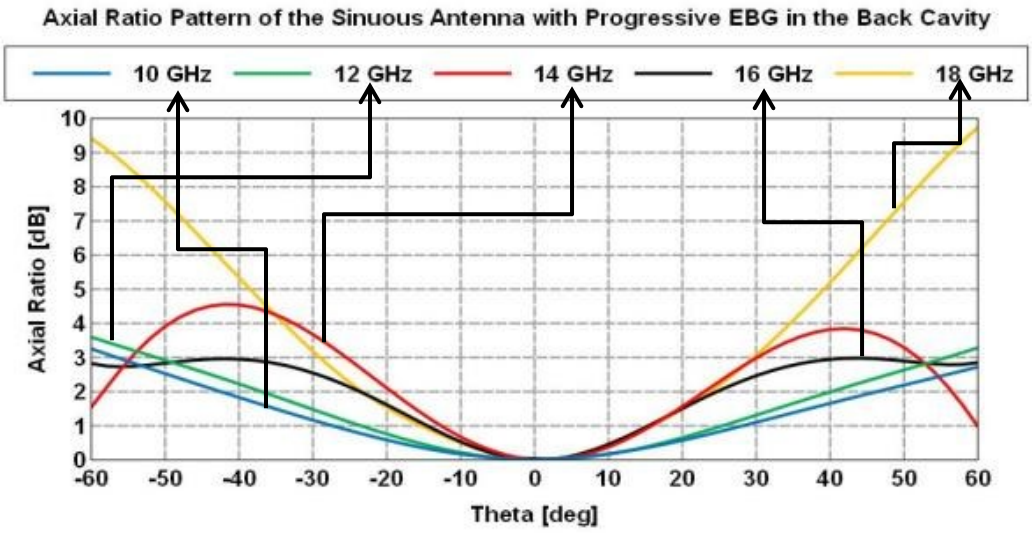

Figure 6.12: Axial ratio pattern of the antenna with progressive EBG loaded back cavity.

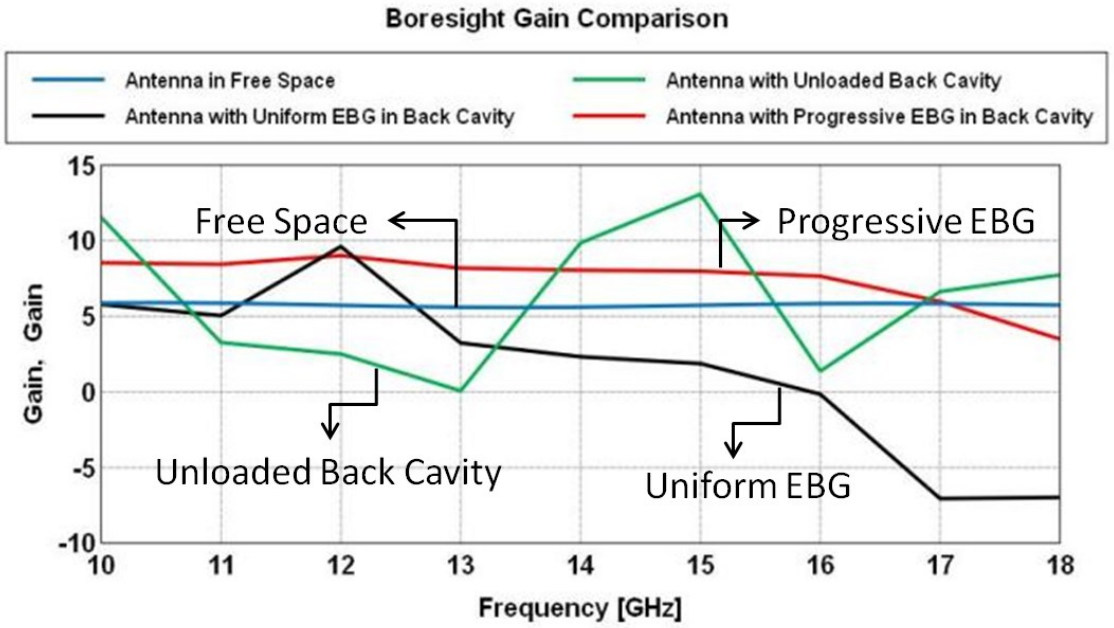

Figure 6.13: Boresight gain comparison of the different antenna configurations.

This section introduced progressive EBG structure, a way to increase the bandwidth of an EBG structure by cascading different size uniform EBGs that resonate close to each other in frequency. The performance of the progressive EBG is validated by loading it inside the cavity of a sinuous

antenna. The far field gain pattern and axial ratio pattern of the antenna is compared with different loadings of the back cavity.

7 UNIFORM HEIGHT PROGRESSIVE EBG STRUCTURES

7.1 Introduction to Uniform Height Progressive EBG Structures

To overcome the limited bandwidth of the uniform EBG surfaces, two broadband designs were developed. A progressive EBG structure uses concentric unit cells that are progressively increasing in size to correspond to decreasing concatenating resonance frequencies to form the required broadband. The height of the different sections may vary as seen in the previous chapter or uniform as shown in Figure 7.1. A stacked EBG structure uses separate layers that cover closely spaced or harmonic frequency bands that form the required broad band. The stacked design is used when the total surface is covered with the broadband, while the progressive design is suitable for surfaces that have distinct identifiable frequency regions in the broadband [50, 51, 52, 53].

The uniform height progressive EBG structure is used with a spiral antenna, as shown in Figure 7.1, and the antennas performance in this setup is compared with the free space performance of the antenna and antenna with a regular uniform EBG structure that resonates at approximately 15 GHz. Figure 7.2 compares the reflection phases off the uniform height progressive EBG and regular EBG structures, computed using commercially available EM simulation tool FEKO. Figure 7.2 shows that the uniform height progressive EBG structure has a wider band gap than regular EBG structure. Band gap is measured as the bandwidth over which the reflection-phase falls between $+90^0$ and -90^0.

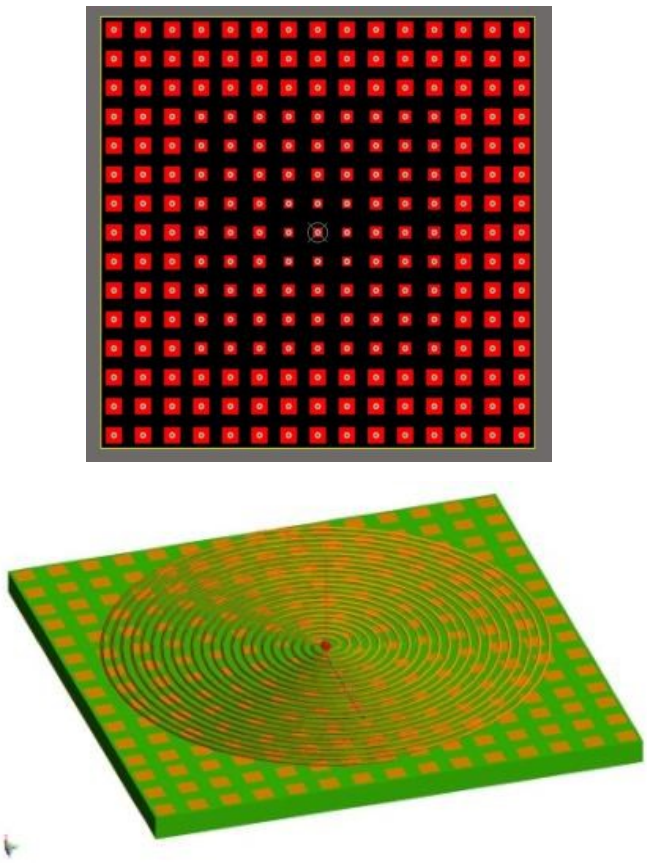

Figure 7.1: (a) Progressive EBG surface layout (b) Spiral antenna over uniform height progressive EBG surface.

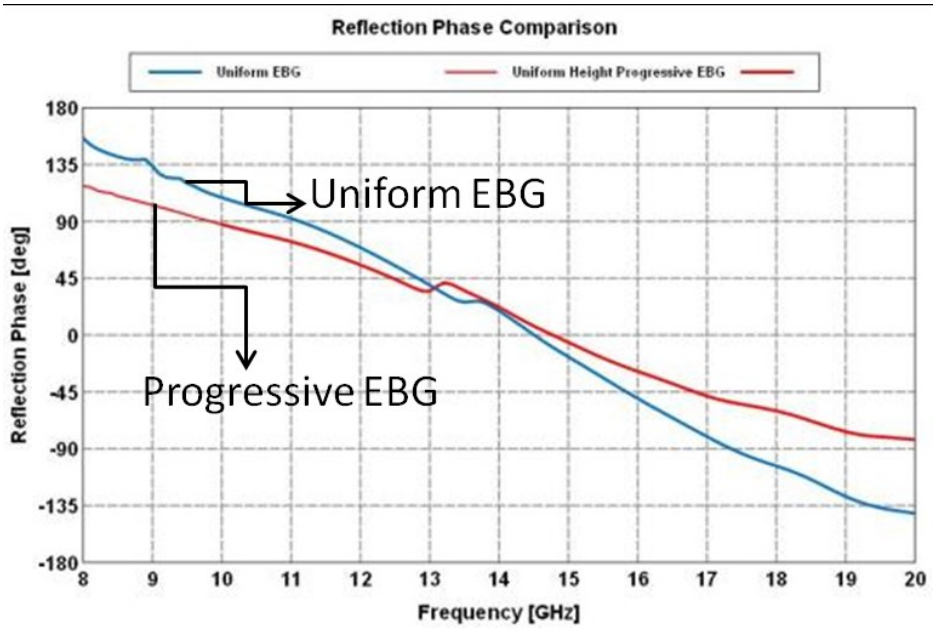

Figure 7.2: Reflection-phase comparison.

7.2 Spiral Antenna over Broadband Progressive EBG Structure

The uniform-height progressive EBG structure is used underneath a spiral antenna and its performance is simulated using the full-wave analysis method-of-moment-based tool FEKO, and the performance is compared to the antenna performance in free space and the performance of the antenna near a regular EBG structure. The spiral over the EBG is shown in Figure 7.1.

The performance of the spiral antenna under different conditions is shown in the next set of Figures. Figure 7.3 shows the gain patterns on the spiral antenna in free space, while Figure 7.4 shows the gain patterns of the spiral antenna placed close to regular EBG structure and Figure 7.5 shows the gain patterns of the spiral antenna placed close to uniform height progressive EBG structure. Figure 7.6 shows the return loss comparison of the spiral antenna under different loadings. Figure 7.7 shows the boresight gain comparison of the spiral antenna under different loadings, while Figure 7.8 shows the boresight axial ratio comparison of the spiral antenna under different loadings. Figures 7.3 through 7.8 show the high gain and high front-to-back ratio of the radiation pattern across the broadband of the spiral antenna near uniform height progressive EBG compared to the spiral antenna near regular EBG. This is accomplished with low profile that is afforded by the reflection-phase characteristics of the broadband EBG. This low profile is in contrast with the higher profile design that uses PEC-backed or absorber-backed cavities. It is clear that the uniform height progressive EBG structure has a wider band gap, compared to the regular EBG structure, which helped in achieving the broadband performance improvement of the spiral when placed near the uniform height progressive EBG structure.

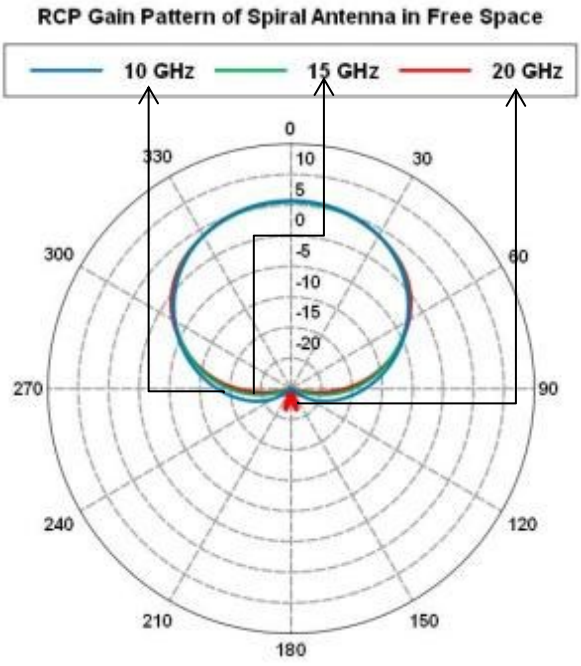

Figure 7.3: Gain patterns of the spiral antenna in free space.

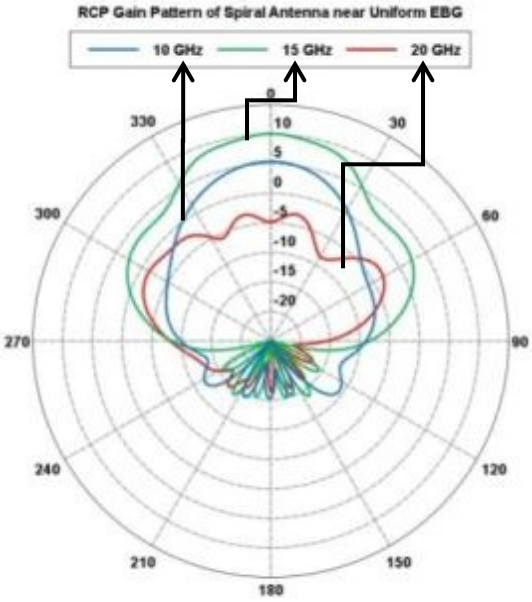

Figure 7.4 Gain patterns of the spiral antenna near regular EBG.

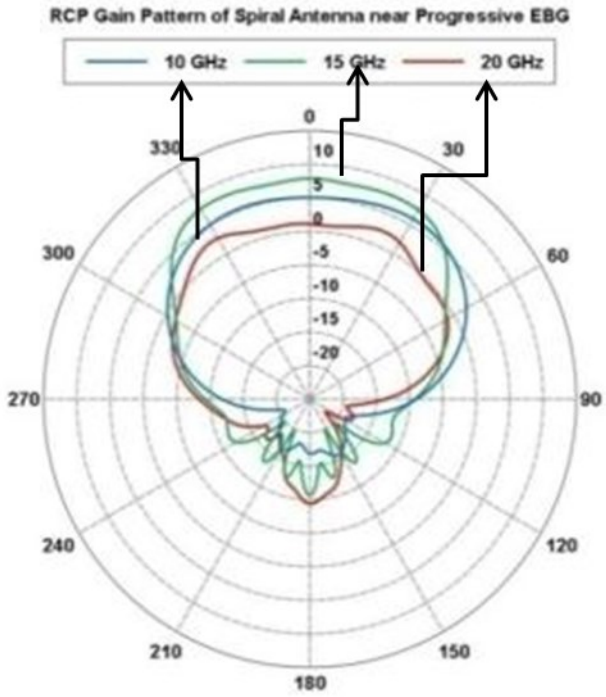

Figure 7.5: Gain patterns of the spiral antenna near uniform height progressive EBG.

Figure 7.6: Return Loss comparison of the spiral antennaunder different loading conditions.

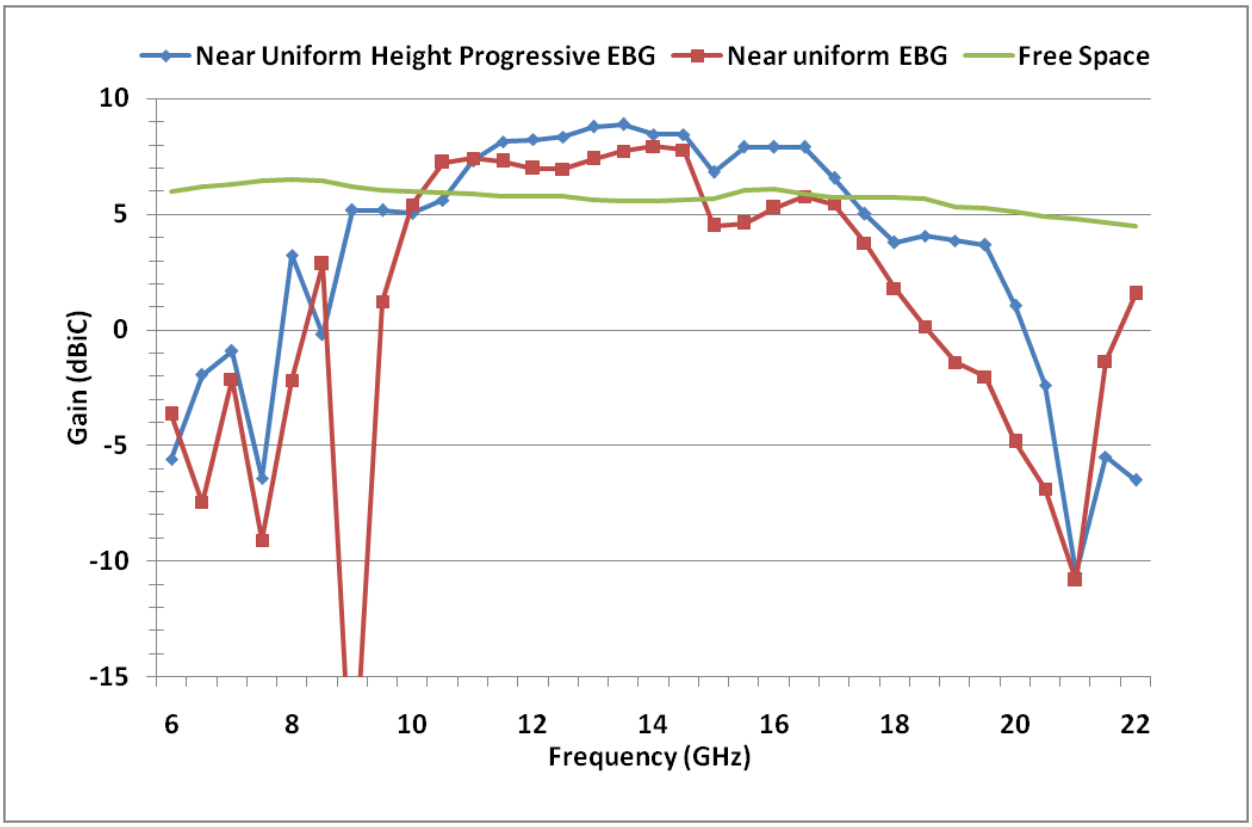

Figure 7.7: Boresight gain comparison of the spiral antenna under different loading conditions.

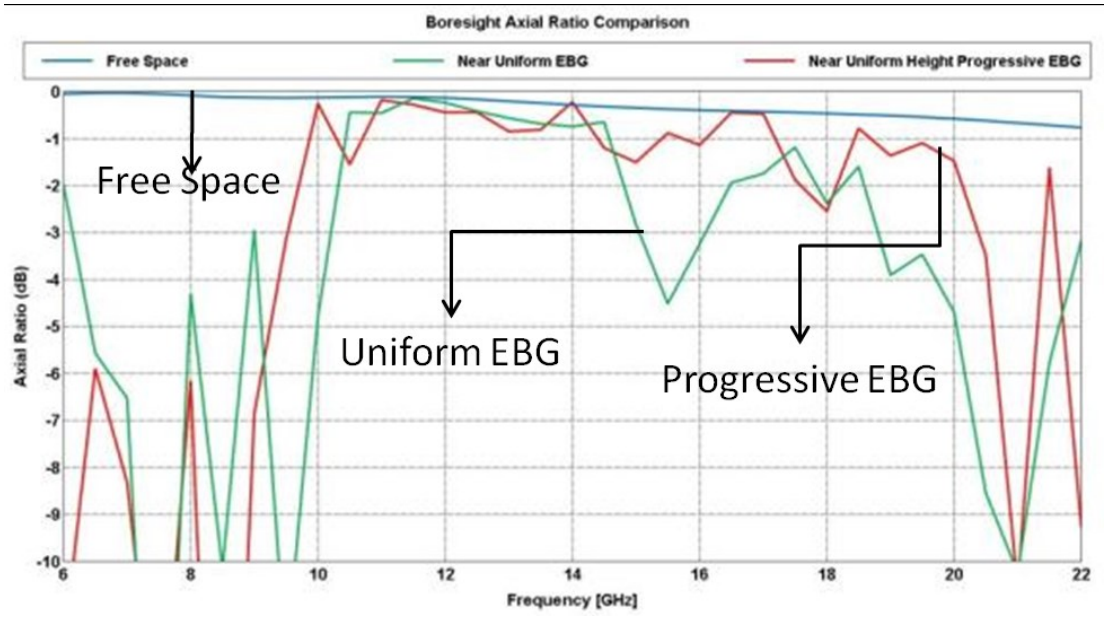

Figure 7.8: Boresight axial ratio comparison of the spiral antenna under different loading conditions.

7.3 Uniform height progressive EBG Structure

Progressive EBG structures, like spiral antennas, resonate at different parts of EBG surface for different frequencies, hence spiral antenna works best with progressive EBG structures. A spiral antenna and a balun, to feed the spiral antenna, are designed to work with progressive EBG. To understand the benefits of progressive EBG, spiral antenna return loss, boresight gain and radiation patterns are compared under different conditions.

Figures 7.9 and 7.10 compare simulated return loss and boresight gain performance respectively of spiral antenna under different conditions. To understand the benefit of progressive EBG over regular EBG, gain patterns of spiral antenna over progressive EBG and regular EBG are compared in Figure 7.11. It is evident from Figure 7.11 that progressive EBG has wider bandwidth compared to regular EBG, as shown in Figure 7.2, which leads to smoother gain patterns over broadband.

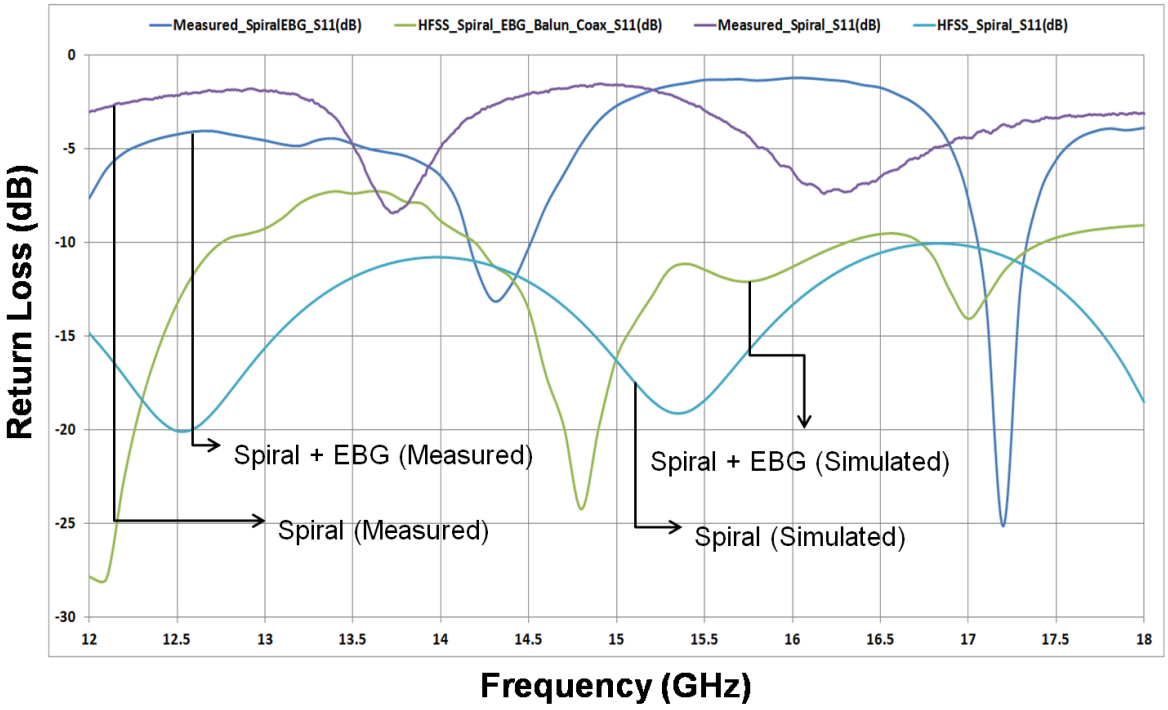

Figure 7.9: Return loss comparison of spiral antenna.

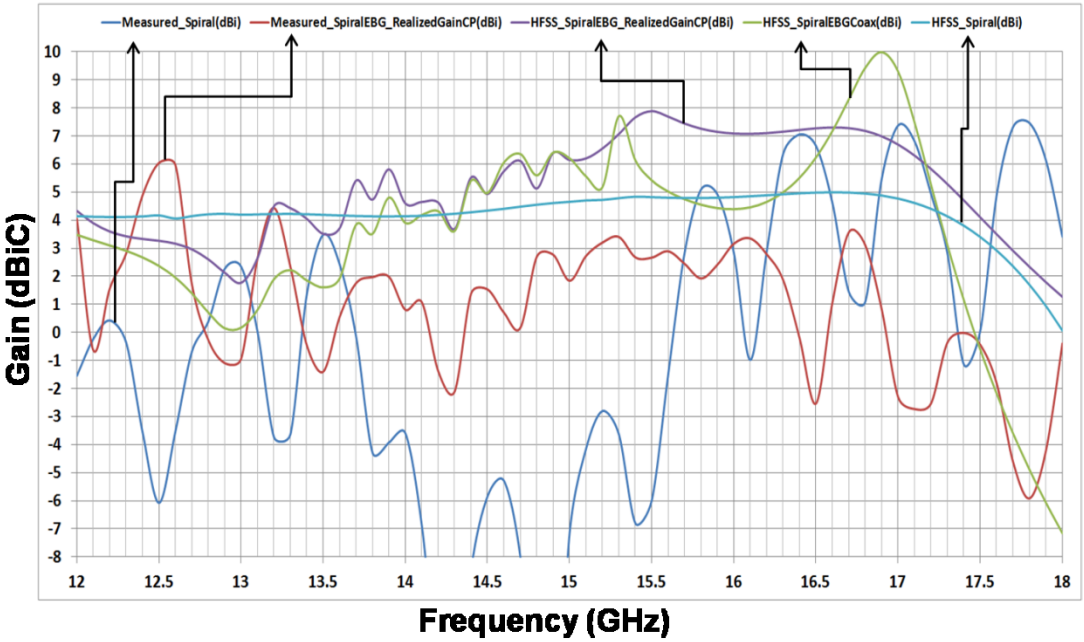

Figure 7.10: Boresight gain comparison of spiral antenna.

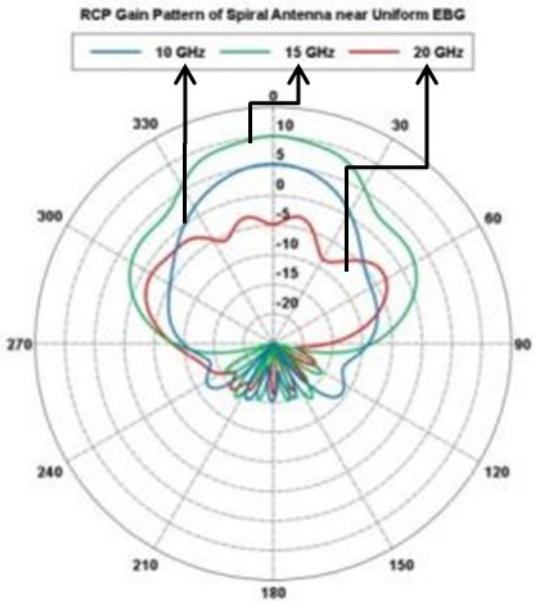

(a)

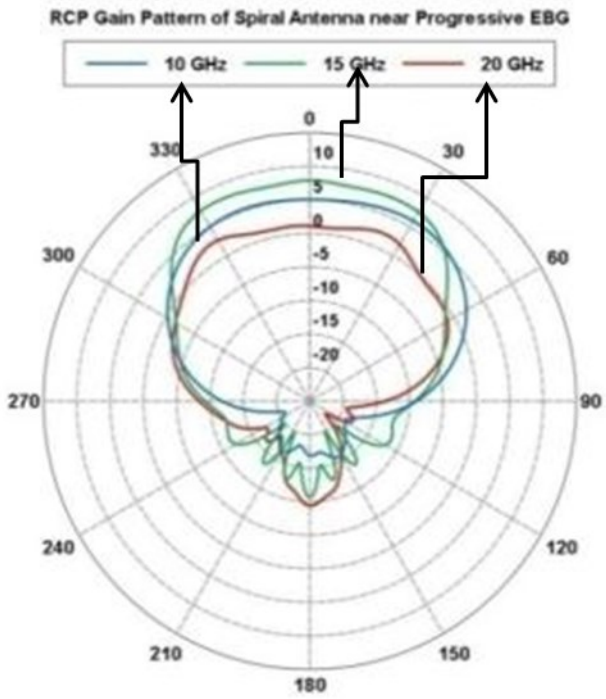

(b)

Figure 7.11: Gain patterns of the spiral antenna near regular (top) and progressive (bottom) EBG.

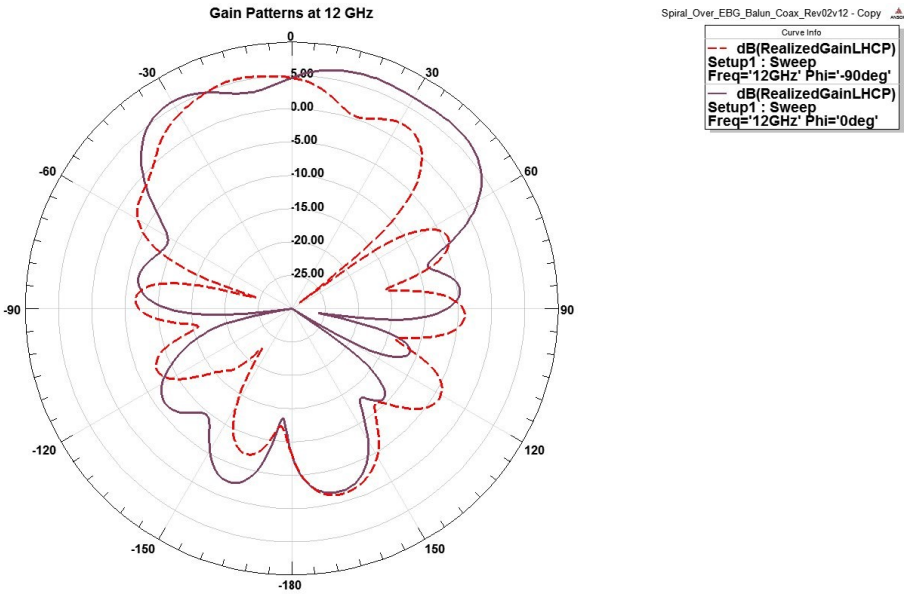

Figure 7.12: Gain patterns of spiral antenna over uniform height EBG Structure at 12 GHz in E-plane (solid) and H-plane (dash).

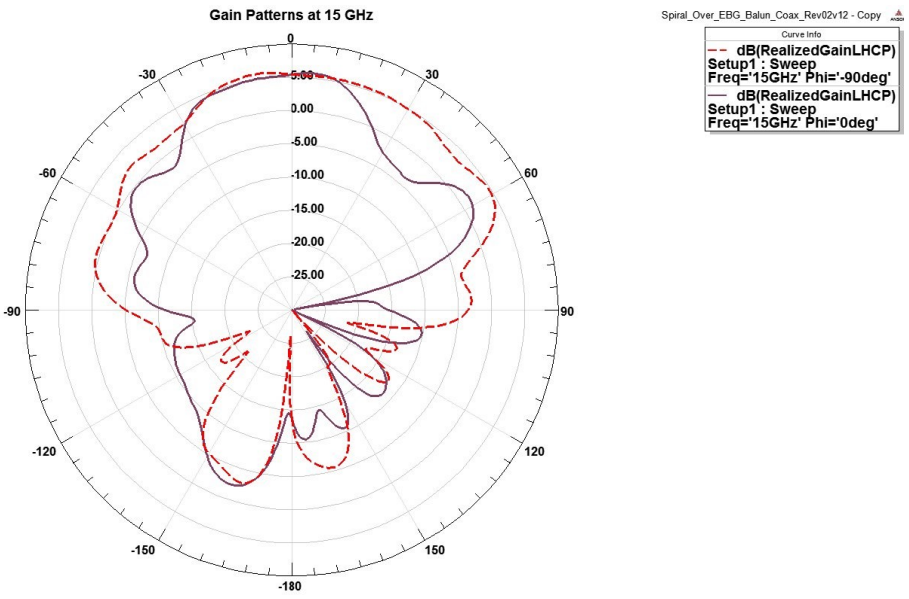

Figure 7.13: Gain patterns of spiral antenna over uniform height EBG Structure at 15 GHz in E-plane (solid) and H-plane (dash).

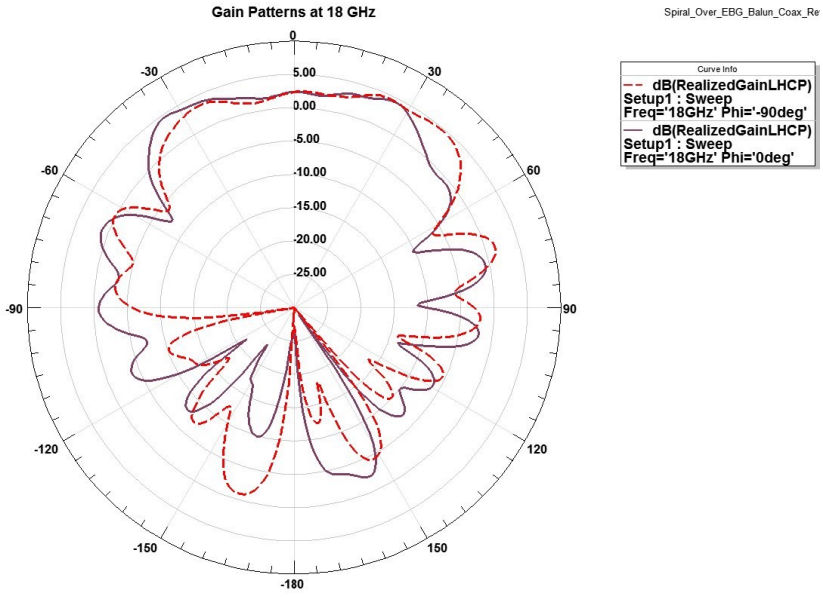

Figure 7.14: Gain patterns of spiral antenna over uniform height EBG Structure at 18 GHz in E-plane (solid) and H-plane (dash).

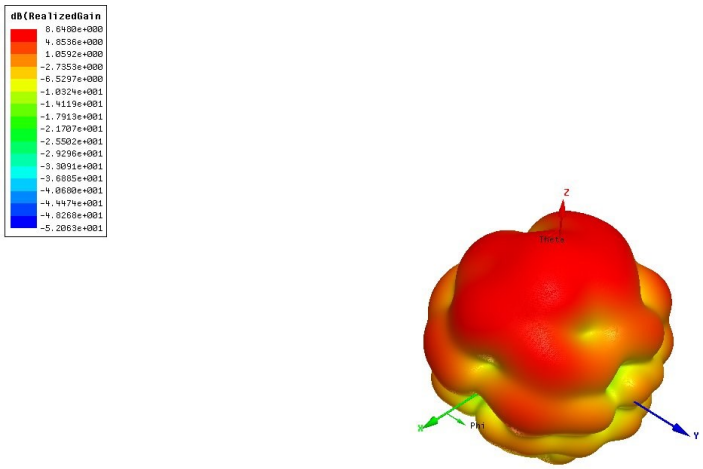

Figure 7.15: 3D Gain pattern of spiral antenna over uniform height EBG Structure at 12 GHz.

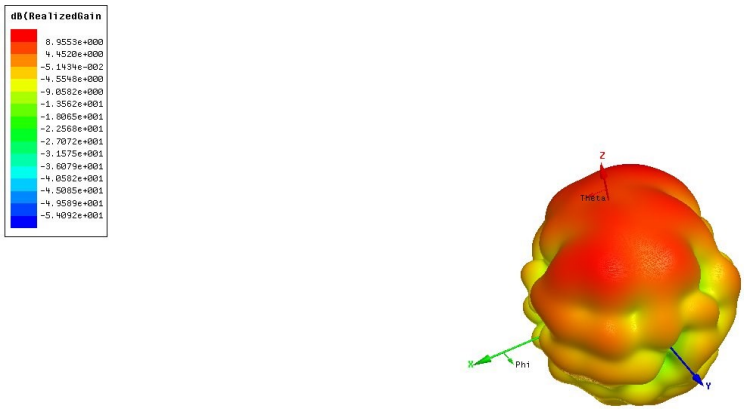

Figure 7.16: 3D Gain pattern of spiral antenna over uniform height EBG Structure at 15 GHz.

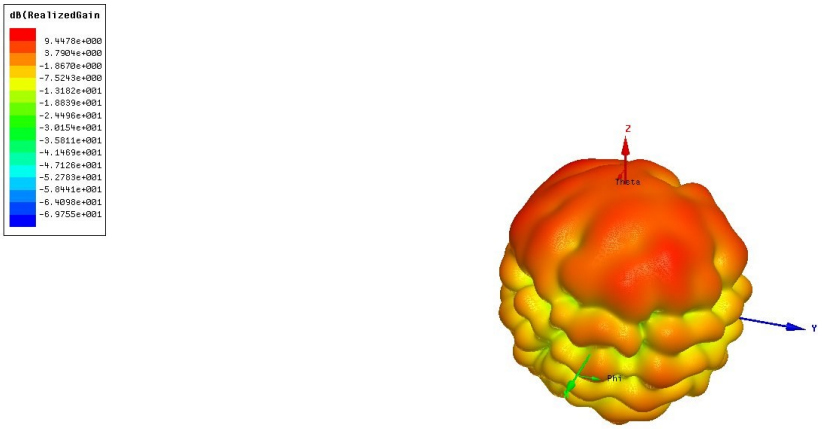

Figure 7.17: 3D Gain pattern of spiral antenna over uniform height EBG Structure at 18 GHz.

It is evident from Figure 7.10 the HFSS simulated boresight gain of spiral antenna increases with progressive EBG, when compared with boresight gain of antenna without progressive EBG.

From Figures 7.10 and 7.11, it is evident that progressive EBG has wider band gap than a uniform EBG and it can be used with a spiral antenna to increase the boresight gain of the spiral antenna while obtaining smoother gain patterns. Figures 7.12 through 7.14 show gain patterns of spiral antenna with uniform height progressive EBG at 12 GHz, 15 GHz and 18 GHz respectively, while Figures 7.15 through 7.17 show 3D patterns of spiral antenna with uniform height progressive EBG at 12 GHz, 15 GHz and 18 GHz respectively. From Figures 7.12 through 7.17 it can be seen that gain patterns are not symmetric because uniform height progressive EBG is not symmetric, with respect to spiral antenna, in both the principal planes. This section showed a way to increase the bandwidth of EBG structures, by progressively cascading uniform EBG structures. A broadband progressive EBG is used with a broadband spiral antenna and return loss,boresight gain and gain patterns of the antenna are compared under different conditions.

8 FABRICATION AND MEASUREMENTS

8.1 Fabrication

Electromagnetic band gap (EBG) structures can be manufactured easily with existing microstrip line and circuit board manufacturing techniques [15, 54, 55]. The UWB antenna and the stacked EBG is built using circuit board etching techniques on Rogers 5880 boards [56] and a coax connector is soldered to the UWB antenna to feed the co-planar waveguide. Spiral antenna, balun and progressive EBG are etched on appropriate dielectric boards (Rogers 5880) and thebalun is soldered to the spiral arms. To accommodate feeding balun a hole is drilled at the center of the progressive EBG, this hole is also used to support and center the feeding balun. Figure 8.1 shows the manufactured and assembled UWB antenna and stacked EBG structure together. Notice the coax cable that is run around the housing of the stacked EBG structure to feed the antenna. The center conductor of the coax cable is soldered to the center line of the coplanar waveguide input to the antenna, while the outer conductor of the coax connector, attached to the connector flange, is soldered to the ground strips of the coplanar waveguide.

The UWB antenna is fed by the TEM wave in coax connector feeding the even mode of the coplanar waveguide. The antenna radiates by the electric field formed between ground strips of the coplanar waveguide and the circular patch element in the antenna. The circular patch element gives the UWB operation of the antenna. Figure 8.2 shows the UWB antenna dimensions, while Figure 8.3 shows the arrangement of the UWB antenna and stacked EBG structure. The entire EBG structure consists of ground plane at the bottom, and an air gap (filled with styro foam) of 3/16 inches followed by EBG circuit on Rogers 5880 board (0.020" thick) followed by an air gap (filled with styro foam) of 3/16 inches followed by EBG circuit on a roger 5880 board (0.020" thick) followed by an air gap (filled with styro foam) of 5/8 inches, followed by another EBG circuit on roger 5880 board (0.020" thick) followed by an air gap of 2.75 inches, which is accomplished by using two styro foam layers of 1.875 inches and 0.875 inches thick. UWB antenna is placed over this entire stacked EBG structure, as shown in Figures 8.1 and 8.3. All the EBG layers are etched on both sides, with one side (closer to the antenna) etched with EBG circuit and the other side completely etched out.

Figure 8.1: Manufactured UWB antenna over stacked EBG structure, along with Coax cable for feeding the antenna.

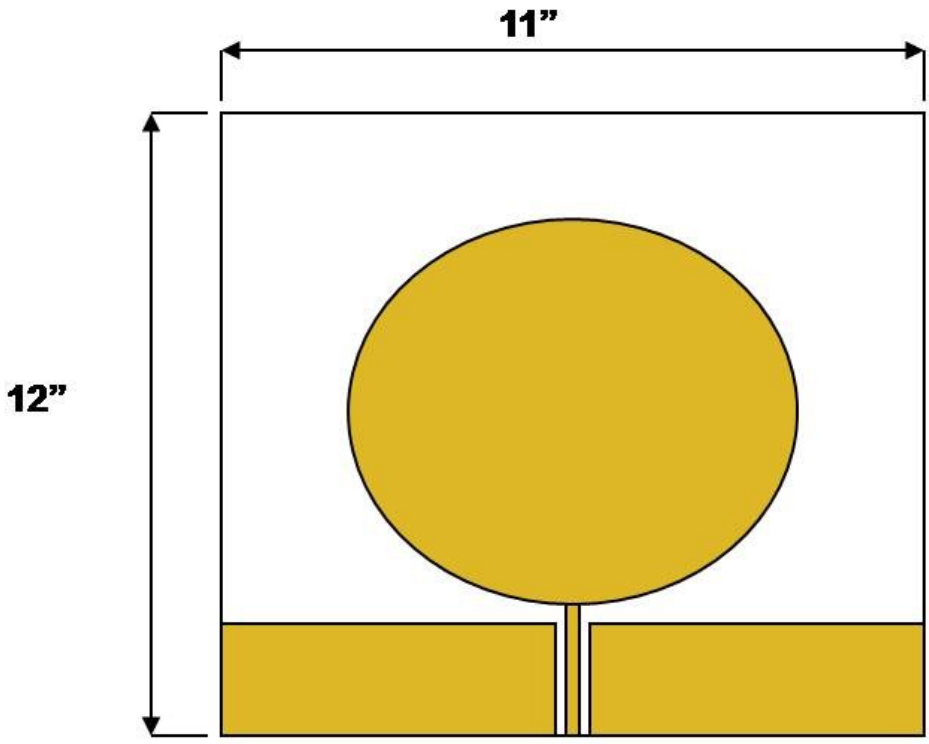

Figure 8.2: UWB antenna used with stacked EBG structure and its dimensions.

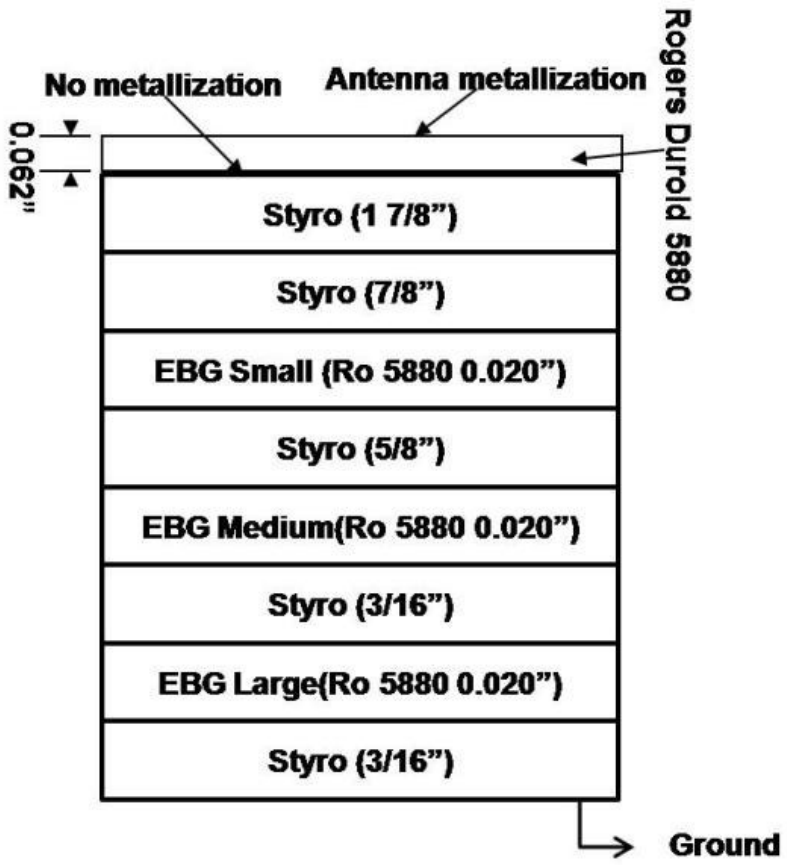

Figure 8.3: Arrangement of the UWB antenna and stacked EBG structure along with dimensions.

Progressive EBG is manufactured, by etching the EBG circuit, on one side and not etching the other side to form ground plane, on Rogers 5880 board which is 0.125 inches thick. Figure 8.4 shows the spiral antenna and progressive EBG structure together along with their dimensions. Notice the rectangular hole in the center of progressive EBG structure for the balun used to feed the spiral antenna. The spiral antenna is fed by a balun, one arm of the spiral antenna is soldered to one of the strips of the balun, and the other arm is soldered to the other arm of the balun. Balun is fed by a coax; the center conductor of the coax is soldered to one of the strips of balun, while the outer conductor of coax is soldered to the other strip of the balun. The spiral antenna is fed by the TEM wave in coax connector feeding the balun, which feed the balanced signal to the arms of the spiral antenna. The circular polarity of the spiral antenna depend on the circular orientation of the arms, with counter clockwise turned spiral antenna giving right hand circular polarization, when looked head-on, and clockwise turned spiral antenna giving left hand circular polarization.

The spiral antenna used is an archimedean spiral antenna, whose air gap between turns is equal to the width of spiral arms; this makes the input impedance of the spiral antenna to be 188 ohms. Balun is designed to transform 50 ohms of the coax connector to 188 ohms of the spiral antenna in the frequency band of interest. The antenna radiates by the electric field formed between the spiral arms of the antenna. Bandwidth of the spiral antenna is determined by the overall size of the spiral antenna and the distance between the spiral arms at the center of the antenna. Figure 8.5 shows manufactured spiral antenna, notice solder joints that connect spiral arms to the feeding balun, also notice progressive EBG structure in the background. Figure 8.6 shows manufactured progressive EBG structure, notice rectangular hole at the center to allow balun through to feed spiral arms.

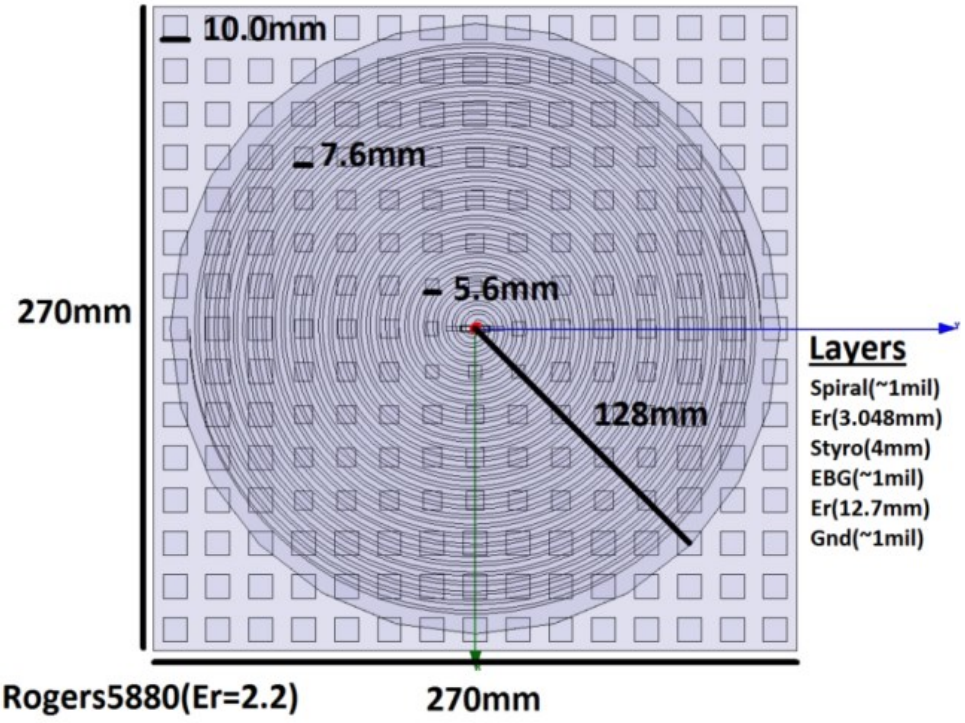

Figure 8.4: Spiral antenna over broadband progressive EBG structure, along with dimensions.

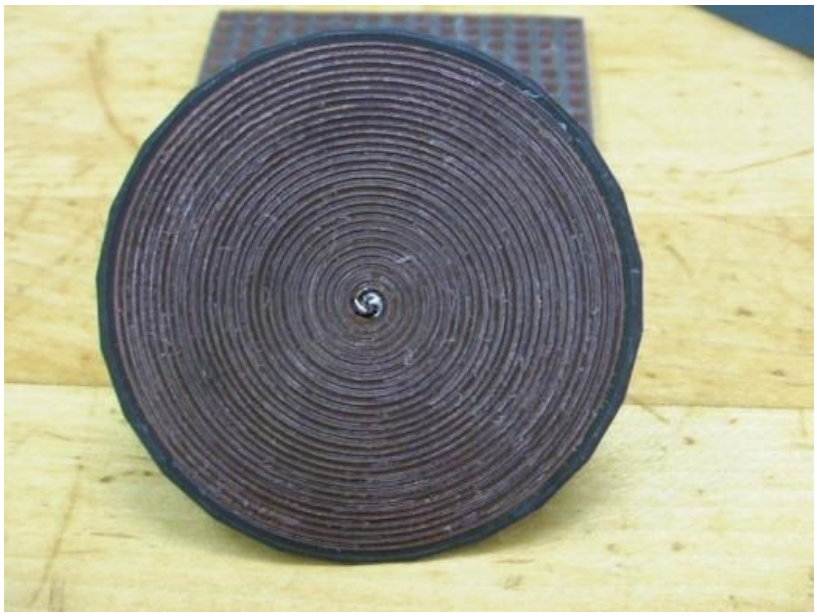

Figure 8.5: Manufactured spiral antenna, notice the solder joints connecting balun arms to spiral arms.

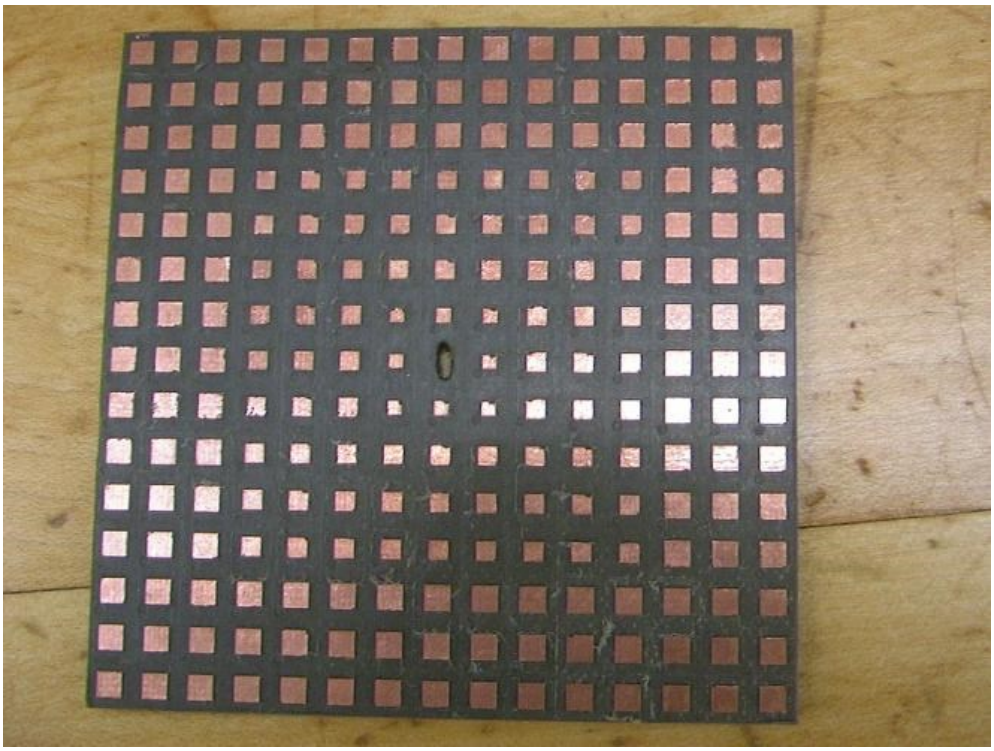

Figure 8.6: Manufactured progressive EBG structure. Notice rectangular hole at the center to allow balun through to feed spiral arms.

Spiral antenna over progressive EBG structure assembly consists of ground plane at the bottom followed by Rogers 5880 followed by EBG circuit followed by air gap (filled with styro foam) of 4mm followed by Rogers 5880 board on which spiral antenna is etched, as shown in Figure 8.4. The fabrication is made much easier by the absence of vias between the patches and ground plane, otherwise vias would need to be drilled between the patches and the ground plane which is time consuming and expensive. Progressive EBG structure is designed to have uniform height even when patch sizes are varying; this made manufacturing a lot easier, by only requiring one dielectric board which is used to etch the entire progressive EBG circuit.

In progressive EBG structures, the capacitance is realized by fields coupled between the patches through the gap, while the inductance is realized by the gap between the patches and the ground plane. For stacked EBG structures, capacitances are realized by coupling between adjacent patches within the same layer and coupling between patches between surrounding layers, while the inductance is realized by the gap between adjacent EBG layers and the ground plane for the bottom layer. The resonance frequency for the individual layer is determined by the tank circuit formed by the effective capacitance and inductance of that layer. The broad band for both the progressive and stacked EBG structures is achieved by cascading, progressively into one layer and vertically in multiple layers respectively, multiple uniform EBG structures similar to cascading multiple sections in a filter to achieve broader desired bandwidth.

8.2 Measurements

Stacked EBG structure is used with UWB antenna to improve the off boresight gain of the antenna comparable to a vivaldi antenna whose size is larger than UWB antenna with stacked EBG. Return loss and off boresight gain of the antenna is measured and compared to the simulated results and the performance of vivaldi antenna. Before any measurements are made, required assembly is completed. This includes assembling the EBG layers with appropriate styro foam layers and packaging the EBG structure properly. The assembled EBG structure is then assembled with styro foam and the suitable antenna and then the required feeding elements are soldered, this include soldering coax connector with cable to the UWB antenna that is then assembled on top the UWB antenna with appropriate styro foam layers. For the progressive EBG structure, spiral antenna is properly installed over it and the balun is routed through the hole in the

progressive EBG and then the spiral arms and balun arms are soldered, making sure the solder joints do not connect one another. Then the coax connector is soldered to the other end of the balun to feed the spiral antenna through the balun. Figure 8.7 shows return loss measurement setup using network analyzer and anechoic chamber. For return loss measurements, one-port network analyzer calibration and one-port measurements are acceptable, in which case it is only necessary to connect one port of the network analyzer to the feed assembly being tested (also referred to as the Device Under Test, or "DUT"). The return loss is measured by the following procedure:

Required Equipment:

1. Network Analyzer (vector or scalar) and test cables and adapters
2. Calibration kit

Measurement Approach:

1. Set up equipment per Figure 8.7, using manufacturer's instructions as a guide.
2. Turn on equipment and allow a necessary stabilization period.
3. Set the network analyzer to sweep the frequency band under test.
4. Calibrate the network analyzer per manufacturer's instructions using appropriate calibration standards as required for the frequency band under test.
5. The following network analyzer settings are recommended for this measurement. They may be changed at the test conductor's discretion.
    a. Measurement - S11 or S22 (depending on network analyzer port being used).
    b. Format - Log Mag, dB (Return Loss).
    c. Scale - 5.0 dB/Div.
    d. Ref level - 0 dB.
    e. Ref position - 1 or 2 divisions from top of display.
    f. Install the necessary waveguide components to interface the network analyzer port to the appropriate test port of the DUT. The horn aperture of the DUT should be loaded into the absorber chamber or a piece of absorber material should be placed in front of the horn aperture.
6. Record the return loss trace to the network analyzer memory and/or print out a hardcopy. Assign a descriptive filename to the trace file and/or indicate on the hardcopy the measurement that was made.

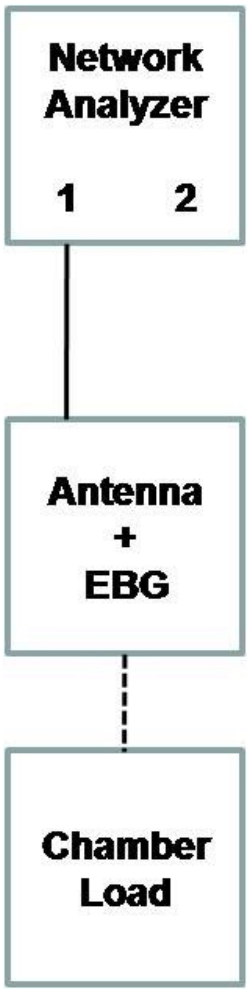

Figure 8.7: Return loss measurement setup.

To measure the gain of DUT, setup shown in Figure 8.8 is used; the following test equipment or its equivalent is utilized:

1. Vector Network Analyzer
2. Signal Source
3. Coax-to-Waveguide adapter(s)
4. Positioner Controller
5. Source horn

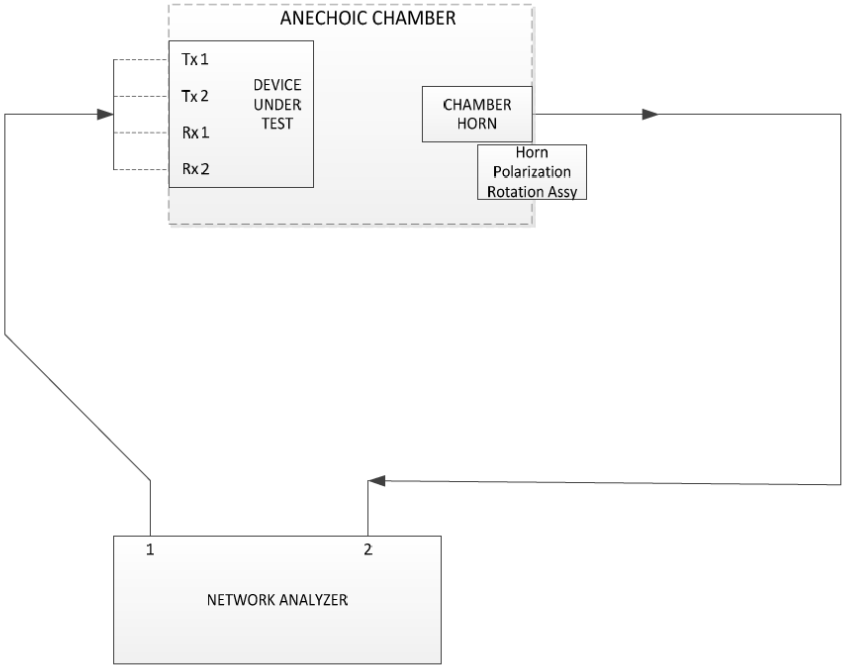

Figure 8.8: Gain measurement setup.

Gain is measured as follows:

1. Set up equipment per Figure 8.8, using manufacturer's instructions as a guide.
2. Turn on equipment and allow a necessary stabilization period.
3. Connect the mixer to input port of the DUT.
    a. For a linear polarized antenna: Ensure that the port is mounted such that the radiation out of the feed horn is vertical. This will be an H-plane cut.
    b. For a circular polarized antenna: Orient the port mounting per the testing requirements.
4. Set the RF signal source to the appropriate frequency band.
5. Adjust the source polarization positioner such that the output signal strength is maximized. Adjust the AUT positioner in azimuth, elevation, and polarization (if applicable) for maximum received signal.
6. Sweep the frequency and record the gain.
7. Use the substitution method to get the gain of DUT.

Return loss of UWB antenna with Stacked EBG and spiral antenna with progressive EBG is measured as described above, but the gain of the of the spiral antenna is measured at boresight, while gain of the UWB antenna is measured at off-boresight using the method described above.

8.3 Measured versus Simulated Results for UWB Antenna over Stacked EBG

The designed and fabricated three layer stacked EBG structure is used with the UWB antenna to enhance its off-boresight peak gain. Shown in Figure 8.9 is the gain of the UWB antenna, and the goal of using the stacked EBG layers is to obtain positive gain for at least 3:1 band.

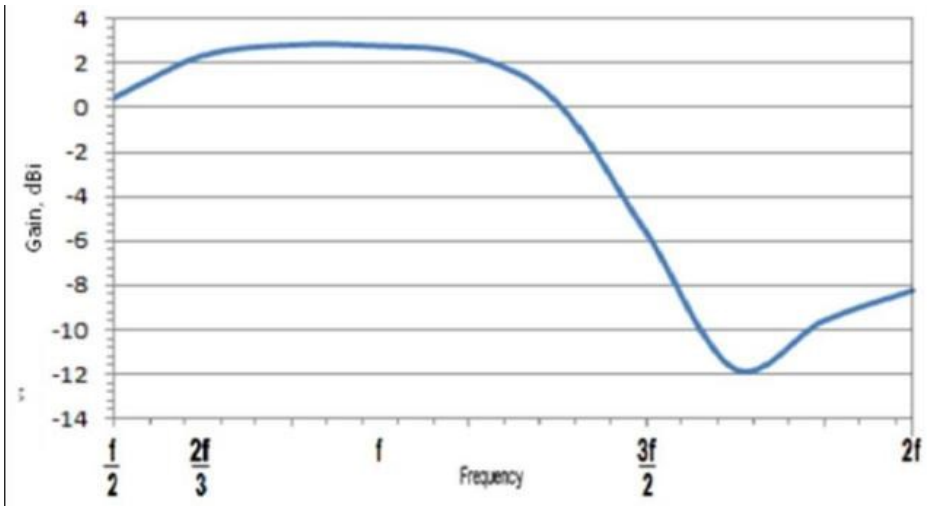

Figure 8.9: Circular Monopole UWB Antenna Gain Performance over 4:1 Frequency Band.

Figure 8.10 shows three layer stacked EBG with UWB monopole antenna over it,the purpose of stacked EBG layers is to reflect the backward radiated energy in phase with respect to forward radiated energy to increase the gain of the antenna in the band of interest.

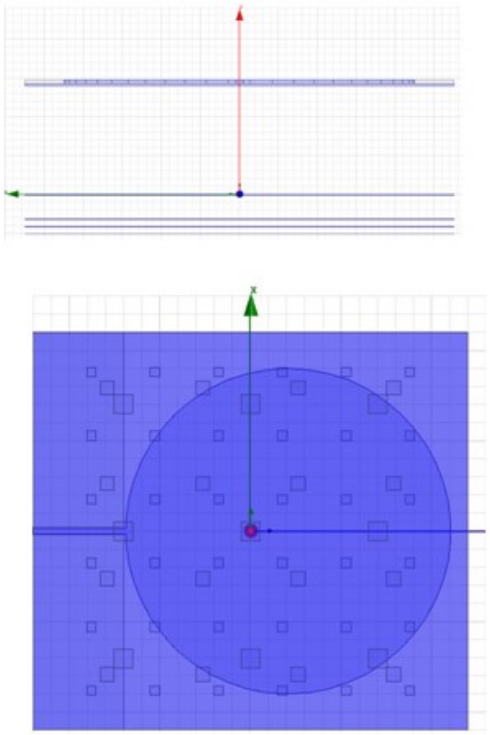

Figure 8.10: UWB antenna over three layer stacked EBG.

The stacked EBG structure is designed to have a band gap roughly from 0.4 GHz to 1.2 GHz. The purpose of designing three layer stacked EBG is to work over broadband and get higher off-boresight gain for the UWB antenna compared to a comparable Vivaldi antenna. Figure 8.11 shows the simulated reflection-phase comparison of the three layer stacked, computed using transmission line analysis from this study and commercially available EM simulation tool HFSS.

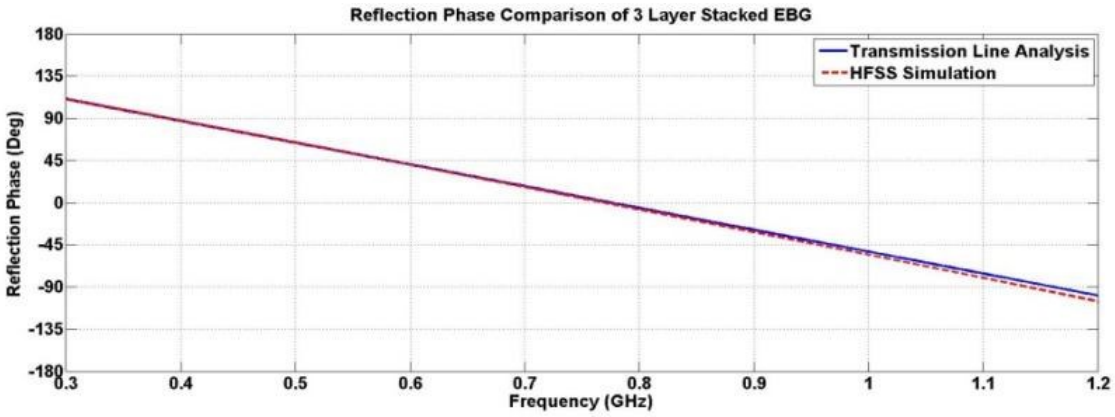

Figure 8.11: Reflection-phase comparison.

Figure 8.12 compares simulated boresight gain of the antenna with and without three layer stacked EBG Structure. Maximum gain of the antenna with three layer stacked is achieved off-boresight, as shown in Figure 8.13. Figure 8.14 shows measured off-boresight gain of the fabricated antenna with three layer stacked EBG.

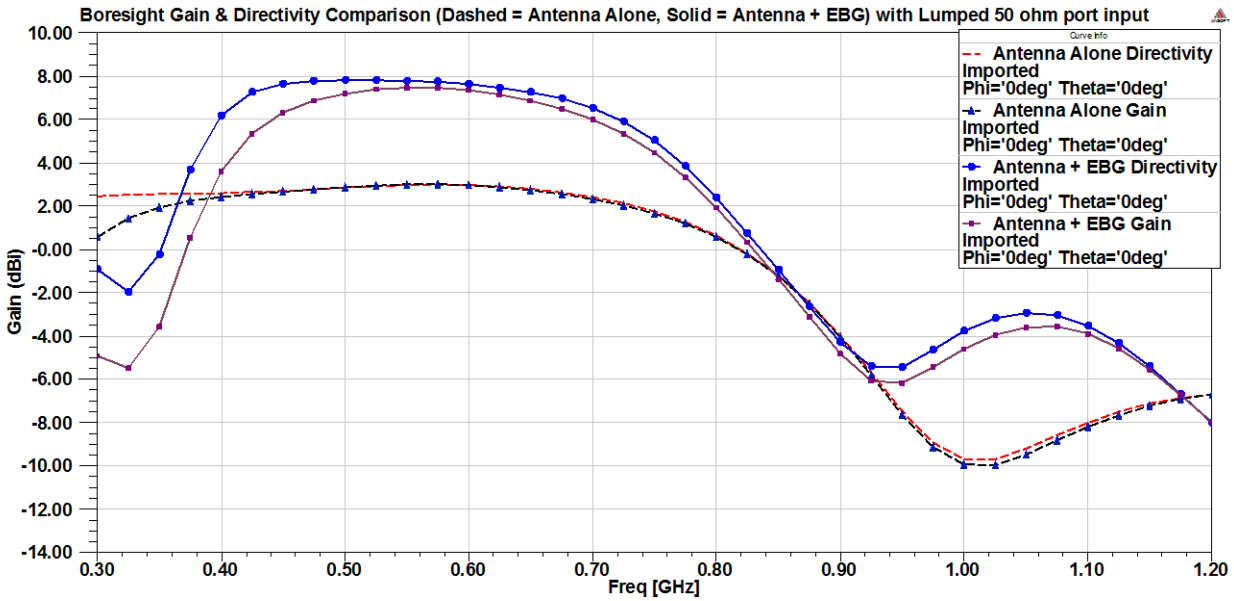

Figure 8.12: Realized Gain and Directivity at Broadside for Circular Monopole in Free Space (dashed) and over 3-Layer EBG Structure (solid).

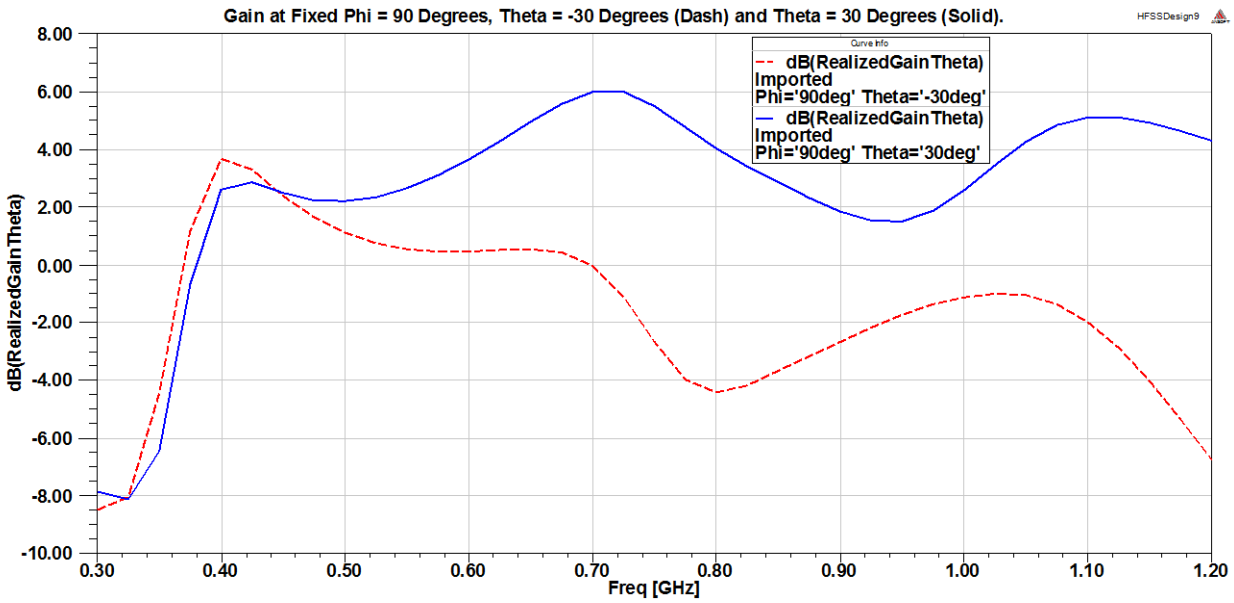

Figure 8.13: Realized Gain of Circular Monopole over 3-Layer EBG Structure at +30^{o} (solid) and -30^{o} (dash) Off Broadside.

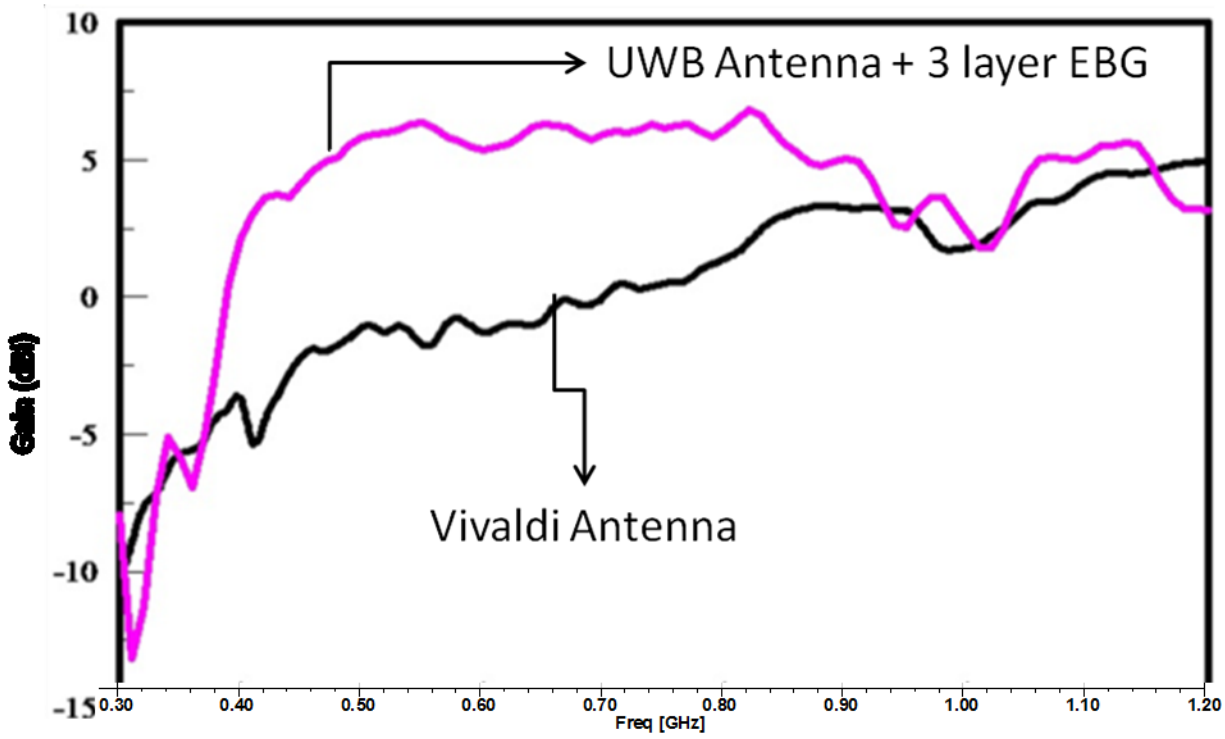

Figure 8.14: Measured Gain of Circular Monopole over 3-Layer EBG Structure (red) versus Measured Gain of Vivaldi Antenna (black) over the Same Frequency Band.

Figure 8.14 shows three layer stacked EBG helped in increasing the boresight gain of the UWB monopole antenna. Simulated and measured off-boresight gains match very well in Figures 8.13 and 8.14. Figure 8.14 shows the UWB monopole antenna with three layer stacked EBG has higher gain than a comparable size Vivaldi antenna, showing the importance of stacked EBG in improving the efficiency of the UWB antenna. This section showed an application of stacked EBG structure, and proved stacked EBG structure can be formed by vertically cascading different size uniform EBGs that resonate close to each other in frequency. The performance of the stacked EBG is validated by using it with a UWB monopole antenna. A prototype is fabricated and the far field gain and return loss of the antenna is compared with simulated results and the concept of stacked EBG structure is validated.

8.4 Measured versus Simulated Results for Spiral Antenna over Progressive EBG

Progressive EBG structures, like spiral antennas, resonate at different parts of EBG surface for different frequencies, hence spiral antenna works best with progressive EBG structures. A spiral antenna and a balun, to feed the spiral antenna, are designed and fabricated to work with progressive EBG. To understand the benefits of progressive EBG, spiral antennas measured and simulated return loss and boresight gain are compared under different conditions. Figure 8.15 shows the fabricated spiral antenna along with solder joints that connect spiral antenna and balun.

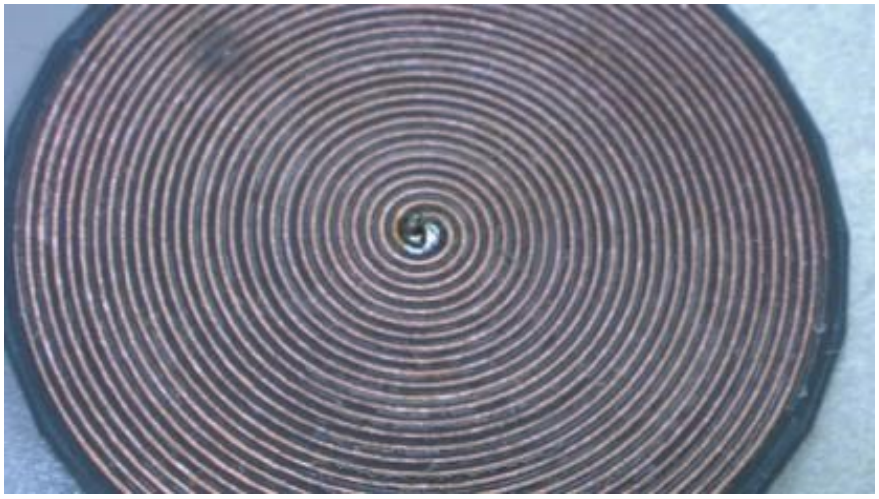

Figure 8.15: Fabricated spiral antenna with solder joints.

Figures 8.16 and 8.17 compare simulated and measured return loss and boresight gain performance respectively of spiral antenna under different conditions.

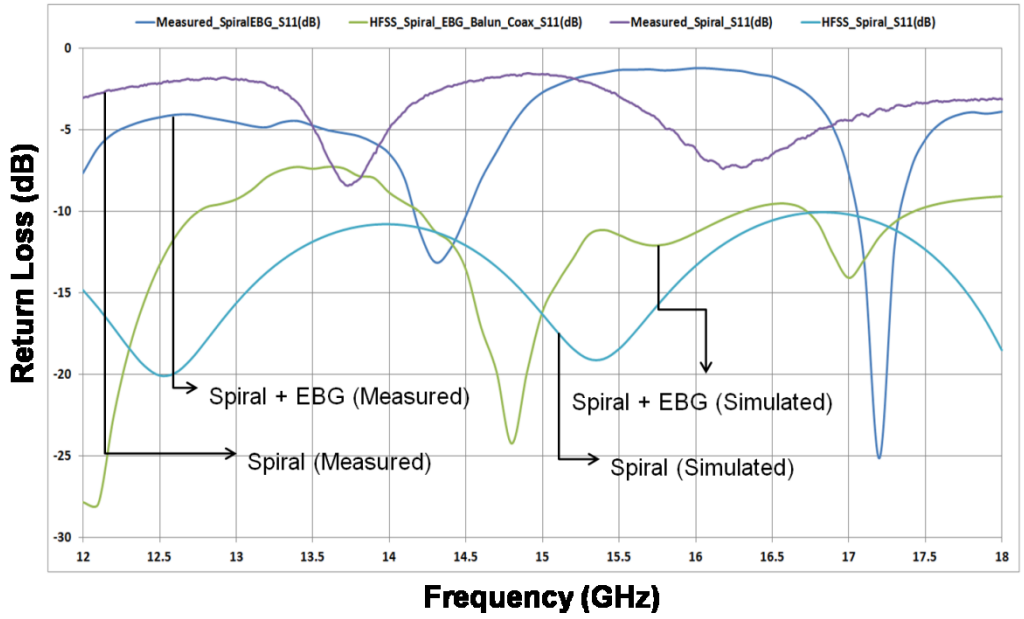

Figure 8.16: Return loss comparison of spiral antenna.

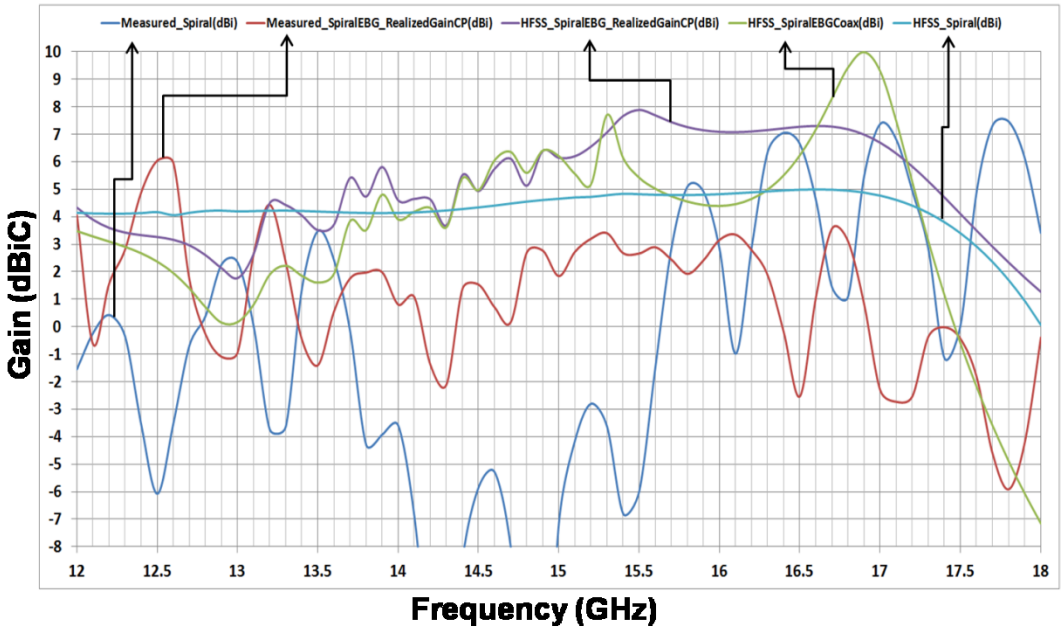

Figure 8.17: Boresight gain comparison of spiral antenna.

It is evident from Figure 8.17 the HFSS simulated boresight gain of spiral antenna increases with progressive EBG, when compared with boresight gain of antenna without progressive EBG. But simulated and measured results do not match, because simulations do not take into account solder

joints [57]. Solder joints cannot be ignored at the frequencies of interest, as their sizes are not negligible compared to wavelength. At high frequencies solder joints can have major impact on return loss, which in turn will affect boresight gain, so effects of solder joint sizes need to be explored. This section showed a way to increase the bandwidth of EBG structures, by progressively cascading uniform EBG structures. A broadband EBG was designed, and fabricated, for a broadband spiral antenna and return loss and boresight gain of the antenna is compared under different conditions. The importance of including the parameters of the solder joint at the antenna feeding point in the design procedure is noted

8.5 Study of Solder Size Effects on Spiral Antenna Performance

To understand the effects of solder joints, solder joints of 0.5 mm diameter are chosen and spiral antenna performance is simulated for varying solder gaps. Figure 8.18 and 8.19 show return loss and boresight gain performance of spiral antenna, respectively, for different solder gaps.

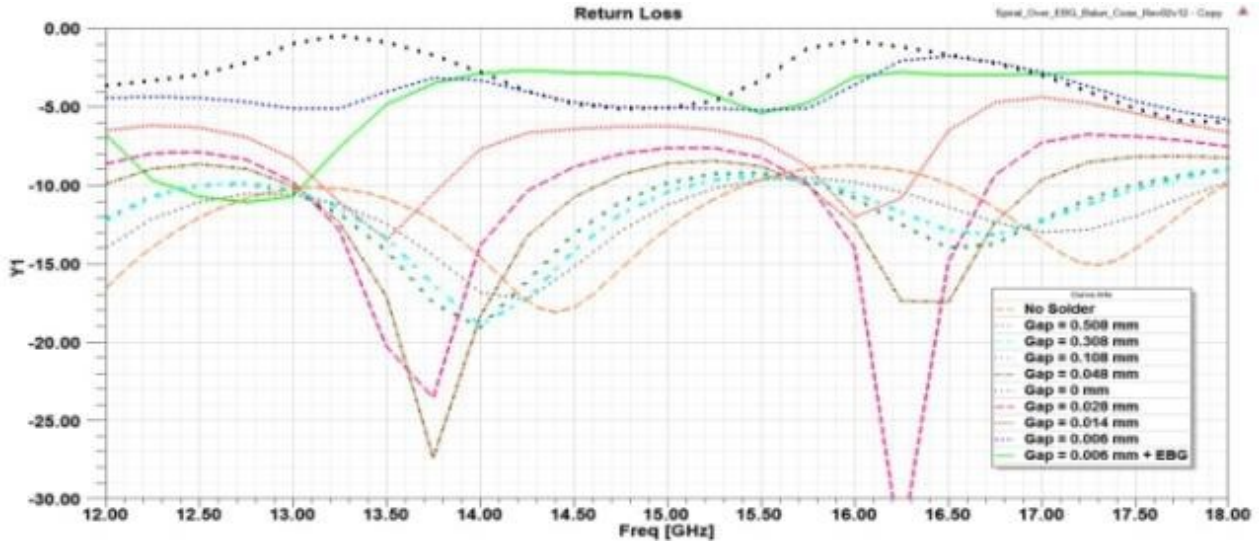

Figure 8.18: Return loss performance comparison of spiral antenna for different solder gaps.

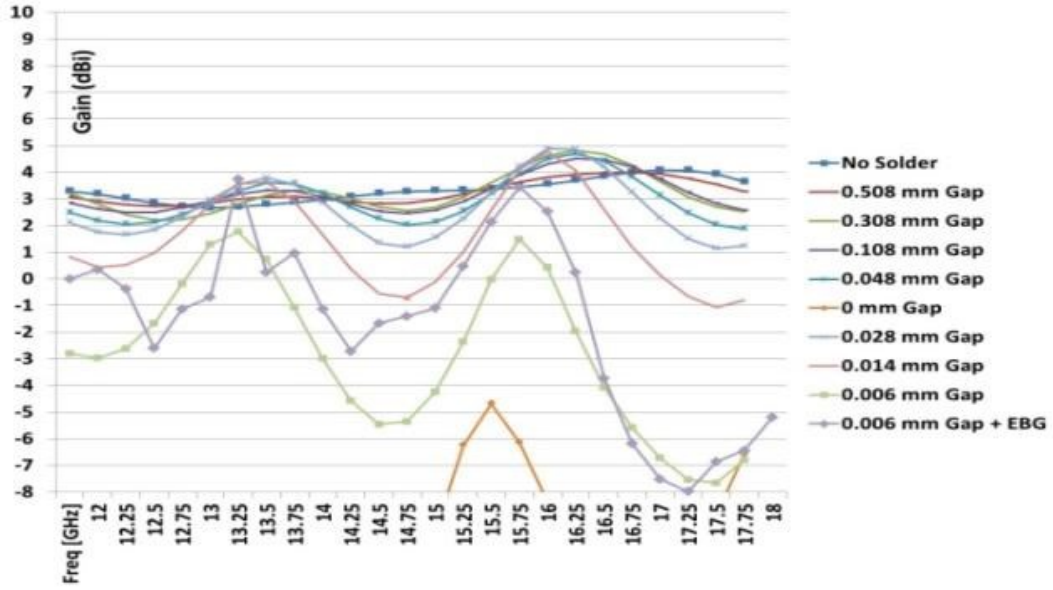

Figure 8.19: Boresight gain performance comparison of spiral antenna for different solder gaps.

Comparing Figure 8.16 with Figure 8.18 and Figure 8.17 with Figure 8.19, it is evident that measured and simulated return loss and boresight gain match for a solder gap of 0.006 mm. This shows the importance of including solder joints in simulations at frequencies under consideration. Solder joints represent lumped reactance, whose electrical size cannot be ignored at frequencies under consideration.The importance of including the parameters of the solder joint at the antenna feeding point in the design procedure is noted. The impact of the solder parameters on return loss and boresight gain is studied to bridge the gap between simulated and measured performance.

9 CONCLUSION ANDFUTUREWORK

9.1 Conclusion

Effects of conductive plane near an antenna have been demonstrated, and analysis of surface waves was carried out. Ground plane near an antenna has several degrading effects on an antenna performance, from unwanted nulls in radiation pattern, reduced radiation efficiency and worse return loss. Ground plane reflects backward radiated EM energy out of phase with respect to forward radiated EM energy which results in destructive addition of EM energies that result in lower gain and unwanted nulls in radiation pattern. One way to solve this problem is by absorbing backward radiated EM energy; this solution was carried out by designing a broadband three layer absorber and validated by loading it inside back cavity of a four arm sinuous antenna and comparing the improvement in performance with respect to an unloaded cavity. Loading the back cavity with absorbers decreases the efficiency of antenna by 50%; a better solution would be to load the back cavity with EBG structure and reflect back ward radiated EM energy in-phase with respect to forward radiated EM energy to constructively add and enhance the performance of the antenna [49, 51, 52].

Electromagnetic band gap structures are studied, analysis established using circuit modeling and transmission line modeling [41, 43] and results were compared with full wave EM simulations. EBG structures suppress surface waves and increase the gain of antenna when used as a ground plane, by reflecting backward radiated EM energy in phase with respect to forward radiated EM energy. EBG structures are equivalent to tank circuit in their band gap, with capacitance represented by gap between metal patches and inductance represented by gap between patches and ground plane. Via less EBG structures were explored and implemented with suitable antennas [49, 50, 51, 52, 53] and a prototype fabricated and measured performance compared with full wave analysis. EBG structures can be used in a number on EM applications from frequency selective surfaces, filtering, surface wave suppression, increasing gain of antennas and miniaturizing antennas for a given gain.

Stacked EBG structures were proposed [48], analyzed, and designed to increase the bandwidth of operation. Stacked EBG was implemented with an Ultra-Wide-Band (UWB) antenna [49], which

radiates at a high gain with high radiation efficiency with consistent radiation pattern over the wide frequency band. Results were compared, with better performance,with the well-known Vivaldi antenna. Measured performance compared well with the full-wave EM simulation and analysis presented in this study.

Progressive EBG surfaces were also proposed [50], designed, and implemented for antennas that radiate over a wide frequency band, with increased gain and radiation efficiency [51, 52]. The progressive dimensions of the EBG match the progressive radiation zones of the antenna. This is unlike the stacked EBG structure, which operates across the wide frequency band across the antenna aperture.

This dissertation presented closed form analysis for different types of EBG structures, using circuit and transmission line analysis [41, 43], and validated the analysis by comparing results to full wave simulations and published results. Analysis in this study was used in designing and introducing stacked and progressive EBG structures [48, 50], for increasing frequency band of EBG structures. Suitable applications for progressive and stacked EBG structures were presented [49, 53], by applying stacked EBG structure to an UWB monopole antenna and progressive EBG structure to a spiral antenna. As mentioned above, it was demonstrated that stacked EBG structures work well with antennas that radiate at the same place for all frequencies, while progressive EBG structures work well with antennas that radiate at different places for different frequencies. Ease of manufacturability of EBG structures was achieved, as part of design process, by designing stacked and progressive EBG structures without vias and progressive EBG structure was designed to have uniform height. Fabrication of EBG structures was carried out and detailed for both progressive EBG and stacked EBG topologies. Design of EBG structures demonstrated that EBG structures can be designed for wanted frequency bands and applied to different types of antennas. This dissertation showed that EBG structures can be modeled and analyzed using image theory, circuit analysis and transmission line analysis, and properties of EBG structures (resonance frequency, surface impedance and reflection phase) can be computed along with EBG bandwidth and necessary conditions for resonance. It is evident that EBG structures can be used as an effective constructive (additive) reflection mechanism to enhance antenna radiation.

9.2 Future Work

Progressive EBG and stacked EBG structures were proposed in this research, and their application in wide band filtering, surface wave suppression and frequency selective surface applications in satellite communications need to be studied and implemented. Satellite communication applications require both pass-band and stop-band of EBG structures to be implemented on sub-reflector to accommodate multiple communication bands on the same reflector. Higher order band gaps of EBG structures need to be explored and applications need to be selected appropriately. The tunability of EBG structures need to be explored for both increasing the bandwidth of EBG structures and changing the band gap of EBG structures at will.

REFERENCES

[1] B. A. Munk, Frequency Selective Surfaces: Theory and Design, New York: John Wiley & Sons, Inc., 2000.

[2] J. D. Joannopoulos, R. D. Meade, and J. N. Winn, Photonic Crystals, Princeton University Press, 1995.

[3] E.Yablonovitch, "Inhibited Spontaneous Emission in Solid-State Physics and Electronics," *Physics Rev. Letter,* pp. 2059-2063, Vol. 58 1987.

[4] Y. Rahmat-Samii and H. Mosallaei, "Electromagnetic band-gap structures: classification, characterization and applications," in *IEE-ICAP symposium*, 2001.

[5] E. Ozbay, A. Abeyta, G. Tuttle, M. Tringides, R. Biswas, T. Chan, C. M. Soukoulis, and K. M. Ho, "Measurement of a three-dimensional photonic band gap in a crystal structure made of dielectric rods," *Phys. Rev. B,* pp. 1945-1948, July 1994.

[6] A. S. Barlevy and Y. Rahmat-Samii, "Characterization of electromagnetic band-gaps composed of multiple periodic tripods with interconnecting vias: concept analysis, and design," *IEEE Trans. Antennas Propagat,* vol. 49, pp. 242-253, 2001.

[7] D. Sievenpiper, L. Zhang, R. F. J. Broas, N. G. Alexopolus, and E. Yablonovitch, "High-impedance electromagnetic surfaces with a forbidden frequency band," *IEEE Trans. Microwave Theory Tech.,* vol. 47, pp. 2059-2074, 1999.

[8] F.-R.Yang, K.-P. Ma,Y. Qian, and T. Itoh, "A uniplanar compact photonic-bandgap (UC-PBG) structure and its applications for microwave circuit," *IEEE Trans. Microwave Theory Tech,* vol. 47, pp. 1509-1514, 1999.

[9] V. Radisic, Y. Qian, R. Coccioli, and T. Itoh, "Novel 2-D photonic bandgap structure for microstrip lines," *IEEE Microw. and Guided Wave Lett.,* vol. 8, no. 2, pp. 69-71, 1998.

[10] C. Caloz and T. Itoh, Electromagnetic Metamaterials: Transmission Line Theory and Microwave Applications, Wiley-IEEE Press, 2005.

[11] Eli Yablonovitch, Henry Everitt, John Higgins "Guest Editorial Electromagnetic Crystal Structures, Design, Synthesis, and Applications," *Journal of Lightwave Technology,* vol. 17, no. 11, pp. 1928-1930, 1999.

[12] "Special issue on meta-materials," *IEEE Trans. Antennas Propag.,* vol. 51, no. 10, 2003.

[13] N. Engheta and R. Ziolkowski, Metamaterials: Physics and Engineering Explorations, John Wiley & Sons Inc., 2006.

[14] G. V. Eleftheriades and K. G. Balmain, Negative Refraction Metamaterials: Fundamental Principles and Applications, Wiley-IEEE Press, 2005.

[15] D. F. Sievenpiper, *High Impedance electromagnetic surfaces,* Ph.D. dissertation, Electrical Engineering Department, University of California, Los Angeles, 1999.

[16] M. Rahman and M. A. Stuchly, "Transmission line – periodic circuit representation of planar microwave photonic bandgap structures," *Microwave Optical Tech. Lett.,* vol. 30, no.

1, pp. 15-19, 2001.

[17] Y. Kim, F. Yang, and A. Elsherbeni, "Compact artificial magnetic conductor designs using planar square spiral geometry," in *Progress In Electromagnetics Research*, 2007.

[18] R. Coccioli, F. R. Yang, K. P. Ma, and T. Itoh, "Aperture-coupled patch antenna on UC-PBG substrate," *IEEE Trans. Microwave Theory Tech.,* vol. 47, pp. 2123-2130, 1999.

[19] R. Gonzalo, P. Maagt, and M. Sorolla, "Enhanced patch-antenna performance by suppressing surface waves using photonic-bandgap substrates," *IEEE Trans. Microwave Theory Tech.,* vol. 47, pp. 2131-2138, 1999.

[20] J. S. Colburn and Y. Rahmat-Samii, "Patch antennas on externally perforated high dielectric constant substrates," *IEEE Trans. Antennas Propagat.,* vol. 47, pp. 1785-1794, 1999.

[21] W. E. McKinzie III, R. B. Hurtado, B. K. Klimczak, J. D. Dutton, "Mitigation of multipath through the use of an artificial magnetic conductor for precision GPS surveying antennas," *Proc. IEEE APS Dig.,* vol. 4, pp. 640-643, 2002.

[22] F. Yang and Y. Rahmat-Samii, "Microstrip antennas integrated with electromagnetic band-gap (EBG) structures: a low mutual coupling design for array applications," *IEEE Trans. Antennas Propagat.,* vol. 51, no. 10, pp. 2936-2946, 2003.

[23] Z. Li and Y. Rahmat-Samii, "PBG, PMC and PEC ground planes: A case study for dipole antenna," in *IEEE APS Int. Symp*, Salt Lake City, UT, 2000.

[24] R.F. Jimenez Broas, D.F. Sievenpiper, and E. Yablonovitch, "A High-Impedance Ground Plane Applied toCellphone Handset Geometry," *IEEE Transactions on Microwave Theory and Techniques,* vol. 49, no. 7, pp. 1262-1265, 2002.

[25] R. Gonzalo, I. Ederra, C. Mann, and P. de Maagt, "Radiation properties of terahertz dipole antenna mounted on photonic crystal," *IEEE Electronics Letters,* vol. 37, no. 10, pp. 613-614, 2001.

[26] M. N. Afsar, Y.Wang and R.Cheung, "Analysis and Measurement of a Broadband Spiral Antenna," *IEEE Antennas and Propagation Magazine,* pp. 59-64, February 2004.

[27] J. A. Kaiser, "The Archimedean Two-Wire Spiral Antenna," *IRE Trans. on Antennas Propagat.,* Vols. AP-8, pp. 312-323, 1960.

[28] R. H. DuHamel, "Dual Polarized Sinuous Antennas,". US Patent 4658262, 14 April 1987.

[29] J. P. Scherer, "The dual polarized sinuous antenna," *Journal of Electronic Defense,* vol. 13, pp. 59-63, 1990.

[30] J. L. Volakis, Antenna Engineering Handbook, New York: McGraw-Hill, 2007.

[31] FEKO, "Computational Electromagnetics EM Software and Systems Pty Ltd," FEKO, [Online]. Available: http:/www.feko.info. [Accessed 23 March 2010].

[32] S. K. Khamas and G. G. Cook, "Optimised Design of a Printed Elliptical SpiralAntenna with a Dielectric Superstrate," *Applied Computational Electromagnetic Society Journal,* vol. 23, pp. 345-351, 2008.

[33] Emerson&. Cuming, "Microwave Products," [Online]. Available: http://www.eccosorb.com.

[Accessed 12 April 2010].

[34] Ansoft, "HFSS: 3D Full-wave Electromagnetic Field Simulation," [Online]. Available: http:/www.ansoft.com. [Accessed 4 August 2011].

[35] M. M. Sigalas, R. Biswas, Q. Li, D. Crounch, W. Lleung, R. Jacobs-Woodbury, B. Lough, S. Nielsen, S. McCalmont, G. Tuttle, and K.M. Ho, "Dipole Antennas on Photonic Band-Gap Crystals . Experiment and Simulation," *Microwave and Optical Technology Letters,* vol. 15, no. 3, pp. 153-158, 1997.

[36] E. R. Brown, C.D. Parker, and E. Yablonovith, "Radiation properties of a planar antenna on a Photonic-Crystal substrate," *Journal of Optic Soc. Am. B,* vol. 10, no. 2, pp. 404-407, 1993.

[37] T.H. Liu, W.X. Zhang, and M. Zhang, "A spiral antenna backed on photonic bandgapmaterial," in *International Symposium on Antennas and Propagation*, Fukuoka, Japan, 2000.

[38] J.M. Baracco, and P. de Maagt, "Radiating element on a photonic bandgap structure for phased array applications," *Proceedings Jina,* vol. 2, pp. 169-172, 2002.

[39] F. Yang, and Y. Rahmat-Samii, "A low profile circularly polarized curl antenna over an electromagnetic bandgap (EBG) surface," *Microwave and Optical technology letters,* vol. 31, pp. 264-267, 2001.

[40] F. Yang and Y. Rahmat-Samii, "Reflection Phase Characterisations of the EBG Ground Plane for Low Profile Wire Antenna Applications," *IEEE Trans. Antennas Propagat.,* vol. 51, no. 10, pp. 2691-2703, 2003.

[41] S. Palreddy, A.I. Zaghloul, "Circuit Analysis of Electromagnetic Band Gap (EBG) Structures," in *URSI-EMTS*, 2013.

[42] Matlab, "The Language of Technical Computing," [Online]. Available: http://www.mathworks.com/. [Accessed 12 December 2011].

[43] S. Palreddy, A.I. Zaghloul, "Transmission line Analysis of Electromagnetic Band Gap (EBG) Structures," in *IEEE APS-URSI*, Memphis, TN, 2014.

[44] S. Perlow, "Analysis of Edge-Coupled Shielded Strip and Slab-line Structures," *IEEE Trans. on Microwave Theory and Techniques,* vol. 35, no. 5, pp. 522-529, 1987.

[45] A. P. Feresidis, A. Chauraya, G. Goussetis, J. C. Vardaxoglou and P. de Maagt, "Multiband Artificial magnetic Conductor Surfaces," in *Proc. IEE Seminar on Metamaterials, for Microwave and (Sub)Millimetre Wave Applications*, London, UK, 2003.

[46] A. Monorchio, G. Manara, L. Lanuzza, "Synthesis of artificial magnetic conductors by using multilayered Frequency Selective surfaces," *IEEE antennas and wireless prop Letters,* vol. 1, pp. 196-199, 2002.

[47] S.A.Tretyakov and S.I.Maslovski, "Thin absorbing structure for all incidence angles based on the use of a highimpedance surfaces," *Microw. Opt. Techn. Let,* vol. 38, no. 3, pp. 175-178, 2003.

[48] S. Palreddy, A.I. Zaghloul, Y. Lee, "An Octave Bandwidth Electromagnetic Band Gap (EBG) Structure," in *European Conference on Antennas and Propagation*, 2012.

[49] A.I. Zaghloul, S. Palreddy, Y. Lee, T. Anthony, "Enhanced-Performance UWB Antenna Using Stacked EBG Surfaces," in *URSI-GASS*, 2014.

[50] A.I. Zaghloul, S. Palreddy, S.J. Weiss, "A Concept for a Broadband Electromagnetic Band Gap (EBG) Structure," in *European Conference on Antennas and Propagation*, 2011.

[51] S. Palreddy, A.I. Zaghloul, R. Cheung, "Performance Comparison of Uniform EBG and Broadband Progressive EBG Inside a Back Cavity of a Spiral Antenna," in *Applied Computational Electromagnetic Society*, 2011.

[52] S. Palreddy, A.I. Zaghloul,S.J. Weiss, "Performance of Spiral Antenna over Broadband Uniform-Height Progressive EBG Surface," in *European Conference on Antennas and Propagation*, 2013.

[53] S. Palreddy, A.I. Zaghloul, T. Anthony, "Spiral Antenna on Broadband Uniform-Height Progressive EBG Structure without Vias," in *IEEE APS-URSI*, 2015.

[54] Rachmansyah, A. Irianto, A.B. Mutiara, "Designing and Manufacturing Microstrip Antenna for Wireless Communication at 2.4 GHz," *International Journal of Computer and Electrical Engineering,* vol. 3, no. 5, pp. 45-48, 2011.

[55] F. Zhao, K.Xiao,W.J. Feng, S.L.Chai, J.J. Mao, "Design and Manufacture of the Wideband Aperture-Coupled Stacked Microstrip Antenna," *Progress in Electromagnetic Research C,* vol. 7, pp. 37-50, 2009.

[56] Rogers Corporation, "RT/Duroid 5880 Laminated," [Online]. Available: http://www.rogerscorp.com/acs/products/32/RT-duroid-5880-Laminates.aspx. [Accessed 7 March 2014].

[57] S. Palreddy, T.Anthony, A.I.Zaghloul, "Effects of Solder in the Feed Junction on Spiral Antenna Performance," in *Applied Computational Electromagnetic Society*, 2015.

PAPERS PRODUCED DURING PH.D STUDY

Conference Papers

1. Sandeep Palreddy, Amir I. Zaghloul, Rudolf Cheung, "An optimized lossy back cavity loaded four arm sinuous antenna," Pages 1-4, APS-URSI 2010.
2. Sandeep Palreddy, Amir I. Zaghloul, Rudolf Cheung,"Study of the Effects of the Back Cavity on a Broadband Sinuous Antenna," ACES 2010.
3. Sandeep Palreddy, Amir I. Zaghloul, Rudolf Cheung, "Performance Comparison of Uniform EBG and Broadband Progressive EBG Inside a Back Cavity of a Spiral Antenna," ACES 2011.
4. A.I. Zaghloul, S. Palreddy, S.J. Weiss, "A Concept for a Broadband Electromagnetic Band Gap (EBG) Structure," Proceedings of the 5th European Conference on Antennas and Propagation (EuCAP), pp 383-387, April 2011.
5. S. Palreddy, A.I. Zaghloul, Y. Lee, "An Octave Bandwidth Electromagnetic Band Gap (EBG) Structure," EuCAP 2012, Pages 3102-3105.
6. Sandeep Palreddy, Amir I. Zaghloul,StevenJ. Weiss, "Performance of Spiral Antenna over Broadband Uniform-Height Progressive EBG Surface," EuCAP, pages 3941-3944, April 2013.
7. S. Palreddy, A.I. Zaghloul, "Circuit Analysis of Electromagnetic Band Gap (EBG) Structures," URSI-EMTS, 2013, Pages 67-70.
8. Sandeep Palreddy, Amir I. Zaghloul, "Transmission line Analysis of Electromagnetic Band Gap (EBG) Structures," APS-URSI, 2014, Pages 1556-1557.
9. Amir I. Zaghloul, Sandeep Palreddy, YounM. Lee, Theodore K. Anthony, "Enhanced-Performance UWB Antenna Using Stacked EBG Surfaces," URSI-GASS 2014, Pages 1-4.
10. Sandeep Palreddy, Amir I. Zaghloul, Theodore K. Anthony, "Spiral Antenna on Broadband Uniform-Height Progressive EBG Structure without Vias," URSI-APS, 2015.
11. Sandeep Palreddy, Theodore K. Anthony,AmirI. Zaghloul, "Effects of Solder in the Feed Junction on Spiral Antenna Performance," ACES, 2015.

Journal Papers

1. Sandeep Palreddy, Amir I. Zaghloul, Rudolf Cheung, "Study of the Effects of the Back Cavity on a Broadband Sinuous Antenna and an Optimized Loaded Back Cavity," ACES Journal, Vol. 26, No. 8, 2011.
2. Sandeep Palreddy, Amir I. Zaghloul, Steven J. Weiss, Youn M. Lee, Theodore K. Anthony, "Methods of Increasing EBG bandwidth and Applications with Antennas," submitting to IEEE Transactions on Antennas and Propagation.
3. Sandeep Palreddy, Amir I. Zaghloul, "Analysis of Electromagnetic Band Gap (EBG) Structures," submitting to IEEE Transactions on Antennas and Propagation.

4. Amir I. Zaghloul, Sandeep Palreddy, Youn M. Lee, Theodore K. Anthony, "Enhanced-Performance UWB Antenna Using Stacked EBG Surfaces and Comparison with Vivaldi Antenna," submitting to IEEE Transactions on Antennas and Propagation.